uOttawa

L'Université canadienne
Canada's university

FACULTÉ DES ÉTUDES SUPÉRIEURES ET POSTOCTORALES

uOttawa

L'Université canadienne
Canada's university

FACULTY OF GRADUATE AND POSDOCTORAL STUDIES

Marc D. Rigden
AUTEUR DE LA THÈSE / AUTHOR OF THESIS

M.Sc. (Microbiology and Immunology)
GRADE / DEGREE

Department of Biochemistry, Microbiology and Immunology
FACULTÉ, ÉCOLE, DÉPARTEMENT / FACULTY, SCHOOL, DEPARTMENT

Determining the role of coiled-coil domain interactions in the oligomerization of DivIVA from *Enterococcus faecalis*

TITRE DE LA THÈSE / TITLE OF THESIS

J-A. Dillon
DIRECTEUR (DIRECTRICE) DE LA THÈSE / THESIS SUPERVISOR

CO-DIRECTEUR (CO-DIRECTRICE) DE LA THÈSE / THESIS CO-SUPERVISOR

EXAMINATEURS (EXAMINATRICES) DE LA THÈSE / THESIS EXAMINERS

K. Dimock

I. Lormier

Gary W. Slater
LE DOYEN DE LA FACULTÉ DES ÉTUDES SUPÉRIEURES ET POSTDOCTORALES / DEAN OF THE FACULTY OF GRADUATE AND POSTDOCORAL STUDIES

Determining the role of coiled-coil domain interactions in the oligomerization of DivIVA from *Enterococcus faecalis*

Marc D. Rigden

Thesis submitted to the
Faculty of Graduate and Postdoctoral Studies
in partial fulfillment of the requirements for the
Master of Science degree in Microbiology and Immunology

Department of Biochemistry, Microbiology and Immunology
Faculty of Medicine
University of Ottawa

Your file Votre référence
ISBN: 0-494-11392-8
Our file Notre référence
ISBN: 0-494-11392-8

Abstract

The involvement of DivIVA in cell division and chromosome segregation has been described in a number of Gram positive organisms. To date, most studies have focused on the effect of overexpression or disruption of DivIVA in various bacterial backgrounds. However, no detailed biochemical study of DivIVA has been conducted to identify which domains are responsible for the different functions of DivIVA. This study examines the coiled-coil domains of DivIVA from the Gram positive coccus *Enterococcus faecalis* to determine their role in oligomer formation. Based on bioinformatics analysis of known DivIVA homologs and *E. faecalis* DivIVA in particular, putative coiled-coil domains were identified at the N-terminal and central regions of DivIVA in all homologs with the N-terminal coiled-coil domain showing the most conservation between species. While the N-terminal and central coiled-coil domains are common to all DivIVA homologs, certain DivIVA homologs including *E. faecalis* DivIVA have a fourth coiled-coil domain located near the C-terminus. Of the four predicted coiled-coil domains of $DivIVA_{Ef}$, disruption of either the N-terminal or C-terminal domains resulted in no change in complex formation as measured by size exclusion chromatography and native gel electrophoresis. In contrast, disruption of the central coiled-coil domains of $DivIVA_{Ef}$ resulted in either decreased complex formation when one of the two domains was disrupted or completely abrogated complex formation when both central domains were disrupted, indicating that the central coiled-coil domains are responsible for complex formation. Based on this information and the recently published transmission electron microscope image of the *Bacillus subtilis* DivIVA

oligomeric complex (Stahlberg *et al.,* 2004), a model for DivIVA oligomerization is proposed.

Additionally, the bank of point mutations and deletions of $DivIVA_{Ef}$ generated in this study was used to identify a region of $DivIVA_{Ef}$ involved in interaction with the novel $DivIVA_{Ef}$ binding protein MLJD1. Using yeast two hybrid studies, interaction between $DivIVA_{Ef}$ and MJLD1 was mapped to residues 60-100 of $DivIVA_{Ef}$. This region is outside the four coiled-coil domains of $DivIVA_{Ef}$, suggesting that interaction between $DivIVA_{Ef}$ and MLJD1 is not dependent on coiled-coil domain interactions. The same bank of mutations can be used to determine the interaction between DivIVA and as yet undiscovered DivIVA-interacting proteins.

Preliminary localization studies of $DivIVA_{Ef}$ in both homologous and heterologous backgrounds were also performed. While no conclusive results were obtained for GFP studies, immunogold electron microscopy of DivIVA in *E. faecalis* showed localization to the division septum and cell poles, similar to DivIVA from other organisms. Once proper GFP localization studies can be carried out, the bank of mutations generated in this study can be used to determine the region(s) of $DivIVA_{Ef}$ involved in division site localization.

Acknowledgements

First and foremost my thanks to Dr. Jo-Anne Dillon for giving me the opportunity to work on this project and guiding me over the last two years. Also to the fearless lab leaders Sandra and Mingmin for their help and guidance to keep me on the straight and narrow path of my project when I started thinking up, planning, and sometimes working on all my little side adventures. The entire lab crew has made these last two years very memorable. Between Jason introducing me to golf (for which I will curse him eternally), Nelson and the panda-without-bamboo pose, Sudeep and his yak-herding talents, Pat and his love-hate relationship with all things technological, Dan and his always cheerful attitude, Val and her love for all things LOTR, and other memorable experiences it's been a great run with a lot of fun, laughs, popcorn awards, and thankfully very few low points. Special thanks to the DivIVA crew (Sandra, Susan, Mingmin, and Dorota) for always being available to bounce ideas off and help come up with new ways of battling and understanding our common protein foe. Of course, none of us could have done any research without Cathy, Anne, Lisa, and the other administrative staff at BMI working tirelessly in the background to make sure we always had everything we needed to perform our Nobel-prize winning experiments. Special thanks also to the staff at the University of Ottawa Core DNA Sequencing and Synthesis facility (Andre, Marc, Hui, and Dan) for making all the primers and doing the seemingly unending sequencing for all my plasmids. I would also like to thank Dr. Peter Anderson (BMI) for the use of his gel filtration equipment and advice concerning these experiments, as well as Dr. Mary Hefford (Health Canada) and her lab staff (primarily Mike Cauchy and Sam Guest) for the use of their Circular Dichroism equipment and help in analyzing and interpreting the

data. Finally, I wish to acknowledge the guidance and support of my thesis advisory committee, Dr. Mary Hefford and Dr. Morris Kates (BMI), as well as my unofficial third committee member Dr. Sandra Ramirez. This project was funded by grant XG 02-075R from the Hospital for Sick Children in Toronto to J.R. Dillon

Table of Contents

List of Figures

List of Tables

List of Abbreviations

AP	Alkaline Phosphatase
dcw	Division and Cell Wall synthesis gene cluster
ddH_2O	Double Distilled water
CD	Circular Dichroism
DivIVA2	$DivIVA_{Bs}$ carrying a Leucine to Proline mutation at residue 120
$DivIVA_{Bs}$	DivIVA protein from *Bacillus subtilis*
$DivIVA_{Ef}$	DivIVA protein from *Enterococcus faecalis*
DNA	DeoxyriboNucleic Acid
EDTA	Ethylenediamine tetra-acetic acid
EtBr	Ethidium Bromide
g	Gravity
GFP	Green Fluorescent Protein
HRP	Horseradish Peroxidase
IgG	Immunogolbulin G
IPTG	Isopropyl-β-D-thiogalatopyranoside
Kan	Kanamyocin
LB	Luria Bertani bacterial culture medium
LMP	Low Melting Point
M	Molar
Min	Minicell gene cluster
MR1	$DivIVA_{Ef\ L29D}$
MR2	$DivIVA_{Ef\ E37P}$
MR3	$DivIVA_{Ef\ E37P,N43P,\ L46D}$
MR4	$DivIVA_{Ef\ E37P,\ N43P,\ L46D,\ L50D,\ L57F}$
MR5	$DivIVA_{Ef\ E37P,\ N43P,\ L46D,\ L50E,\ L57F}$
MR6	$DivIVA_{Ef\ 1\text{-}190}$
MR7	$DivIVA_{Ef\ \Delta 130\text{-}190}$
MR8	$DivIVA_{Ef\ \Delta 60\text{-}190}$
MR9	$DivIVA_{Ef\ \Delta 60\text{-}130}$
MR10	$DivIVA_{Ef\ L143P}$
MR11	$DivIVA_{Ef\ L104P}$
MR12	$DivIVA_{Ef\ L104P,\ L143P}$
MR13	$DivIVA_{Ef\ L104P,\ I125P}$
MR14	$DivIVA_{Ef\ L104P,\ I125P,\ L143P}$
MR15	$DivIVA_{Ef\ L104P,\ I115P,\ I125P}$
MR16	$DivIVA_{Ef\ L104P,\ I115P,\ I125P,\ L143P}$
MRE	Mean Residue Ellipticity
MWCO	Molecular weight cut-off
OD	Optical Density
PBP2B	Penicillin Binding Protein, involved in bacterial cell division
PBS	Phosphate Buffered Saline
PCR	Polymerase Chain Reaction
rpm	Revolutions per minute
SDS	Sodium dodecyl sulphate

SDS-PAGE	Sodium dedecyl sulphate polyacrylamide gel electrophoresis
SDM	Site Directed Mutagenesis
STI	Soybean Trypsin Inhibitor
TBS	Tris-buffered saline
TTBS	Tris buffered saline with 0.05% Tween-20
TEM	Transmission Electron Microscopy
UV	Ultraviolet light
V	Volt
W	Watts
X-gal	5-bromo-4-chloro-3-indolyl-β-D-galactopyranoside

Introduction

One of the key processes in both cellular and bacterial survival is co-ordination of proper cell division. In order to ensure their survival, cells must ensure that their progeny contain an equal amount of all the genetic and cellular materials present in the parent cell. While significantly less complex than their eukaryotic cousins, the regulatory systems of prokaryotes ensure proper division septum placement and creation of identical daughter cells.

1.1 Regulation of cell division site placement

The cytokinetic event in prokaryotes is performed by the tubulin homolog FtsZ (Bi and Lutkenhaus, 1991). FtsZ is a GTPase capable of homooligomerization and forms a ring associated with the bacterial membrane which constricts and eventually separates the parent cell into two daughter cells (Bi and Lutkenhaus, 1991; Bramhill and Thompson, 1994). The assembly of the FtsZ ring serves as a recruitment site for other cell division related proteins including ZipA, FtsA, FtsQ and other proteins associated with the division and cell wall synthesis (dcw) gene cluster (Rothfield and Justice, 1997; Dewar and Dorazi, 2000; Margolin 2001, 2003). The formation of the FtsZ ring is the first known step in cell division and occurs before complete nucleoid separation (Bi and Lutkenhaus, 1991).

Unless properly regulated, FtsZ can polymerize and constrict at any point along the bacteria, leading to elongated filaments and minicells, both of which can lead to a non-viable bacterial cell population (Begg and Donachie, 1985). The mechanisms which control division septum placement have been studied extensively in Gram negative organisms such as *Escherichia coli* (Fu *et al.*, 2001; Pichoff and Lutkenhaus, 2001; Rothfield *et al.*, 2001; Shih *et al.*, 2003) and, in our laboratory, *Neisseria gonorrhoeae*

(Francis *et al.*, 2000; Ramirez-Arcos *et al* 2001a,b, 2002, 2004a; Szeto *et al.*, 2001, 2004). In Gram negative organisms, division septum placement is co-ordinated by a combination of nucleoid occlusion and the tripartite Min system (Harry, 2001). The presence of the bacterial nucleoid, which is the region containing the bacterial chromosome, inhibits formation of the FtsZ ring (Sun and Margolin, 2004). While the mechanism used by nucleoid occlusion to regulate FtsZ placement is largely unknown (Sun and Margolin, 2004), the regulatory mechanism of the Min system has been well defined.

The Min system is comprised of three proteins designated MinC, MinD, and MinE, all of which are expressed from the *minB* locus (de Boer *et al.*, 1989). MinC is responsible for regulating placement of FtsZ and acts by depolymerising any FtsZ structures (Hu *et al.*, 1999). In order to perform its function, MinC is dependent on MinD, an ATPase which reversibly binds to MinC and recruits it to the cell membrane, and MinE which controls the localization of the MinCD complex (Rothfield *et al.*, 2001; Ramirez-Arcos *et al.*, 2001a,b, 2002, 2004a; Shih *et al.*, 2003, Szeto *et al.*, 2001, 2004). In this model of septum placement control, the three Min proteins undergo dynamic oscillation controlled by the interactions of MinD and MinE (Raskin and de Boer, 1999, Figure 1). This continual oscillation results in maintaining a low concentration of the division inhibitor MinC at the middle of the cell (Rothfield *et al.*, 2001; Ramirez-Arcos *et al* 2001a, b, 2004a). This high concentration of MinC blocks cell division from occurring at the cell poles and thus only permits division at the middle of the cell.

Figure 1 - Schematic diagram of Gram negative Min-dependent midcell site selection.

A) Following MinD dimerization and association of MinC in the cytoplasm, the MinCD protein complex localizes to the cell membrane at or near the cell poles. B) A MinE ring forms near the midcell and activates the ATPase activity of MinD. C) Due to the effect of MinE, the MinCD protein complex dissociates from the cell membrane dissociate and return to the cytoplasm. MinC and MinD then diffuse along a concentration gradient towards the opposite cell pole. D) Upon reaching the opposite cell pole where the concentration of MinE is lowest, the MinCD complex re-forms and re-associates with the cell membrane. Once MinE reaches the cell poles, the ring dissociates and re-forms at midcell, repeating the cycle. This minimizes the concentration of MinC at the middle of the cell, allowing FtsZ to polymerize and form a cytokinetic ring.

Figure 1

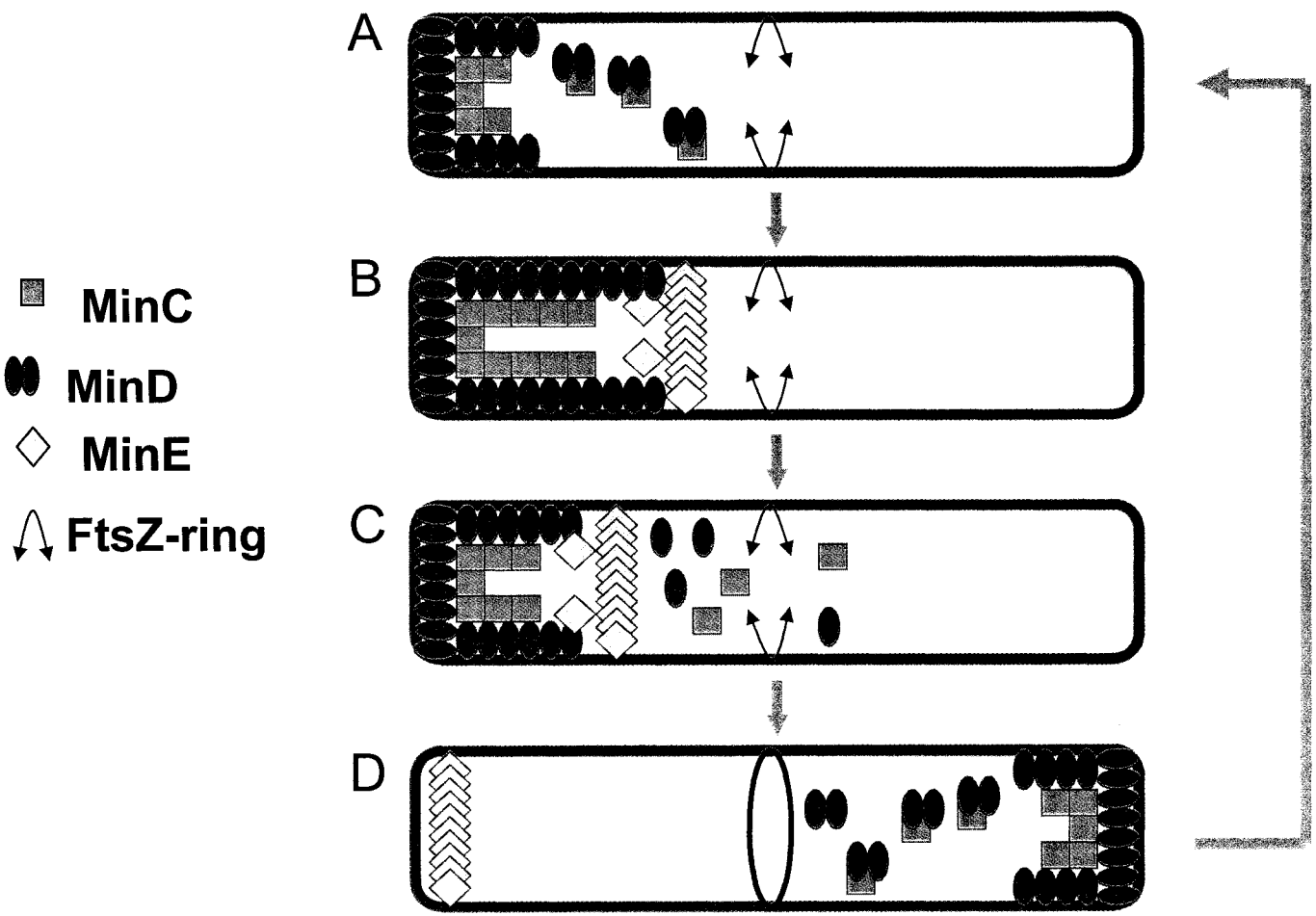

1.2 Division site localization in coccal-shaped organisms

While the same mechanisms of division site selection are used for both bacilli and cocci, the lack of an obvious midcell in cocci adds a new dimension to septal localization. Specifically, due to the lack of an obvious midcell, cocci must use a different method to define the midcell for septum placement (Ramirez-Arcos *et al.,* 2001b). However, it has been demonstrated that the Min proteins from cocci are functional when expressed in a bacillus background (Ramirez-Arcos *et al.,* 2001a,b, 2002, 2004a; Szeto *et al.,* 2001, 2004), indicating that the fundamental process of septum regulation involving the Min proteins is similar regardless of cell shape.

1.3 Cell Division in Gram positive organisms

While the Min protein model has been well characterized, the model only applies to Gram negative organisms and not to Gram positive organisms. Some Gram positive species, such as *Bacillus subtilis*, have homologs of MinC and MinD, however there are no MinE homologs found in Gram positive organisms. Thus, these organisms use a different mechanism to regulate proper cell division.

1.4 Identification and characterization of divIVA

In the early 1970's, Reeve *et al.* used nitrosoguanidine mutagenesis to identify genes involved in *B. subtilis* cell division (Reeve *et al.,* 1973). This work identified two novel genes, one of which was designated *divIVA,* which disrupted proper cell division in *B. subtilis* when mutated by nitrosoguanidine and produced a high proportion of minicells devoid of DNA following division (Reeve *et al.,* 1973). More than twenty years following the identification of *divIVA*, experiments performed independently by two different researchers characterized the unaltered *divIVA* gene product and proposed that

DivIVA replaces MinE as the topological specificity factor for Min protein function in Gram positive organisms (Cha and Stewart, 1997; Edwards and Errington, 1997).

1.4.1 Role of DivIVA in Gram Positive Cell Division

Although no direct interaction between DivIVA and MinD has been demonstrated, localization patterns of MinD in *B. subtilis* in the presence and absence of DivIVA have demonstrated the connection between the two proteins (Marston *et al.*, 1998; Marston and Errington, 1999). Unlike the dynamic oscillation pattern observed for MinD in Gram negative species, MinD does not oscillate in a Gram positive background and instead remains sequestered at the cell poles in the presence of DivIVA while in the absence of DivIVA, MinD is found distributed throughout the cell (Martson *et al.*, 1998, Figure 2). This polar sequestering of MinD, and by association MinC, by DivIVA minimizes the concentration of the division inhibitor MinC at midcell and allows proper midcell division to occur. However, many Gram positive organisms lack homologs of all the Min proteins but still have DivIVA homologs. Therefore, these organisms must utilize a hitherto undescribed method to control proper septum placement.

1.4.2 Chromosomal location of divIVA

In the majority of the species containing DivIVA homologs, the *divIVA* gene is found slightly downstream of the division and cell wall (*dcw*) gene cluster and immediately upstream of the isoleucyl tRNA synthetase gene (Cha and Stewart 1997; Massidda *et al.*, 1998). Although *divIVA* and several upstream genes are transcriptionally related to the *dcw* gene cluster, disruption of the genes upstream of *divIVA* does not affect its expression (Cha and Stewart, 1997; Fadda *et al.*, 2003).

Figure 2 - Schematic diagram of MinCD/DivIVA cell division.

A) DivIVA associates with the cell poles and sequesters the MinCD division inhibitor complex away from the middle of the cell allowing the FtsZ cytokinetic ring to assemble at midcell. B) DivIVA associates with the new cell pole during FtsZ contraction and marks it as a used site of cell division. C) Following septation, the MinCD complex is drawn to the newly-formed cell poles and sequestered there by DivIVA.

Figure 2

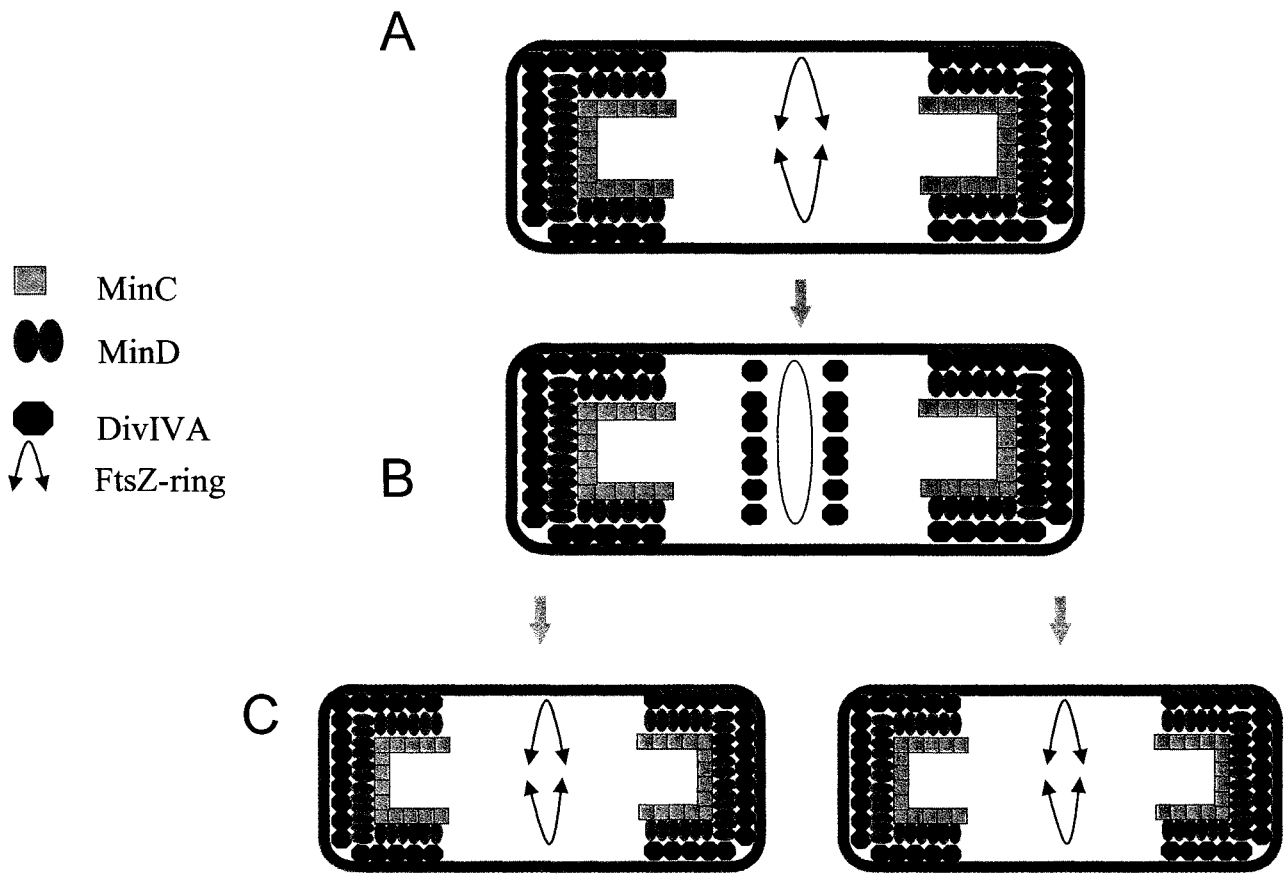

1.4.3 Biological function of DivIVA

The exact role of DivIVA in bacterial cell division and chromosome segregation remains largely unknown. While *divIVA* has been suggested to be non-essential in *S. pneumoniae* (Fadda *et al.,* 2003), the *divIVA* homologs of *B. subtilis, Brevibacterium lactofermentum, E. faecalis* and *Streptomyces coelicolor* have been shown to be essential genes (Edwards and Errington, 1997; Marston and Errington, 1999; Thomaides *et al.,* 2001; Flardh, 2003a,b; Ramos *et al.,* 2003; Ramirez-Arcos *et al.,* 2004b). Overexpression or disruption of *divIVA* results in severe defects in cell morphology, including inhibition of septation, swelling of cells, and filamentation depending on the host species (Cha and Stewart, 1997; Ramos *et al.,* 2003; Ramirez-Arcos *et al.*, 2004b).

1.4.4 DivIVA localizes to sites of cell division

DivIVA has been shown to localize to sites of nascent and used cell division under a variety of experimental conditions. DivIVA from *B. subtilis* ($DivIVA_{Bs}$) has been shown to localize to sites of cell division not only in its native host by also when expressed heterologously in *E. coli* (Edwards and Errington, 1997; Edwards *et al.,* 2000; Ding *et al.,* 2002). The localization of DivIVA is so specific that it has been proposed as a model system to demonstrate cytology-based protein-protein interactions (Ding *et al.,* 2002). Similar to the yeast two hybrid system that relies on dimerization to activate a reporter gene (Chien *et al.,* 1991), this cytology screen involves tagging the protein of interest with DivIVA or GFP and expressing both fusion proteins in the same cell. If the protein or proteins of interest interact, GFP is localized to the cell poles while the fluorescence remains distributed through the cytoplasm if the proteins do not interact (Ding *et al.,* 2002). While it was originally suggested that $DivIVA_{Bs}$ localization

depended on FtsZ, PBP2B, and other proteins in the cell division complex, experiments using outgrowing spores of *B. subtilis* have demonstrated that $DivIVA_{Bs}$ can localize to previous sites of cell division independently (Marston *et al.,* 1998; Hamoen and Errington, 2003; Harry and Lewis, 2003). These studies suggest that DivIVA recognizes a hitherto unidentified marker of sites of cell division. This marker is likely found in both prokaryotes and eukaryotes since $DivIVA_{Bs}$ has been shown to localize to division sites in the eukaryotic fission yeast *Schizosaccharomyces pombe* (Edwards *et al.,* 2000).

1.4.5 DivIVA is a multifunctional protein

Although the primary function of DivIVA appears to be in cell division, a second role in chromosome segregation has been demonstrated in *B. subtilis* (Errington, 2001; Thomaides *et al.,* 2001; Wu and Errington, 2003). While direct interaction between $DivIVA_{Bs}$ and DNA has not been demonstrated, the absence of $DivIVA_{Bs}$ in *B. subtilis* cells undergoing sporulation results in spores devoid of chromosomal material (Thomaides *et al.,* 2001). $divIVA_{Bs}$ expression has been demonstrated to decrease during sporulation, indicating that the $DivIVA_{Bs}$ marking the used sites of cell division are involved in this process (Thomaides *et al.,* 2001). It has been proposed that $DivIVA_{Bs}$ acts as a polar anchor and interacts with the RacA/Spo0J/Soj chromosome segregation machinery (Wu and Errington, 2003). In this model of chromosome segregation, Soj and Spo0J interact with the region of the bacterial chromosome associated with bi-directional replication, also known as the *oriC* region (Wu and Errington, 2003). Once the association between *oriC* and Soj/Spo0J is formed, RacA acts in conjunction to bring the *oriC* and the remainder of the chromosome to the cell pole, where it is anchored by

DivIVA (Wu and Errington, 2003). However, no direct interaction between DivIVA and RacA or Soj/Spo0J has been demonstrated.

1.4.6 Interaction between DivIVA and other cellular proteins

As mentioned previously, while DivIVA is believed to interact with MinD and components of the chromosome segregation machinery, no direct interactions between the proteins has been observed. Using an *E. faecalis* genomic library screen, Liao *et al.* identified a novel *E. faecalis* DivIVA ($DivIVA_{Ef}$) interacting protein, which has been named MLJD1 (Liao *et al.*, unpublished). MLJD1 is a hypothetical protein with homologs in several Gram positive bacteria. Sequence analysis of MLJD1 suggests it contains two CBS, or Cystathionine Beta Synthase domains, located in the central and C-terminal regions. CBS domains are usually found in pairs on proteins and are implicated in membrane binding and protein-protein interactions of both cytoplasmic and nuclear proteins (Bateman, 1997; Nath *et al.*, 2002). Recently, it was found that CBS domains can act as energy sensors by binding to molecules such as ATP or AMP (Scott *et al.*, 2004). The N-terminus of MLJD1 contains a predicted DNA binding domain belonging to the DeoR protein family (Roy *et al.*, 2002; Wiegert and Schumann, 2003). Liao *et al.* have also demonstrated that MLJD1 self-interacts, forming a homomultimeric complex and affects bacterial cell division when expressed heterologously in *E. coli.* (Liao *et al.*, unpublished).

1.4.7 DivIVA forms a homooligomeric complex

To date, DivIVA oligomerization has only been studied using the *B. subtilis* homolog while experiments on the DivIVA homologs from other organisms including *S. pneumoniae, B. lactofermentatum* and *S. coelicolor* have focused primarily on protein

localization. Unlike most cell division proteins that form complexes with other proteins, $DivIVA_{Bs}$ has been shown to form a homooligomeric complex comprising between 6-10 monomers (Muchova *et al.*, 2002 a, b; Stahlberg *et al.*, 2004). This oligomerization appears to be independent of buffer and pH conditions (Muchova *et al.*, 2002b). While the original *divIV-A1* mutation, an alanine to threonine substitution at residue 78 (A78T), disrupts proper $DivIVA_{Bs}$ function, studies by Muchova *et al* have shown that this mutation has no effect on the oligomerization state of DivIVA (Cha and Stewart, 1997; Muchova *et al.*, 2002a). In contrast, Muchova *et al* also demonstrated that a leucine to proline mutation at residue 120 (L120P) reduces the oligomerization by 50% with no noticeable effect on $DivIVA_{Bs}$ function. The results of these studies suggest that oligomerization is not critical for the biological function of DivIVA. However, upon closer inspection of the native gel electrophoresis results presented by Muchova *et al.*, there is evidence that a portion of the DivIVA present in the purified DivIVA2 ($DivIVA_{Bs\ L120P}$) sample maintained the full oligomeric structure (Muchova *et al.*, 2002a). As such, it is not clear whether oligomer formation is necessary for proper DivIVA function.

1.4.8 Structure of the DivIVA oligomeric complex solved by Transmission Electron Microscopy

Due to the difficulty in crystallizing the oligomeric complex (Muchova *et al.*, 2002b), a transmission electron microscopy (TEM) study was used to determine the quaternary structure of $DivIVA_{Bs}$ (Stahlberg *et al.*, 2004). $DivIVA_{Bs}$ forms an elongated particle with protrusions at both ends to resemble a "doggy-bone". *In vitro*, this doggy bone forms the base unit of a larger lattice of DivIVA built by overlap of the base units

by either end to end interaction or interaction through the central portion of the protein to form a two dimensional network. Since DivIVA does not require any of the known cell division proteins to localize to the cell poles, it is possible that DivIVA can help in creating the cell polarity needed in processes such as *B. subtilis* sporulation and *S. coelicolor* tip extension (Stahlberg *et al.*, 2004).

1.5 Rationale for using Enterococcus faecalis as a model organism

Similar to the selection of *N. gonorohoeae* to study Min protein function in cocci, Dr. Dillon's lab chose to examine the cell division of the coccus *Enterococcus faecalis* to determine whether the function of DivIVA is similar in both bacilli and cocci. Also, since *E. faecalis* lacks homologs of MinC and MinD, studying *E. faecalis* will help elucidate how cell division regulation occurs in this and other Gram positive organisms that lack Min proteins. *E. faecalis* is a Gram positive coccus found as a normal part of the mammalian intestinal microflora and can be transmitted through fecal contamination of soil, sewage, and water (Aarestrup *et al.,* 2002; Tannock and Cook, 2002). In humans, *E. faecalis* can cause severe conditions such as bacteremia and endocarditis and is one of the leading causes of nosocomial infections in pediatric hospital wards (Gilmore *et al.,* 2002). Like most bacteria, *E. faecalis* has been developing resistance to numerous antibiotics over the years and today is resistant at varying degrees to β-lactams, aminoglycosides, glycopeptides, chloramphenicol, and tetracycline (Kak and Chow, 2002). The genome of *E. faecalis* contains approximately 33% mobile DNA elements, which is believed to contribute to the transfer of antimicrobial resistance between species (Paulsen *et al.,* 2003).

1.6 Coiled-coil mediated protein-protein interactions

Bioinformatic analysis of various DivIVA homologs suggests that the protein has a high propensity for forming coiled-coil domains, which are known to be involved in dimerization and oligomerization of a large variety of proteins and structures (Lupas, 1996). Coiled-coil domains are the main structural element of a large class of fibrous proteins including keratin, myosin, and fibrinogen, as well as transcription factors including leucine zippers (Lupas *et al.,* 1991; Lupas, 1996). As illustrated in Figure 3, coiled-coil domains are characterized by a repeating heptad motif with positions A and D being hydrophobic and providing the interaction interface while residues B, C, E, F, and G are generally hydrophilic (Lupas, 1996, Figure 3A). These heptads pack together into a "knobs-into-holes" orientation so that the A and D residues are interacting with their counterparts on the adjoining heptad (Figure 3B). The number of helices present in a coiled-coil domain is dependent on the amino acid composition of the A and D positions. A predominance of either leucine or isoleucine in both positions generally produces a trimeric structure, a predominance of leucine at position A and isoleucine in position D results in tetramers while the opposite arrangement results in dimers (Lupas, 1996). Also, the amino acids in positions E and G can interact between coils and determine whether the domains will pack either in a parallel or antiparallel configuration. Coiled-coil domains have been demonstrated to mediate protein-protein interactions in a wide range of proteins including prokaryotic proteins such as the mating pair formation protein TrhB (Gilmour *et al.,* 2003) and flagellar hook protein (Gugolya *et al.,* 2003), eukaryotic proteins, including the mitotic protein NuMA (Harborth *et al.,* 1999), receptor associated factors such as TRAF2 (Park *et al.,* 1999) and tropomyosin (Lupas, 1996) as well as viral

Figure 3 - Orientation of the A through G residues in the heptad repeat of a coiled-coil domain.

A) Top view of the interaction between coiled-coil domains is mediated by interaction between residues A and D. B) Side view of coiled-coil interaction showing the arrangement of the A and D residues into a "knobs into holes" orientation. Figure adapted from http://cis.poly.edu/~jps/coilcoil.html

Figure 3

A

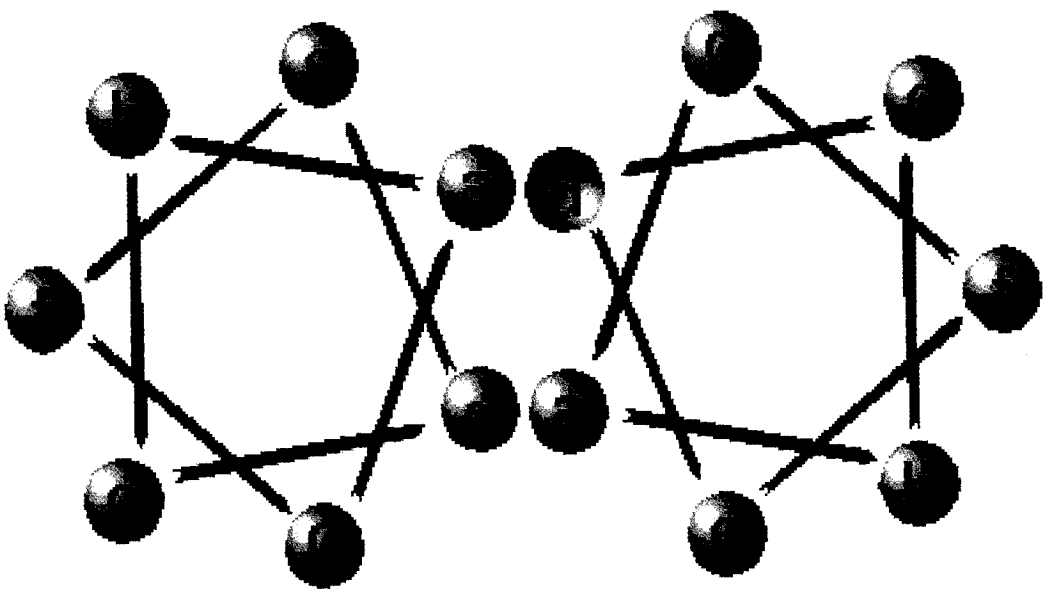

B

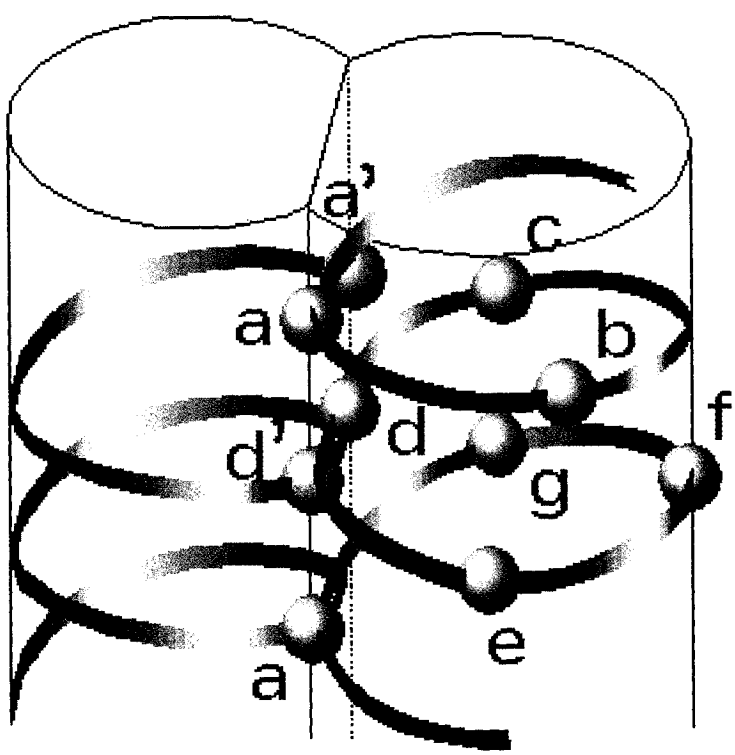

helper component proteins such as the *Cauliflower mosaic virus* protein P2 (Hebrard *et al.*, 2001).

1.7 Hypothesis and Objectives

My hypothesis is that coiled-coil domain interactions are responsible for the oligomerization of DivIVA from *E. faecalis*. In order to test this hypothesis and examine some other characteristics of $DivIVA_{Ef}$, the following objectives were completed:

1) Bioinformatic analysis of DivIVA
    a. Comparison of known DivIVA homologs to determine regions likely involved in oligomer formation and other properties of DivIVA
    b. Coiled-coil domain analysis of $DivIVA_{Ef}$ to select residues for site directed mutagenesis
2) Site Directed Mutagenesis of $DivIVA_{Ef}$
    a. Disruption of the N-terminal coiled-coil domain
    b. Disruption of the C-terminal coiled-coil domain
    c. Disruption of the Central coiled-coil domains
3) Purification and analysis of the effects of coiled-coil disruptions on the oligomerization of mutated $DivIVA_{Ef}$
    a. Size Exclusion Chromatography
    b. Native Gel Electrophoresis
    c. Yeast Two Hybrid Analysis
4) Mapping the interaction between $DivIVA_{Ef}$ and $MLJD1_{Ef}$

5) Localization of DivIVA$_{Ef}$ in homologous and heterologous backgrounds

a. GFP localization in *E. coli* and *B. subtilis*

b. Immungold localization in *E. faecalis*

Materials and Methods

2.1 Strains and Growth Conditions

Bacterial and yeast strains used in this study can be found in Table 1. *E. coli* strains XL1-Blue and DH5α were used for cloning purposes, *E. coli* C41(DE) was used for protein expression and purification due to its increased ability to express proteins at higher levels than other *E. coli* strains and *E. coli* PB103 for GFP localization experiments due to its uniform size and shape. *E. coli* cells were grown at 37°C in Luria-Bertani (LB) media (Difco, Detroit, MI) supplemented with 50 μg/mL kanamycin or 100 μg/mL ampicillin or on LB agar plates containing either 50 μg/mL kanamycin or 100 μg/mL ampicillin when required. *Saccharomyces cerevisiae* strain SFY526 (Clontech, Palo Alto, CA) was used for yeast two-hybrid assays. *S. cerevisiae* SFY526 was grown at 30°C on either yeast extract-peptone-adenine-dextrose (YPAD) or synthetic dropout (SD) medium as described in the Clontech Yeast Two-Hybrid manual. *Enterococcus faecalis* strains JH2-2 and JHSR1 were used for immunogold localization and Western blot analysis and were grown on Brain Heart Infusion (BHI) media (Difco) supplemented with either 125 μg/mL erythromycin or 125 μg/mL erythromycin and 1000 μg/mL kanamycin respectively. *Bacillus subtilis* strain 1756 (Edwards and Errington, 1997) was used for GFP localization experiments and was grown on LB agar plates supplemented either with 5 μg/mL erythromycin before transformation or 5 μg/mL erythromycin and 5 μg/mL chloramphenicol after transformation. Transformed *B.* subtilis 1756 colonies were also grown on Starch-Agar plates (Difco) to verify double crossover disruption of *amyE*. Following overnight culture, the amylase activity of the *B.*

Table 1 – Strains used in this study

Strain	Relevant Genotype	Source/Reference
E. coli XL1-Blue	*hsdR17 supE44 recA1 endA1 gyrA46 thi relA1 lac*/F` [*proAB*$^+$ *lacI*^{q} *lacZ*DM15::Tn*10*(Tet^r)]	Stratagene
E.coli DH5α	*sup*E44Δ*lac*U169 (80*lacZΔM15) hsd*R17 *rec*A1 *end*A1 *gyr*96 *thi*-1 *rel*A1	Gibco-BRL
E. coli C-41	B F *dcm ompT hsdS* (r_B m_B) gal λ(DE3) and containing at least one additional uncharacterized mutation	Miroux and Walker, 1996 [1]
E. coli PB103	*dad*R1 *trp*E61 *trp*A62 *tna*-5 *purB*$^+$	Ramirez-Arcos *et al.*, 2001a[2]
S. cerevisiae SFY526	*MATa ura3-52 his3-200 ade2-101 lys2-801 trp1-901 leu2-3 112 can^r gal4-542 gal80-538 URA3::GAL1$_{UAS}$-GAL1$_{TATA}$ -lacZ*	Clontech
E. faecalis JH2-2	Rif^R, Fus^R	ATCC strain 29212
E. faecalis JHSR1	JH2-2 *divIVA::kan*	Ramirez-Arcos *et al.*, 2004b
B. subtilis 1756	*divIVA*::pSG1043 (P_{divIVA} – *lacZ ermC* P_{spac} *divIVA*	Edwards and Errington, 1997[3]

[1] Gift from J.E. Walker
[2] Gift from P. de Boer
[3] Gift from J. Errington

subtilis colonies was tested visually by addition of iodine. Colonies with positive amylase activity presented a clear zone around the colony, indicating the starch in the media was being degraded by amylase and consequently the colony did not contain a disruption of *amyE*.

2.2 Bioinformatic analysis of DivIVA$_{Ef}$

All DivIVA sequence information was collected from The Institute for Genomic Research (TIGR) database (http://www.tigr.org). Sequences were aligned using the Multalin interface (http://prodes.toulouse.inra.fr) with identity defined as greater than 90% sequence homology and similarity defined as 50-90% sequence homology. Coiled-coil domain predictions were performed using the Coils, Paircoil, and MultiCoil software on the Expasy website (http://www.expasy.org) using the default settings for the Coils and MultiCoil program and a probability cut off of 0.2 for the Pair coils program. Restriction analysis of *divIVA$_{Ef}$* was performed using Webcutter (http://rna.lundberg.gu.se/cutter2/). Isoelectric point and charge calculations were performed using IEP (http://bioweb.pasteur.fr/seqanal/interfaces/iep.html).

2.3 Polymerase Chain Reaction (PCR) and Site Directed Mutagenesis (SDM)

All primers used in this study are listed in Table 2 and were designed manually based on the *divIVA$_{Ef}$* (EF1002) sequence available in the TIGR database. All PCR reactions were performed in a Perkin-Elmer Gene Amp 9600 thermocycler (Perkin Elmer, Wellesly, MA) using the following program: 5 minutes at 94°C; 30 amplification cycles consisting of denaturation at 94°C for 15 seconds, annealing for 15 seconds at temperatures indicated for each reaction, and extension at 72°C for either one minute (PCR) or six minutes (SDM). Following the amplification cycles, the reactions were

incubated for 5 minutes at 72°C, then maintained at 4°C until removed from the thermocycler.

2.3.1 General method for PCR amplification

PCR reactions to amplify wild type and mutant *divIVA$_{Ef}$* used the following recipe: 75.5 µl ddH_2O, 10 µl of 10X Thermopol Buffer (MBI Fermentas, Burlington, Ontario), 10 µl template DNA consisting of either 10 µg/mL plasmid or 0.5 McFarland Standard (Remel, Lenexa, KA) bacterial cultures suspended in ddH_2O, 2 µl of 10 mM dNTP (MBI Fermentas), 1 µl of each primer dilute to a concentration of 0.2 µg/µL and 0.5 µl *Taq* DNA polymerase (MBI Fermentas). SDM reactions used the same recipe as listed above with the following changes: 75.9 µl ddH_2O and 0.1 µl *Vent* DNA polymerase instead of *Taq* DNA polymerase (MBI Fermentas). Primers were as indicated for each plasmid.

2.3.2 Construction of mutant DivIVA$_{Ef}$ by site directed mutagenesis (SDM)

All primer synthesis and DNA sequencing were performed by the University of Ottawa Core DNA Sequencing and Synthesis Facility (UOCDSSF). Restriction sites are underlined for each primer where appropriate (Table 2). Wild-type *divIVA$_{Ef}$* was amplified from *E. faecalis* strain JH2-2 (Table 1) using primers IVApET-1 and IVApET-2 (Table 2) to incorporate *Nde*I and *Xho*I restriction sites at the 5` and 3` ends respectively. Annealing temperature for this reaction was 47°C. Following digestion with *Nde*I and *Xho*I, *divIVA$_{Ef}$* was cloned into pET30a (Table 3) previously digested with the same enzymes to generate pSRDiv (Table 3). This plasmid adds a 6xHis tag to the C-terminus of DivIVA$_{Ef}$ which will be used to facilitate protein purification.

Table 2 – Oligonucleotide primers used in this study

Primer	Sequence (5`→ 3`)[1]	Restriction Endonuclease Site	Product
IVApET1	5` GCGCCATATGGCATTAACTCCATTAGA 3`	*Nde*I	*divIVA*$_{Ef}$ 5` end
IVApET2	5` GCGCCTCGAGTTTTGATTCTTCTTCAA 3`	*Xho*I	*divIVA*$_{Ef}$ 3` end, no stop codon
IVApET3	5` GCGCCTCGAGTTCCTTAACTGCTGTATG 3`	*Xho*I	*divIVA*$_{Ef}$ 1-190, no stop codon
L29D-F	5` GACTTT**GA**TGATCAAAGTCACACG 3`	*Bcl*I	*divIVA*$_{Ef}$ L29D
L29D-R	5`ATCTACATCGTCTTGGTTATAGC 3`	None	
E37P-F	5` CGTGATTA**TCCGG**ATGCATTAC 3`	*Bsp*EI	*divIVA*$_{Ef}$ E37P
E37P-R	5` TGTGACTTGATCTAAAAAGTC 3`	None	
N43P/ L46D-F	5` CAAAAA**CCA**CGT GAA**GAC**GAGAAATC 3`	*Bsa*AI and *Bbs*I	*divIVA*$_{Ef}$ N43P and L46D
N43P/ L46D-R	5` TAATGCATCCGATAATCACGTGTG 3`	None	
L50D/ L57F-F	5` GCAGAAGAAAAA**TTT**CAATACTTC 3`	*Xmn*I	*divIVA*$_{Ef}$ L57F
L50D/ L57F-R	5` GTGTTT**GTC**TGATTTCTC**GTC**TTC 3`	None	*divIVA*$_{Ef}$ L46D and L50D
L104P-F	5` CCAAAGAAACC**CCC**GTAGAAGCTG 3`	Removes *Xcm*I	*divIVA*$_{Ef}$ L104P
L104P-R	5` CTTGGTTATCTGCCGAAGTGATAATC 3`	None	
I115P-F	5` CAAATGCAATG**CCC**GCAGATGCTG 3`	*Aci*I	*divIVA*$_{Ef}$ I115P
I115P-R	5` ATTTACGTTCAGCTTCTAC**GGG**GGTTTC 3`	Removes *Xcm*I	*divIVA*$_{Ef}$ L104P
I125P-F	5` GAAATCAACACAA**CCG**TTAGCAGAAGCA 3`	Removes *Dde*I	*divIVA*$_{Ef}$ I125P
I125P-R	5` CGTTCAGCATCTGCAATCATTGC 3`	None	
L143P-F	5` GAAACAGAAGAC**CCT**AAGAAGAAAAC 3`	*Dde*I	*divIVA*$_{Ef}$ L143P
L143P-R	5` CCCAGCTAATTGACGGGCACGTTC 3`	None	
IVA-1	5` GCGCGAATTCATGGCATTAACTCCATTAGA 3`	*Eco*RI	*divIVA*$_{Ef}$ 5` end
IVA-2	5` GCGCGGATCCCTATTTTGATTCTTCTTCAA 3`	*Bam*HI	*divIVA*$_{Ef}$ 3` end
IVA-5	5` GCGCGGATTCATGGCATTAACTCCATTAGA 3`	*Bam*HI	*divIVA*$_{Ef}$ 5` end
IVA-6	5` GCGCGGATCCTTCCTTAATGCTGTATG 3`	*Bam*HI	*divIVA*$_{Ef}$ 1-190

[1] Restriction endonulease sites are underlined, Mutagenized codons are indicated in bold

IVA-7	5` GCGCCTGCAGGAAGTATTGTAATTTTTCTTC 3`	*Pst*I	*divIVA*$_{Ef}$ 1-60
IVA-8	5` GCGCCTGCAGGAAATTCTTGATGAACAAG 3`	*Pst*I	*divIVA*$_{Ef}$ 190-233
IVA-9	5` GCGCCTGCATAATTGCTTCTGCTAAGATTTG 3`	*Pst*I	*divIVA*$_{Ef}$ 1-130
IVA-10	5` GCGCCTGCAGATTGAACGTGCCCGTCAATAAG 3`	*Pst*I	*divIVA*$_{Ef}$ 130-233
Iva-GFP1	5` GCGCCCATGGTTTTTGATTCTTCTTCAA 3`	*Nco*I	*divIVA*$_{Ef}$ 3` end, no stop codon
IVA-Xyl	5` GCGCGAATTCAGAGGTGAAGGAATATGGCATTAAC 3`	*Eco*RI	*divIVA*$_{Ef}$ 5` end with RBS[2]
GFP-3-BAM	5` GCGCGGATCCTTATTGTACAGCTCGTCC 3`	*Bam*HI	*egfp* 3` end

[2] Ribosomal binding site

Table 3 - Plasmids used in this study

Plasmid	Relevant Genotype	Source
pET30a	Kan^R P_{T7}::6xHis	Novagen
pSRDiv	Kan^R P_{T7}::*divIVA*$_{Ef}$-6xHis	Ramirez-Arcos *et al.*, 2004b
pMR1	Kan^R P_{T7}::*divIVA*$_{Ef}$(L29D) - 6xHis	This study
pMR2	Kan^R P_{T7}::*divIVA*$_{Ef}$ (E37P) - 6xHis	This study
pMR3	Kan^R P_{T7}::*divIVA*$_{Ef}$ (E37P, N43P, L46D) - 6xHis	This study
pMR4	Kan^R P_{T7}::*divIVA*$_{Ef}$(E37P, N43P, L46D, L50D, L57F) - 6xHis	This study
pMR5	Kan^R P_{T7}::*divIVA*$_{Ef}$(E37P, N43P, L46D, L50E, L57F) - 6xHis	This study
pMR6	Kan^R P_{T7}::*divIVA*$_{Ef}$(1-190) - 6xHis	This study
pMR7	Kan^R P_{T7}::*divIVA*$_{Ef}$(Δ130-190) - 6xHis	This study
pMR8	Kan^R P_{T7}::*divIVA*$_{Ef}$(Δ60-190) - 6xHis	This study
pMR9	Kan^R P_{T7}::*divIVA*$_{Ef}$(Δ60-130) - 6xHis	This study
pMR10	Kan^R P_{T7}::*divIVA*$_{Ef}$(L143P) - 6xHis	This study
pMR11	Kan^R P_{T7}::*divIVA*$_{Ef}$ (L104P) - 6xHis	This study
pMR12	Kan^R P_{T7}::*divIVA*$_{Ef}$(L104, L143P) - 6xHis	This study
pMR13	Kan^R P_{T7}::*divIVA*$_{Ef}$(L104P, I115P) - 6xHis	This study
pMR14	Kan^R P_{T7}::*divIVA*$_{Ef}$(L104P, I115P, L143P) -6xHis	This study
pMR15	Kan^R P_{T7}::*divIVA*$_{Ef}$(L104P, I115P, I125P) -6xHis	This study
pMR16	Kan^R P_{T7}::*divIVA*$_{Ef}$(L104P, I115P, I125P, L143P) -6xHis	This study
pGAD424	Amp^R P_{ADH1}[1]::*gal4*(AD)[2]	Clontech
pGBT9	Amp^R P_{ADH1}::*gal4*(BD)[3]	Clontech

[1] P_{ADH1}: Yeast promoter which regulates expression of *gal*4
[2] Encodes the activation domain (AD) of GAL4
[3] Encodes the DNA-binding domain (BD) of GAL4

pSRAD-Div	Amp^R P_{ADH1}::*gal4*(AD)-*divIVA*$_{Ef}$	Ramirez-Arcos *et al.*, 2004b
pSRBD-Div	Amp^R P_{ADH1}::*gal4*(BD)-*divIVA*$_{Ef}$	Ramirez-Arcos *et al.*, 2004b
pMR1-AD	Amp^R P_{ADH1}::*gal4*(AD)-*divIVA*$_{Ef}$ (L29D)	This study
pMR1-BD	Amp^R P_{ADH1}::*gal4*(BD)-*divIVA*$_{Ef}$ (L29D)	This study
pMR2-AD	Amp^R P_{ADH1}::*gal4*(AD)-*divIVA*$_{Ef}$ (E37P)	This study
pMR2-BD	Amp^R P_{ADH1}::*gal4*(BD)-*divIVA*$_{Ef}$ (E37P)	This study
pMR3-AD	Amp^R P_{ADH1}::*gal4*(AD)-*divIVA*$_{Ef}$ (E37P, N43P, L46D)	This study
pMR3-BD	Amp^R P_{ADH1}::*gal4*(BD)-*divIVA*$_{Ef}$ (E37P, N43P, L46D)	This study
pMR4-AD	Amp^R P_{ADH1}::*gal4*(AD)-*divIVA*$_{Ef}$ (E37P, N43P, L46D, L50D, L57F)	This study
pMR4-BD	Amp^R P_{ADH1}::*gal4*(BD)-*divIVA*$_{Ef}$ (E37P, N43P, L46D, L50D, L57F)	This study
pMR5-AD	Amp^R P_{ADH1}::*gal4*(AD)-*divIVA*$_{Ef}$ (E37P, N43P, L46D, L50E, L57F)	This study
pMR5-BD	Amp^R P_{ADH1}::*gal4*(BD)-*divIVA*$_{Ef}$ (E37P, N43P, L46D, L50E, L57F)	This study
pMR6-AD	Amp^R P_{ADH1}::*gal4*(AD)-*divIVA*$_{Ef}$ (1-190)	This study
pMR6-BD	Amp^R P_{ADH1}::*gal4*(BD)-*divIVA*$_{Ef}$ (1-190)	This study
pMR7-AD	Amp^R P_{ADH1}::*gal4*(AD)-*divIVA*$_{Ef}$ (Δ130-190)	This study
pMR7-BD	Amp^R P_{ADH1}::*gal4*(BD)-*divIVA*$_{Ef}$ (Δ130-190)	This study
pMR8-AD	Amp^R P_{ADH1}::*gal4*(AD)-*divIVA*$_{Ef}$ (Δ60-190)	This study
pMR8-BD	Amp^R P_{ADH1}::*gal4*(BD)-*divIVA*$_{Ef}$ (Δ60-190)	This study
pMR9-AD	Amp^R P_{ADH1}::*gal4*(AD)-*divIVA*$_{Ef}$ (Δ60-130)	This study
pMR9-BD	Amp^R P_{ADH1}::*gal4*(BD)-*divIVA*$_{Ef}$ (Δ60-130)	This study

pMR10-AD	Amp^R P_{ADH1}::*gal4*(AD)-*divIVA*$_{Ef}$ (L143P)	This study
pMR10-BD	Amp^R P_{ADH1}::*gal4*(BD)-*divIVA*$_{Ef}$ (L143P)	This study
pMR12-AD	Amp^R P_{ADH1}::*gal4*(AD)-*divIVA*$_{Ef}$ (L104P, L143P)	This study
pMR12-BD	Amp^R P_{ADH1}::*gal4*(BD)-*divIVA*$_{Ef}$ (L104P, L143P)	This study
pMR15-AD	Amp^R P_{ADH1}::*gal4*(AD)-*divIVA*$_{Ef}$ (L104P, I115P, I125P)	This study
pMR15-BD	Amp^R P_{ADH1}::*gal4*(BD)-*divIVA*$_{Ef}$ (L104P, I115P, I125P)	This study
pMR16-AD	Amp^R P_{ADH1}::*gal4*(AD)-*divIVA*$_{Ef}$ (L104P, I115P, I25P, L143P)	This study
pMR16-BD	Amp^R P_{ADH1}::*gal4*(BD)-*divIVA*$_{Ef}$ (L104P, I115P, I25P, L143P)	This study
pGAD-MLJD1c	Amp^R P_{ADH1}::*gal4*(AD)-*mljd1c*	Liao *et al.*, unpublished
pGBT-MLJD1c	Amp^R P_{ADH1}::*gal4*(BD)-*mljd1c*	Liao *et al.*, unpublished
pDSW209	Amp^R P_{trc}[4]::*gfp*	Weiss et al., 1999[5]
pMRGFP-Div	Amp^R P_{trc}::*gfp-divIVA*$_{Ef}$	This Study
pEGFP	Amp^R P_{lac} ::*egfp*	Clontech
pMRDiv-GFP	Amp^R P_{lac} ::*divIVA*$_{Ef}$-*egfp*	This Study
pJPR1	Amp^R, Cm^R, *5`amyE 3`amyE*, xylose inducible P_{xyl} promoter	Jones *et al.*, 2001[6]
pJPR-Div-GFP	Amp^R, Cm^R, *5`amyE 3`amyE*, P_{xyl} *divIVA*$_{Ef}$-*egfp*	This Study

[4] P_{trc} was mutated at the -10 and -35 regions.
[5] Gift from W. Margolin
[6] Gift from J. Errington

Site directed mutants were designed to both disrupt the predicted coiled-coil domains and modify the restriction profile of *divIVA*$_{Ef}$. Unless otherwise indicated, mutations and deletions of *divIVA*$_{Ef}$ were constructed by SDM using pSRDiv as a template to facilitate subsequent protein purification. Recircularization of SDM products was performed by phosphorylating the SDM product followed by self-ligation as follows: following PCR, the SDM DNA was purified using the Qiagen PCR clean kit (Qiagen Inc., Mississagua, Ontario). The phosphorylation reaction was carried out using the following recipe: 15 µl DNA purified from the SDM reactions, 2 µl of 10X PNK buffer A (MBI Fermentas), 1 µl of 100 mM dATP and 2 µl T4 polynucleotide kinase (MBI Fermentas). Reactions were incubated for one hour at 37°C, then the phosphorylated DNA was purified using a Qiagen PCR clean kit, then self-ligated using the following recipe: 17 µl phosphorylated DNA, 2 µl 10X ligase buffer (MBI Fermentas) and 1 µl T4 DNA ligase (MBI Fermentas). Ligations were incubated for 30 minutes at 37°C and transformed into *E. coli* XL1-Blue using the heat shock method without further manipulation (Sambrook *et al.*, 1980).

2.3.2.1 N-terminal point mutations

To introduce a leucine to aspartic acid mutation at residue 29 (L29D) into pSRDiv to produce pMR1 (Table 3), primers L29D-F and L29D-R (Table 2) and an annealing temperature of 52°C were used. This mutation introduces a *Bcl*I restriction site to *divIVA*$_{Ef}$. Following recircularization and transformation, colonies were screened following the diagram shown in Figure 4. The screening protocol was used for all plasmids constructed in this study. Briefly, to screen for the correct plasmid size colonies were picked using a sterile toothpick and resuspended in 25 µL ddH_2O. Following

Figure 4 - Flow chart detailing the general method for the introduction of point mutations into *divIVA*$_{Efbv}$ SDM.

Specifically, the L29D mutation is shown in detail. A) Starting from the parental plasmid, primers are designed to anneal in opposite directions with one (or both) encoding the mutation of interest (denoted by the asterisk) and the entire plasmid is amplified by SDM. B) Following SDM amplification, the linearized DNA is phosphorylated and self-ligated to create a circular plasmid and transformed into *E. coli* XL1-Blue. C) Colonies that were able to grow on the selected media are screened using the "Cracking" method to ensure that the correct sized plasmid was formed during recircularization and transformation. D) The *divIVA*$_{Ef}$ gene from plasmids of the correct size (6.0 kb) is PCR amplified and screened for the presence/absence of the restriction site introduced by the mutation. Only those plasmids that carried *divIVA*$_{Ef}$ genes that showed the expected digest pattern were sequenced to ensure no other mutations or frameshifts were present.

Figure 4

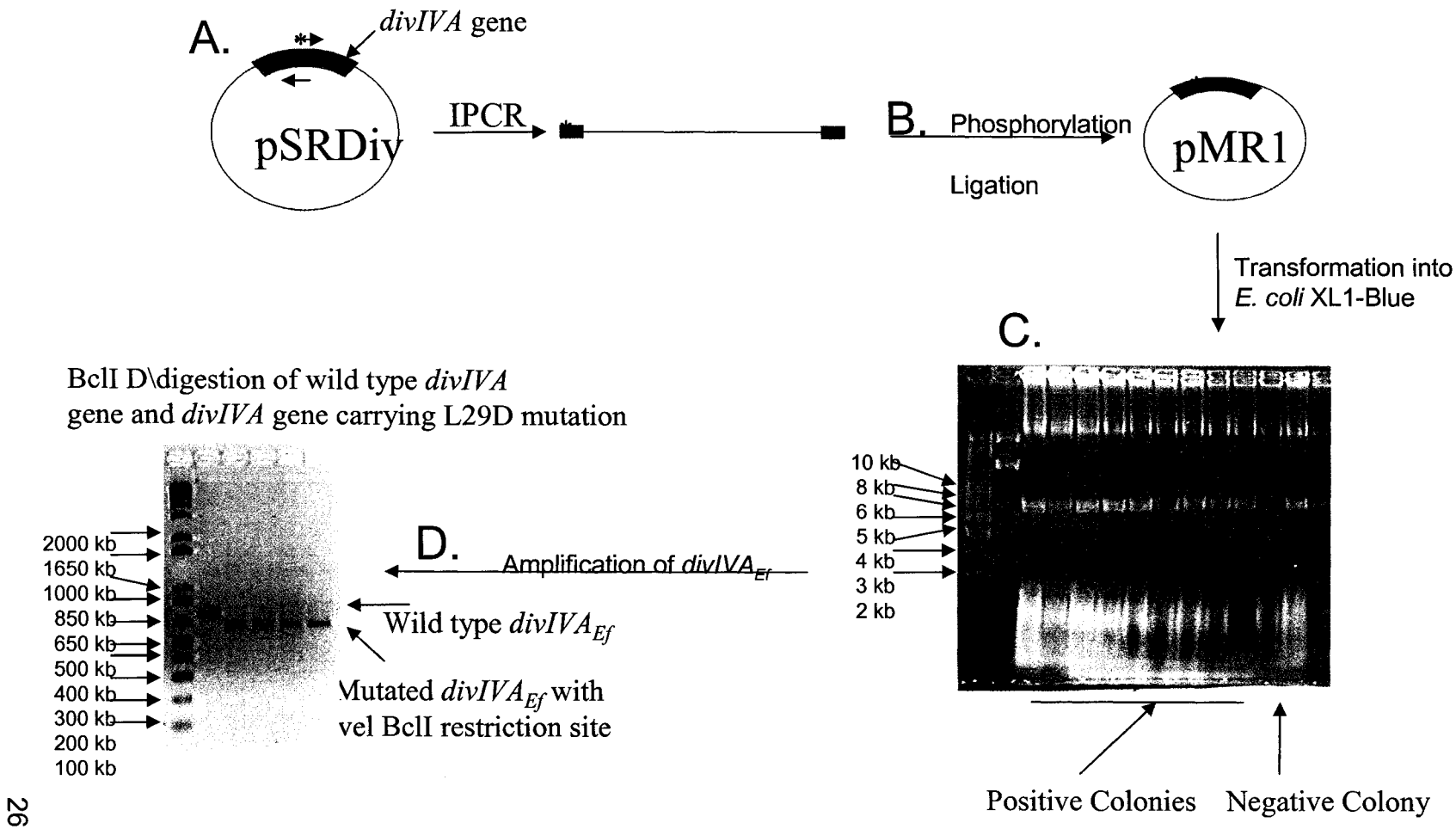
A.
divIVA gene
pSRDiv
IPCR
B.
Phosphorylation
Ligation
pMR1
Transformation into
E. coli XL1-Blue
C.
10 kb
8 kb
6 kb
5 kb
4 kb
3 kb
2 kb
Positive Colonies
Negative Colony
BclI D\digestion of wild type divIVA
gene and divIVA gene carrying L29D mutation
2000 kb
1650 kb
1000 kb
850 kb
650 kb
500 kb
400 kb
300 kb
200 kb
100 kb
D.
Amplification of divIVA$_{Ef}$
Wild type divIVA$_{Ef}$
Mutated divIVA$_{Ef}$ with
vel BclI restriction site

resuspension, the toothpick was used to streak a fresh LB agar plate containing appropriate selective markers to maintain the colony. 25 µL cracking solution, prepared just prior to use and made up of 9 parts cracking buffer (11 mM EDTA, pH 8.0, 11% glycerol, 38.5 mM SDS, 0.83 mM bromophenol blue) and 1 part 1M NaOH, was added to the cell suspension and incubated at room temperature for five minutes to lyse the cells. The suspension was then loaded into a 1% agarose gel and electrophoresed using TAE buffer (40 mM Tris base, 0.1% acetic acid, 1 mM EDTA) for one hour at 100 V. Following electrophoresis, the gel was stained using ethidium bromide (EtBr) for 20 minutes, destained in ddH_2O, and imaged using UV light in an Alpha Innotech Corporation MultiImage light cabinet (Alpha Innotech Corporation, San Leandro, CA). Once colonies carrying the correct size plasmid were identified, *divIVA*$_{Ef}$ was amplified by PCR using primers IVA-1 and IVA-2 (Table 2). Annealing temperature and extension time were 47°C and 60 seconds respectively and 10 µL of a colony suspension of approximately 0.5 MacFarland turbidity units used as template (Remel). Following PCR amplification, the PCR products were digested for 18 hours at 37°C with *Bcl*I using the following recipe: 13 µL ddH_2O, 4 µL PCR DNA, 2 µL NE Buffer 3 (New England Biolabs, Beverly, MA) and 1 µL *Bcl*I (New England Biolabs). 5 µL DNA loading buffer (40% sucrose, 0.25% bromophenol blue) was added to the reaction following incubation and the entire volume loaded onto a 1% agarose gel and electrophoresed and stained as described above. Colonies carrying the mutated *divIVA*$_{Ef}$ as determined by restriction digest analysis were sequenced to ensure only the desired L29D mutation was present.

Introduction of a glutamic acid to proline mutation at residue 37 (E37P) into pSRDiv to create pMR2 (Table 3) was accomplished using primers E37P-F and E37P-R

(Table 2), and an annealing temperature of 52°C. Screening for the E37P mutation was as described for L29D using the introduced *Bsp*EI restriction site and NE Buffer 3.

Two additional mutations, aspargine to proline at residue 43 (N43P) and leucine to aspartic acid at residue 46 (L46D) were added to pMR2 to disrupt the first half of the N-terminal coiled-coil domain to create pMR3 (Table 3). To generate this construct, pMR2 was used as template with primers N43P/L46D-F and N43P/L46D-R (Table 2) and an annealing temperature of 43°C. The presence of the mutations was verified as described previously using *Bsa*AI (N43P) and *Bbs*I (L46D) with NE Buffers 3 and 2 respectively.

To disrupt the entire predicted N-terminal coiled-coil domain two additional mutations, leucine to aspartic acid at residue 50 (L50D) and leucine to phenylalanine at residue 57 (L57F), were added to pMR3 to generate pMR4 (Table 3). This construct was generated using pMR3 as a template with primers L50D/L57F-F and L50D/L57F-R (Table 2) with an annealing temperature of 45°C. Screening was carried out as described above using the introduced *Xmn*I (L57F) and NE Buffer 2. During DNA sequencing, an unexpected leucine to glutamic acid mutation at residue 50 (L50E) was found in one of the clones during sequencing. Since this construct also completely disrupted the N-terminal coiled-coil domain, it was kept and designated pMR5 (Table 3) and contains mutations E37P, N43P, L46D, L50E, and L57F.

2.3.2.2 Creation of a C-terminal deletion

Creation of a C-terminal truncation of the last 43 residues of $DivIVA_{Ef}$ ($DivIVA_{Ef\ 1\text{-}190}$) has the dual function of removing the C-terminal coiled-coil domain and shortening $DivIVA_{Ef}$ to approximately the same length as $DivIVA_{Bs}$. The truncation was

constructed using pSRDiv as a template and primers IVApET-1 and IVApET-3 (Table 2) and an annealing temperature of 47°C to incorporate *Nde*I and *Xho*I restriction sites at the 5` and 3` ends respectively. Following digestion with *Nde*I and *Xho*I, the truncated *divIVA*$_{Ef}$ was cloned into pET30a previously digested with the same enzymes to generate pMR6 (Table 3).

2.3.2.3 Deletions and point mutations of the central coiled-coil domains

For all deletions of the central coiled-coil domains, pSRDiv was used as template. To remove the first of the central coiled-coil domains consisting of residues 60-130 (DivIVA$_{Ef\,\Delta 60\text{-}130}$), SDM using primers IVA-7 and IVA-10 (Table 2) and an annealing temperature of 55°C were used to generate pMR9 (Table 3). To remove the second of the central domains consisting of residues 130-190 (DivIVA$_{Ef\,\Delta 130\text{-}190}$), SDM using primers IVA-8 and IVA-9 (Table 2) were used with an annealing temperature of 50°C to generate pMR7 (Table 3). Removal of both central coiled-coil domains consisting of residues 60-190 (DivIVA$_{Ef\,\Delta 60\text{-}190}$) was performed using primers IVA-7 and IVA-8 and an annealing temperature of 50°C to generate pMR8 (Table 3). SDM products involving central coiled-coil domain deletions were digested with *Pst*I before recircularization. Screening for the *divIVA*$_{Ef}$ deletions was performed as described previously with the following change. Following confirmation of the correct sized plasmid and insert amplification using primers IVA-1 and IVA-2 as described above, the insert size was determined by electrophoresis using a 1% agarose gel. Colonies carrying the correct sized insert were sent for DNA sequencing.

To create point mutations in the central coiled-coil domains, SDM was used to introduce leucine to proline mutations at residues 104 (L104P) and 143 (L143P) to

pSRDiv to generate pMR11 and pMR10 respectively (Table 3). These mutations disrupt the first and second of the central coiled-coil domains respectively. For L104P, primers L104P-F and L104P-R (Table 2) were used with an annealing temperature of 47°C. Introduction of the L104P mutation abrogates a native *Xcm*I site in *divIVA*$_{Ef}$ allowing for screening as described above using NE Buffer 2. For L143P, primers L143P-F and L143P-R (Table 2) were used with an annealing temperature of 50°C. The L143P mutation was screened as described previously using the *Dde*I restriction site introduced to *divIVA*$_{Ef}$ and NE buffer 3.

A combination of the L104P and L143P mutations was created to simultaneously disrupt both central coiled-coil domains by SDM using pMR10 as a template with L104P-F and L104P-R primers. Screening was conducted as described for pMR11 and the resulting plasmid was designated pMR12 (Table 3).

To further abrogate the central coiled-coil domains, isoleucine to proline mutations at residue 125 (I125P) were added to pMR11 and pMR12 by SDM to generate L104P/I125P (pMR13, Table 3) and L104P/I125P/L143P (pMR14, Table 3) respectively. In both cases, primers I125P-F and I125P-R (Table 2) and an annealing temperature of 50°C were used. Introduction of I125P removes a native *Dde*I restriction site and the removal of this site was used for screening purposes using NE Buffer 3.

One additional mutation, isoleucine to proline at residue 115 (I115P), was also added to pMR13 and pMR14 to ensure complete abrogation of the central coiled-coil domains. To incorporate the I115P mutation, SDM was performed using primers I115P-F and I115P-R (Table 2) and an annealing temperature of 43°C to generate pMR15 (L104P/I115P/I125P, Table 3) and pMR16 (L104P/I115P/I125P/L143P, Table 3)

respectively. The I115P mutation introduces an *AciI* restriction site, which was used for screening purposes as described above with NE Buffer 3.

2.4 Protein Induction and Purification

To overexpress the mutant and wild type DivIVA$_{Ef}$ proteins, *E. coli* C41 (DE3) was transformed with plasmids derived from pET30a (pSRDiv, pMR1-16). Colonies were subcultured in Luria Bertani (LB) medium supplemented with 50 μg/mL kanamycin (LB-Kan$_{50}$) and incubated for 18 hours at 37°C with shaking at 250 rpm. Following the 18 hour incubation, cultures were diluted 1:20 in fresh LB-Kan$_{50}$ and incubated for two hours at 37°C with shaking at 250 rpm prior to induction. Protein expression was induced by addition of ispropyl-β-D-thiogalatopyranoside (IPTG, MBI Fermentas) to a final concentration of 0.4 mM followed by incubation for three hours at 37°C at 250 rpm. Following induction, cultures were pelleted by centrifugation for 5 minutes at 5000 rpm in a Sorvall RC5C ultracentrifuge (Mandel Scientific, Guelph, Ontario), with a SW-55 rotor. Cells were then washed two times with phosphate buffered saline (PBS: 136 mM NaCl, 2.7 mM KCl, 10 mM Na_2HPO_4, 1.8 mM KH_2PO_4, pH 7.4), aliquoted, and frozen at -20°C until sonication and purification.

To separate the soluble and insoluble protein components, induced cells were resuspended in 5 mL of appropriate binding buffer (described below) and lysed by sonication using a sonic dismembrator 60 (Fisher Scientific, Ottawa, ON). Sonication was performed using 3 cycles of ten 1-second bursts at 15 W with a 1 minute time interval on ice between cycles. Following sonication, the cell extract was spun at 25,000 rpm for 25 minutes at 4°C in an L8-55M ultracentrifuge (Beckman Counter, Fullerton,

CA) using a SW55 swinging bucket rotor. The soluble supernatant was removed from the insoluble debris by decantation and stored at 4°C until used for purification.

In order to purify protein from the soluble fractions, two different immobilized metal affinity chromatography (IMAC) resins were employed. His-bind resin (Novagen, Darmstadt, Germany), which uses nickel as the immobilized metal, was used for the majority of the samples while TALON resin (Clontech), which uses cobalt as the immobilized metal, was used for samples that bound poorly to His-bind resin.

2.4.1 His-bind resin purifications

For purifications involving His-bind resin, the binding buffer comprised 5mM imidazole, 500 mM NaCl and 20 mM Tris-HCl, pH 7.9. Following sonication and fractionation, the soluble fraction was passed over resin pre-equilibrated with charge buffer (50 mM $NiSO_4$) followed by binding buffer. Once the soluble fraction was passed through the resin, the bound proteins were washed with binding buffer containing increasing concentrations of imidazole (up to 100 mM). Samples were eluted from the resin using elution buffer (250 mM imidazole, 500 mM NaCl, 20 m Tris-HCl, pH 7.9). Following sample elution, the resin was washed using strip buffer (100 mM EDTA, 500 mM NaCl, 20 mM Tris-HCl, pH 7.9) and stored at 4°C in strip buffer. This method of purification was used for wild type $DivIVA_{Ef}$, as well as MR1 through MR5, MR7, and MR11 through MR16.

2.4.2 TALON resin purifications

For purifications involving TALON resin (Clontech), the binding buffer consisted of 300 mM NaCl, and 50 mM NaH_2PO_4, pH 7.0. Following sonication and fractionation as described above, the soluble fraction was incubated for 30 minutes with gentle

agitation at room temperature with resin pre-equilibrated with binding buffer. The resin was then pelleted by centrifugation at 500 g for two minutes using a J-6B swinging bucket centrifuge (Beckman Coulter). The supernatant was removed and the resin resuspended in two bed volumes of binding buffer and gently agitated at room temperature for 10 minutes. Following incubation, the resin was pelleted as before and washed until 30 bed volumes of binding buffer were exchanged. After the final resuspension, the resin was transferred to a polypropylene column and allowed to settle. The resin was then washed with wash buffer (300 mM NaCl, 50 mM NaH_2PO_4, pH 7.0) containing increasing concentrations of imidazole (5-50 mM). Protein was eluted from the resin using elution buffer (300 mM NaCl, 50 mM NaH_2PO_4, 150 mM imidazole, pH 7.0). Any remaining protein was removed from the resin by washing using 20 mM MES, pH 5.0 and the resin was subsequently stored at 4°C in 20% ethanol containing 0.1% sodium azide. This purification method was used for MR6, MR9, and MR10

Regardless of the method of purification, protein samples were concentrated using a Centricon 10,000 MWCO concentrator (Millipore, Billerica, MA). Protein samples purified using His-resin were dialyzed using PBS while those purified using TALON resin were dialyzed using TALON binding buffer to remove the excess imidazole. Dialysis and concentration was performed prior to analysis by native gel electrophoresis or gel filtration.

The presence of the 6xHis tag incorporated by expression from pET30a for purification purposes likely has no effect on oligomerization. Experiments conducted on the *B. subtilis* DivIVA homolog have demonstrated that the oligomer state is identical for $DivIVA_{Bs}$ in both the presence and absence of the 6xHis tag (Muchova *et al.*, 2002a).

2.5 Protein Electrophoresis

Protein purity and relative concentration were analysed by sodium dodecyl sulphate polyacrylamide gel electrophoresis (SDS-PAGE) using the protocol described by Sambrook *et al.,* (1980). Briefly, two phase gels consisting of a 5% stacking and 12% resolving layers were used to separate the proteins. Sample preparation involved adding loading buffer (62.5 mM Tris-HCl, pH 6.8, 2% SDS, 25% glycerol, 0.01% bromophenol blue) to each sample in a 1:5 ratio followed by boiling the samples for 5 minutes to ensure complete denaturation. Electrophoresis was conducted using 5 mM Tris-HCl, 50 mM glycine and 0.1% SDS, pH 8.3 as the running buffer at 100V until the bromophenol blue dye exited the gel. Unless used for Western blotting, gels were stained with Coomassie brilliant blue (Sambrook *et al.,* 1980) and destained using a 45% methanol, 10% acetic acid solution. In order to determine relative protein concentration, densitometric analysis was performed following destaining using AlphaEase version 5.04 (Alpha Innotech). This relative concentration was used to ensure equal sample loading for Western blotting and native gel electrophoresis.

For urea SDS-PAGE analysis, 5M urea was added to each of the stacking and resolving gels, as well as the running buffer to ensure complete sample denaturation. 5 μL of 10M urea was added to each sample prior to boiling and gels were stained with Sypro Ruby protein stain (Bio-Rad) overnight and destained for 2-3 hours with water the following morning.

2.6 Circular Dichroism (CD) Analysis

CD analysis of purified DivIVA$_{Ef}$ and proteins containing N-terminal mutations was performed using a Jasco J-810 spectropolarimeter (Jasco Inc., Easton, MD). Protein

samples dialyzed in PBS were analyzed using a cuvette with a path length of 0.2 mm and the average of five scans was used to determine the experimental ellipticity at each wavelength. Mean Residue Ellipticity (MRE) was calculated using the equation MRE = (100q x MW)/(C x L x R) where q represents the experimental ellipticity (in millidegrees [mdeg]), MW represents the mass of the protein (in Daltons), C represents the concentration of the protein sample (in mg/mL), L represents the path length of the cuvette (in cm) and R represents the number of residues in the protein (adapted from http://www.huhaha.com/pages/knowledge_pages/cd_unit.html). To compare spectra, the MRE was plotted against wavelength.

2.7 Mass Spectrometry Analysis

Purified DivIVA$_{Ef}$ was subjected to SDS-PAGE electrophoresis and stained with Coomassie brilliant blue as described above. Bands were excised from the gel following destaining and sent to the Queen's University Protein Discovery group for MALDI-TOF Mass Spectrometry analysis.

2.8 Glycosylation assay

In order to determine whether DivIVA$_{Ef}$ undergoes post-translation glycosylation, purified DivIVA$_{Ef}$ along with Horseradish Peroxidase (HRP, positive control), and Soybean Trypsin Inhibitor (STI, negative control) were subjected to SDS-PAGE electrophoresis. Following electrophoresis, the gel was fixed by immersion in 50% methanol for 30 minutes. Following fixation, the gel was washed twice in 3% acetic acid, then incubated for 15 minutes in oxidizing solution from the Pierce GelCode Glycoprotein staining kit (Pierce, Rockford, IL). Following oxidation, the gel was washed with 3% acetic acid as described above. After washing, the gel was incubated in

GelCode Glycoprotein Staining reagent (Pierce) for 15 minutes followed by 5 minutes in reducing solution. The gel was washed 5 times with 3% acetic acid, then rinsed with distilled water and imaged using the Alpha Innotech Corporation MultiImage light cabinet.

2.9 Size exclusion chromatography analysis

Gel filtration analysis was carried out using an HR16/50 column packed manually with approximately 100 mL of either Superdex-200 resin or Superose-6 resin (Amersham Biosciences, Montreal, QC) which differ in their fractionation range as per manufacturer's instructions and equilibrated with either PBS or TALON extraction buffer depending on which sample was being analyzed. Flow rate was maintained at 0.7 mL/min. 500 µl of purified proteins was injected onto the column and fractions collected using a Pharmacia Frac-3000 fraction collector. Elution volumes from 1-30 mL were not collected, 30-60 mL were collected in 0.5 ml intervals for samples having a full oligomeric complex and 1.0 mL intervals for samples having disrupted complexes, and elutions from 60-90 ml were collected in 1.0 ml intervals for full oligomeric samples and 0.5 mL intervals for samples with disrupted complexes.

Following sample collection, the protein elution profile was constructed as follows: 20 µl of BioRad protein assay dye was pipetted into each well of a 96 well microtitre plate. 100 µl of each fraction was added to each well and absorbance recorded on a Spectra Shell microplate reader (Tecan, Maennedorf, Switzerland) at 595 nm. The elution profile for each sample was compared to the elution profile of standards purchased from Amersham Biosciences to determine the molecular mass of the protein complex. The standard curve was constructed by determining the column void volume

(V_o), the total bed volume (V_t) and the elution volume (V_e) for each standard. These values were then used to determine the partition coefficient (K_{av}) for each standard using the equation $K_{av} = (V_e-V_o)/(V_t-V_o)$. This value was plotted against the log of the molecular weight of the standard and a line of best fit was determined. Following calculation of the K_{av} for the various DivIVA$_{Ef}$ samples, the calculated protein complex mass was determined then divided by the bioinformatically determined monomer mass to determine the number of DivIVA$_{Ef}$ monomers present in the complex.

2.10 Native Gel Electrophoresis

Gradient Tris-HCl gels were purchased from BioRad. Loading buffer (40% glycerol, 0.01% bromophenol blue, 62.5 mM Tris-HCl, pH 6.8) was added to purified protein samples in a 1:5 ratio. Electrophoresis was conducted using 192 mM glycine, 25 mM Tris-HCl, pH 8.3 at 100 V until the bromophenol blue dye ran off the gel. Gels were stained with Coomassie brilliant blue as described above unless used for Western blot analysis.

2.11 Western Blot

Following protein electrophoresis, samples were transferred to Hybond-C Nitrocellulose (Amersham Biosciences) for one hour at 100V. For Western blots of native gels, membranes were stained with Ponceau Red (0.1% Ponceau Red, 5% acetic acid), the standards marked, and destained using ddH_2O. The remainder of the protocol was identical for Westerns of both native and denatured proteins. Membranes were blocked for one hour at room temperature with either 3% skim milk in TBS (50 mM Tris, 1.25 M NaCl) containing 0.05% Tween-20 (TTBS) for α-DivIVA$_{Ef}$ (Ramirez-Arcos *et al.*, 2004b) blots or 3% BSA in TTBS for α-His (Qiagen) blots. Following blocking,

membranes were washed three times with TTBS, then incubated overnight at 4°C with primary antiserum dilute 1:1000 in TTBS with gentle agitation.

The following morning, the membranes were washed three times with TTBS and incubated for one hour with either alkaline phosphatase (AP) conjugated goat α-rabbit IgG for α-DivIVA$_{Ef,}$ (Bio-Rad, Mississagua, Ontario) or AP conjugated goat α-mouse IgG for α-His (Bio-Rad) dilute 1:3000 in TTBS. Membranes were then washed three times with TTBS and developed using Attophos (Promega, Madison, WI). Samples were visualized using UV light in an Alpha Innotech Corporation MultiImage light cabinet.

2.12 Yeast two hybrid analysis

Following confirmation of the *divIVA$_{Ef}$* sequences, wild type and mutated *divIVA$_{Ef}$* genes, with the exception of *divIVA$_{Ef\text{-}MR6}$* (described below), were PCR amplified using primers IVA-1 and IVA-2 to incorporate *Eco*RI and *Bam*HI at the 5` and 3` ends respectively. Following purification and digestion, the *divIVA$_{Ef}$* genes were cloned into both pGAD424 and pGBT9 (Clontech, Table 3) previously digested with *Eco*RI and *Bam*HI. Screening of the resultant plasmids was performed by releasing the insert by restriction endonuclease digestion to verify the correct size prior to DNA sequencing. The resultant plasmids were named after their pET30a counterparts but with an AD suffix for clones in pGAD424 and a BD suffix for clones in pGBT9. For example, the constructs containing *divIVA* amplified from pMR1 and cloned into pGAD424 and pGBT9 were named pMR1-AD and pMR1-BD respectively (Table 3). For the C-terminal DivIVA$_{Ef}$ truncation, pSRDiv was used as template with primers IVA-1 and IVA-6 (Table 2) with the remainder of the protocol unchanged.

Following DNA sequence confirmation of the fusion, plasmids were transformed into *Saccharomyces cerevisiae* SFY526 as indicated by the Clontech Yeast Two Hybrid manual. Plasmids were tested both individually and in combination with their corresponding partner (e.g. pMR3-AD + pMR3-BD), as well as with the wild type $DivIVA_{Ef}$ when no interaction between the mutated proteins was detected. Following three days incubation at 30°C, activation of the β-Galactosidase reporter gene was tested using a colony lift assay. Briefly, sterile filter discs were pressed over the yeast colonies, the filters frozen in liquid nitrogen for 10 seconds, and allowed to thaw at room temperature. Once thawed, the filters were placed in petri dishes on a second filter pre-soaked with Z-buffer (60 mM Na_2HPO_4, 40 mM NaH_2PO_4, 10 mM KCl, 1 mM $MgSO_4$) supplemented with 0.27% β-mercaptoethanol and 0.3 μg/mL X-gal (5-bromo-4-chloro-3-indolyl-β-D-galactopyranoside, MBI Fermentas) and incubated at room temperature until either the colonies turned blue or 24 hours, whichever came first. Only colonies where both plasmids were required to activate the reporter gene were further quantified using the liquid culture assay method (Clontech).

2.13 Mapping of interaction between $DivIVA_{Ef}$ and MLJD1

In order to determine what region of $DivIVA_{Ef}$ is responsible for interaction with MLJD1, yeast two hybrid experiments were performed as described above. Interaction testing was carried out using $DivIVA_{Ef}$ that either a) had the N-terminal coiled-coil domain completely disrupted (MR5), b) was lacking the second coiled-coil domain (MR9), c) was lacking the third coiled-coil domain (MR7) or d) was lacking the C-terminal 43 amino acids (MR6). The various $DivIVA_{Ef}$ constructs were tested in combination with pGAD-MLJD1c and pGBT-MLJD1c (Table 3) as appropriate.

Interaction between the various DivIVA$_{Ef}$ constructs and MLJD1 was determined using the colony lift assay as described above.

2.14 Localization of DivIVA$_{Ef}$

2.14.1 GFP localization in heterologous backgrounds

2.14.1.1 Localization in Escherichia coli

In order to examine DivIVA$_{Ef}$ localization in a Gram negative background, GFP fusions to DivIVA$_{Ef}$ were constructed at both the N and C terminal domains. For the N-terminal fusion, wild type *divIVA$_{Ef}$* was PCR amplified using primers IVA-1 and IVA-2 as described previously. Following amplification and digestion with *Eco*RI and *Bam*HI, the *divIVA$_{Ef}$* gene was cloned into pDSW209 (Weiss *et al.*, 1999, Table 3) previously digested with the same enzymes. DNA sequencing was used to verify a proper fusion between GFP and DivIVA$_{Ef}$ and the resultant plasmid was named pMRGFP-Div (Table 3).

For the C-terminal fusion, wild type *divIVA$_{Ef}$* was PCR amplified using primers IVA-5 and IvaGFP-1 (Table 2) to incorporate *Bam*HI and *Nco*I at the 5` and 3` ends respectively. Following amplification and digestion, the *divIVA$_{Ef}$* gene was cloned into pEGFP (Clontech, Table 3) previously digested with the same enzymes. Fusion between DivIVA$_{Ef}$ and GFP was confirmed by DNA sequencing and the resulting plasmid was named pMRDiv-GFP (Table 3).

Following sequence confirmations, pMRGFP-Div and pMRDiv-GFP, along with their respective cloning vectors (pDSW209 and pEGFP) were transformed into *E. coli* PB103 using the heat shock method (Sambrook *et al.*, 1980). Following transformation, colonies were subcultured into LB broth containing 100 μg/mL ampicillin and IPTG

ranging from 0.5-2.0 mM. Once the cultures reached mid-exponential phase (OD_{600} . 0.6), a 2 µL aliquot was mixed with 2 µL of liquified 2% low melting point (LMP) agarose, placed on a microscope slide, and fluorescence observed using an Olympus BX61 microscope equipped with a Photometrics CoolSnap ES camera and Image Pro (Version 4.5.1) software.

2.14.1.2 Localization in Bacillus subtilis

To observe the localization of $DivIVA_{Ef}$ in a Gram positive background, *$divIVA_{Ef}$-gfp* was amplified from pMRDiv-GFP using primers IVA-Xyl and GFP-3-Bam (Table 2) to incorporate *Eco*RI and *Bam*HI at the 5` and 3` ends respectively. Following amplification and digestion, the *$divIVA_{Ef}$-gfp* fusion was cloned into pJPR1 (Jones *et al.*, 2001, Table 3) previously digested with the same enzymes. The sequences of both *$divIVA_{Ef}$* and *gfp* were confirmed by DNA sequencing. The resulting plasmid was named pJPR-Div-GFP (Table 3).

Following sequencing, pJPR-Div-GFP was transformed into *Bacillus subtilis* strain 1756 as follows: 10 mL MD Medium (61.4 mM K_2HPO_4, 44.1 mM KH_2PO_4, 2.87 mM sodium citrate, 2% glucose, 0.005% L-Tryptophan, 0.0011% ferric ammonium citrate, 0.25% L-aspartic acid, 3 mM $MgSO_4$) containing 0.1% casamino acids, 5 µg/mL erythromycin and 0.1 mM IPTG was inoculated with 5-10 colonies of *B. subtilis* 1756 and incubated at 37°C and 250 rpm shaking until OD_{600} reached ~1.2. Following incubation, an equal volume of MD medium containing 5 µg/mL erythromycin and 0.1 mM IPTG was added and the culture incubated for 1 hour at 37°C and 250 rpm. 800 µL of culture was then added to 1.5 mL eppendorf tubes containing either 1 µg/mL pJPR-Div-GFP or pJPR1 and incubated for 20 minutes, 37°C, 250 rpm. Following the 20

minute incubation, 25 μL of 20% casamino acids was added to each tube followed by incubation for 75 minutes at 37°C and 250 rpm agitation. Aliquots ranging from 150 μL to 300 μl were then plated onto LB agar plates containing 5 μg/mL erythromyocin, 5 μg/mL chloramphenicol, and 0.1 mM IPTG and incubated at 37°C overnight.

Since pJPR1 is designed to integrate into the amylase gene of *B. subtilis*, transformants were screened for disrupted *amyE*. To test for *amyE* disruption, colonies were subcultured onto starch agar plates and incubated overnight at 37°C. Plates were then flooded with Lugol's solution (5% iodine, 10% potassium iodide, 20% acetic acid) for 2-3 minutes and the remaining solution drained by decanting. Colonies that did not contain disruptions of *amyE* were not stained by the Lugol's solution and appeared as clear zones.

To induce expression of DivIVA$_{Ef}$-GFP in *B. subtilis*, colonies containing disrupted *amyE* genes were subcultured overnight at 37°C in S medium (0.2% $[NH_4]_2SO_4$, 0.6% KH_2PO_4, 1.4% K_2HPO_4, 0.1% sodium citrate, 0.02% $MgSO_4$, 1% casamino acids, 20 μg/mL L-tryptophan, 0.056% $MnSO_4$, filter sterilized to remove precipitated $MnSO_4$) containing 5 μg/mL erythromyocin and 5 μg/mL chloramphenicol. The following morning, 300 μL of the overnight cultures were subcultured into four different tubes containing 3 mL of fresh S-medium supplemented with either no supplement, 0.1 mM IPTG, 0.1mM IPTG and 0.5% D-xylose, or 0.5% D-xylose and cultures incubated at 30°C, 250 rpm until mid-exponential phase (OD_{600} ~ 0.7). 2 μL of the cultures was then added to 2 μL of liquified LMP agarose on a microscope slide and fluorescence observed as described above.

2.14.2 Immunogold localization of DivIVA$_{Ef}$ in Enterococcus faecalis

To localize DivIVA$_{Ef}$ in its native host, immunoelectron microscopy was performed in collaboration with Peter Rippstein at the University of Ottawa Heart Institute. Localization was performed using *E. faecalis* strain JH2-2 and rabbit polyclonal α-DivIVA$_{Ef}$. Final antiserum dilution was 1:250 and samples were visualized using a Jeol 1230 Electron Microscope equipped with a digital AMT camera.

Results

3.1 Bioinformatic Analysis of DivIVA$_{Ef}$

Using multiple sequence alignment software, the sequences of 28 known DivIVA homologs (as of August 24, 2004) were compared (Fig 5). The resulting alignment shows moderate conservation (28.3% similarity, 21.6% identity) in the first 70 residues with the region between residues 40-55 showing the highest conservation while the remainder of the protein is poorly conserved (15.5% similarity, 5.6% identity) between species. This corresponds to residues 30-45 of DivIVA$_{Ef}$ since the *E. faecalis* sequence begins at residue 10 of the overall alignment (Figure 5).

Due to differences in the computational algorithms used to generate coiled-coil domain predictions, each program generated a slightly different result for DivIVA$_{Ef}$. Figure 6 shows the predictions for DivIVA$_{Ef}$ using the Coils MTIDK matrix (A), the Coils MTK matrix (B), Paircoil (C) and MultiCoil (D) online programs. Since N-terminal and central coiled-coil domains were present regardless of the software used in the prediction, only the Coils MTIDK matrix will be presented in this study.

Despite the low sequence homology, the predicted coiled-coil domains for the various DivIVA proteins showed similar trends. Figure 7 shows the predicted coiled-coil domains of the DivIVA homologs from *E. faecalis* (A), *B. subtilis* (B), *Staphylococcus aureus* (C) and *Mycobacterium avium paratuberculosis* (D). Each prediction features a highly certain coiled-coil domain (p = 100%) located approximately between residues 25 and 60. After this initial domain, there was a gap or region of low probability followed by a second region with a high likelihood of coiled-coil domain formation that spanned the central region of the protein. While this region varied greatly in terms of localized

Figure 5 - Multiple sequence alignment of 29 known DivIVA homologs.

Consensus characters appearing in red have >90% sequence homology and those in blue have 50-90% homology. With regards to the symbols presented in the consensus (bottom lone), # represents either Asparagine (N), Aspartic acid (D), Glutamine (Q), or Glutamic acid (E). % represents either Leucine (L) or Methionine (M). ! represents either Isoleucine (I) or Valine (V). The strains from top to bottom are: *Enterococcus faecalis, Lactobacillus plantarum, Staphylococcus agalactiae, Streptoccus pyogenes, Streptococcus mutans, Staphylococcus mitis, Streptococcus pneumoniae, Bacillus anthracis, Bacillus cereus, Oceanobacillus iheyensis, Bacillus halodurans, Bacillus subtilis, Listeria innocua, Listeria monocytogenes, Clostridium acetobutylicum, Clostridium tetani, Clostridium perfringes, Thermoanaerobacter tengcongensis, Bdellovibrio bacteriovorus, Desulfovibrio vulgaris hildenborough, Geobacter sulfurreducens, Deinococcus radiodurans, Mycobacterium avium paratuberculosis, Tropheryma whipplei, Mycoplasma mycoides, Lactobacillus johnsonii, Lactococcus lactis, Staphylococcus aureus,* and *Staphylococcus epidermidis*

Figure 5

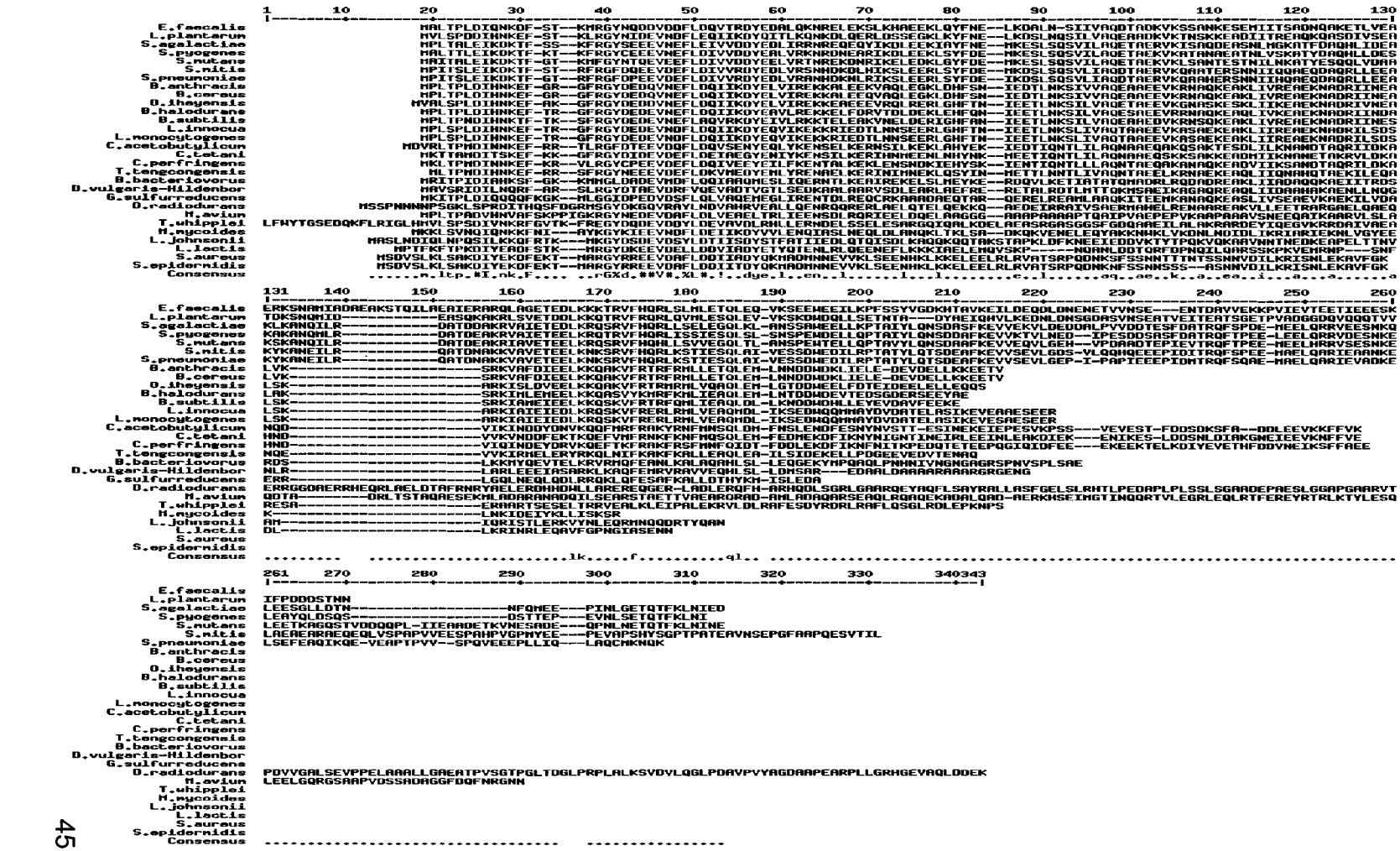

Figure 6 - Predicted coiled-coil domains for $DivIVA_{Ef}$

A) Coils with MTIDK matrix with no weight at positions A and D, B) Coils with MTK matrix with no weight at positions A and D, C) Paircoil using a probability cutoff of 0.2 (represented by the dashed line) and D) MultiCoil using default settings. For A, B, and C, the three different traces represent the size of the amino acid window used in the prediction.

Figure 6

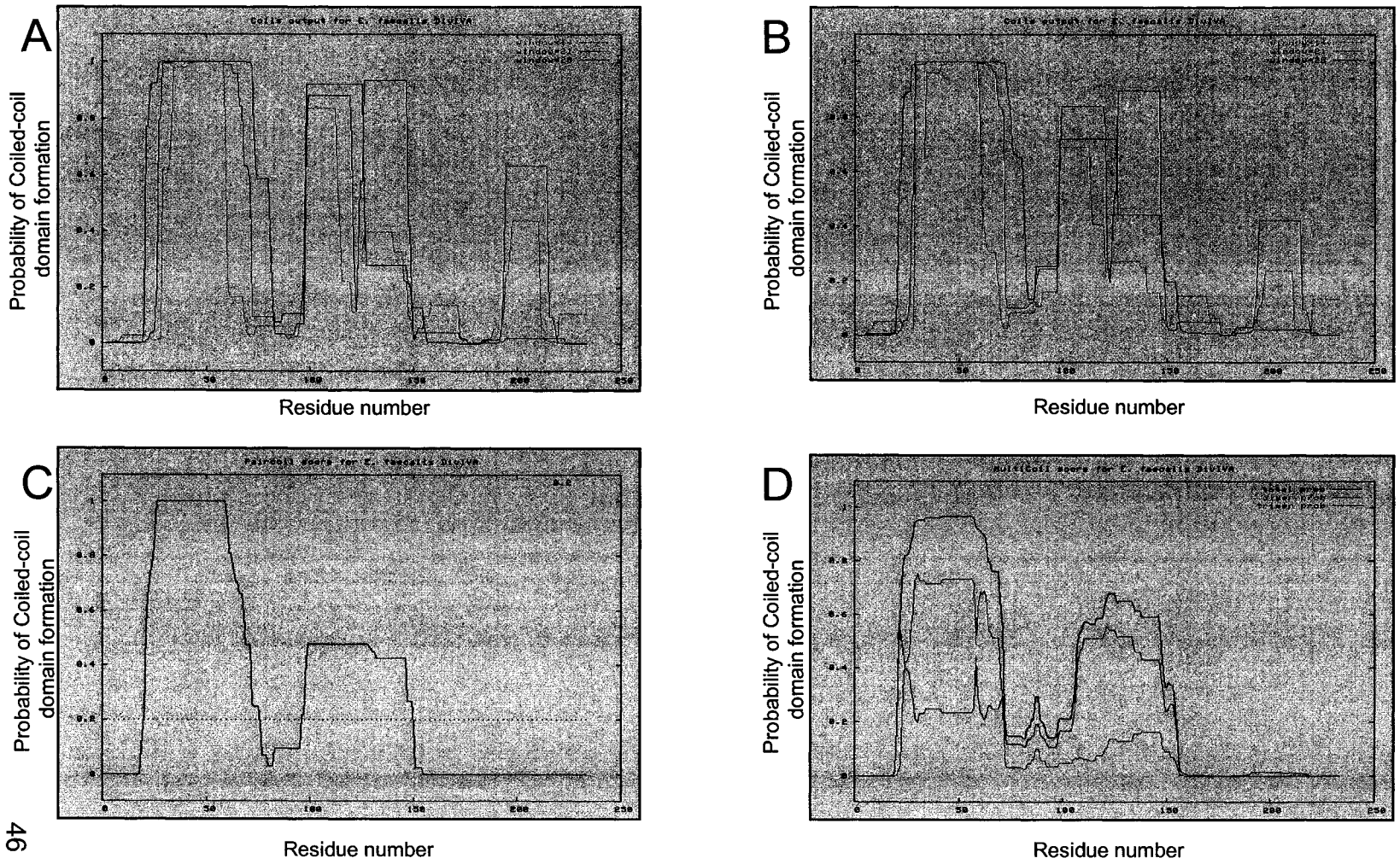
A
B
C
D
Probability of Coiled-coil domain formation
Residue number

Figure 7 - Coiled-coil domain predictions using the Coils program for DivIVA homologs

A) *Enterococcus faecalis*, B) *Bacillus subtilis*, C) *Staphylococcus aureus* and D) *Mycobacterium avium paratuberculosis*. The three window sizes define how many residues were examined simultaneously.

Figure 7

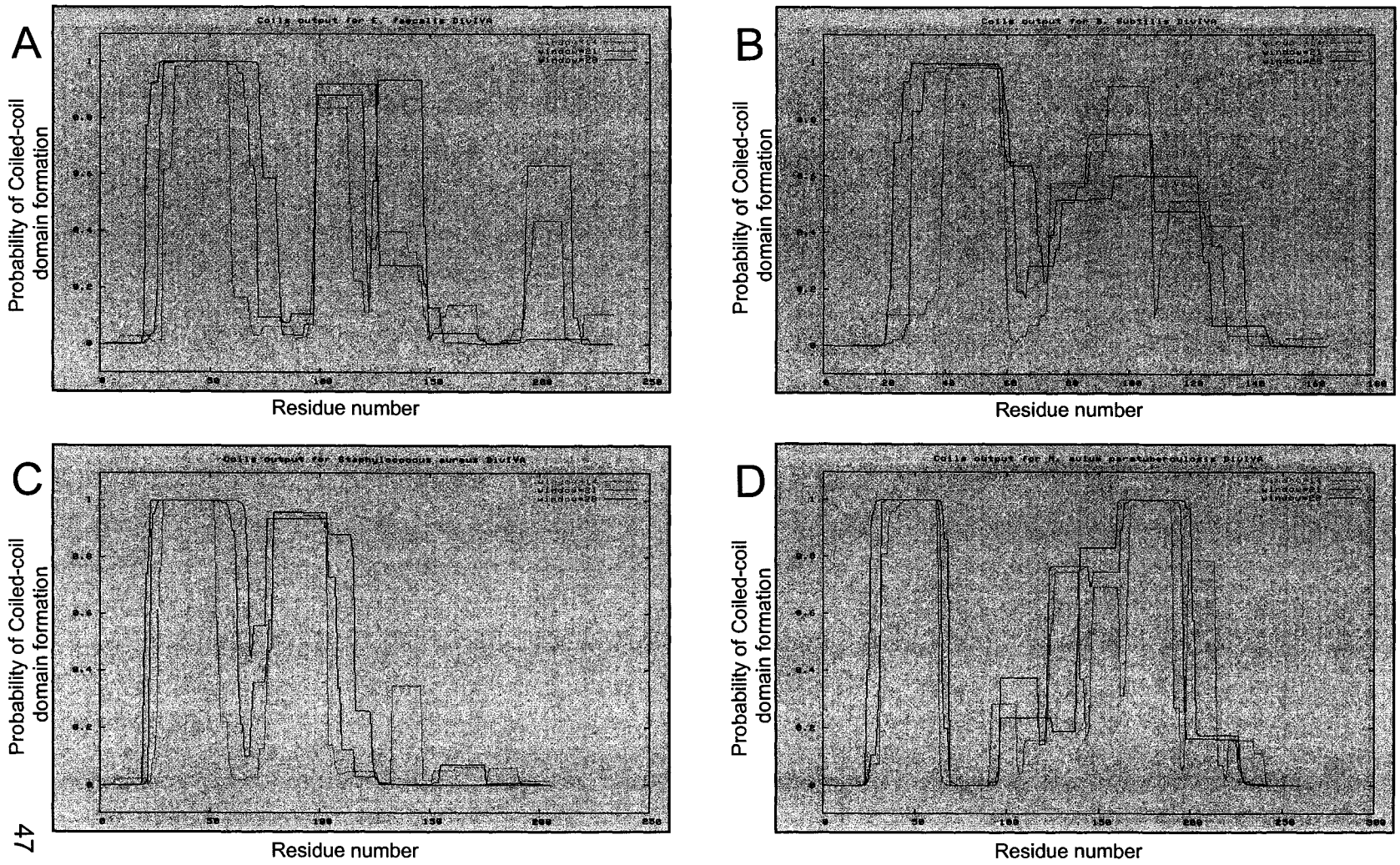
A
Probability of Coiled-coil domain formation
Residue number
B
Probability of Coiled-coil domain formation
Residue number
C
Probability of Coiled-coil domain formation
Residue number
D
Probability of Coiled-coil domain formation
Residue number

probabilities (50-100%) and possible number of domains (as defined by the peaks), it was always present. However, the C-termini of the various proteins varied greatly with some homologs such as DivIVA$_{Ef}$ (Figure 7A) having a low probability domain (40-70%) and others homologs such as DivIVA$_{Sa}$ (Figure 7C) lacking a coiled-coil domain. A residue-per-residue assignment of the coiled-coil domain registers for DivIVA$_{Ef}$ generated using Paircoil analysis, as well as the location of the various mutations created to disrupt the coiled-coil domains and the peptides identified by MALDI-TOF analysis, is shown in Figure 8.

As mentioned previously, coiled-coil domains can exist in different forms. As shown in Figure 6D, Multicoil analysis of DivIVA$_{Ef}$ predicts that the N-terminal coiled-coil domain is composed primarily of two stranded domains while the central domain is primarily three stranded. Other DivIVA homologs show a similar two-stranded preference for the N-terminal coiled-coil domain with some homologs predicted to have a mix of two stranded and three stranded character for the central coiled-coil domains (data not shown).

3.2 Discrepancy between the observed and predicted molecular weight of DivIVA$_{Ef}$

While bioinformatics predicts that DivIVA$_{Ef}$ should have a molecular mass of 27 kDa, samples run in denaturing SDS-PAGE gels against known standards indicate that DivIVA$_{Ef}$ has a mobility corresponding to approximately 40 kDa (Figure 9a). To confirm that only DivIVA$_{Ef}$ was being purified from the *E. coli* lysates, mass spectrometry analysis of the purified protein band as well as the secondary band (indicated by the arrow in Figure 9A) was performed. The MALDI-TOF analysis of both the major and secondary bands identified only peptides that corresponded exactly to

Figure 8 – Detailed sequence information of $DivIVA_{Ef}$

Assignment of heptad positions specific to $DivIVA_{Ef}$ as defined by Paircoil are listed below the primary amino acid sequence. The central coiled-coil region is predicted to have two separate domains with the second domain shown in italics. The locations of point mutations created to study the effect of coiled-coil domain disruption in this study are indicated by arrows with the mutagenized amino acid listed above the arrow. Locations of residues involved in creating DivIVA deletions are indicated by the star. Peptides identified by MALDI-TOF analysis are underlined.

Figure 8

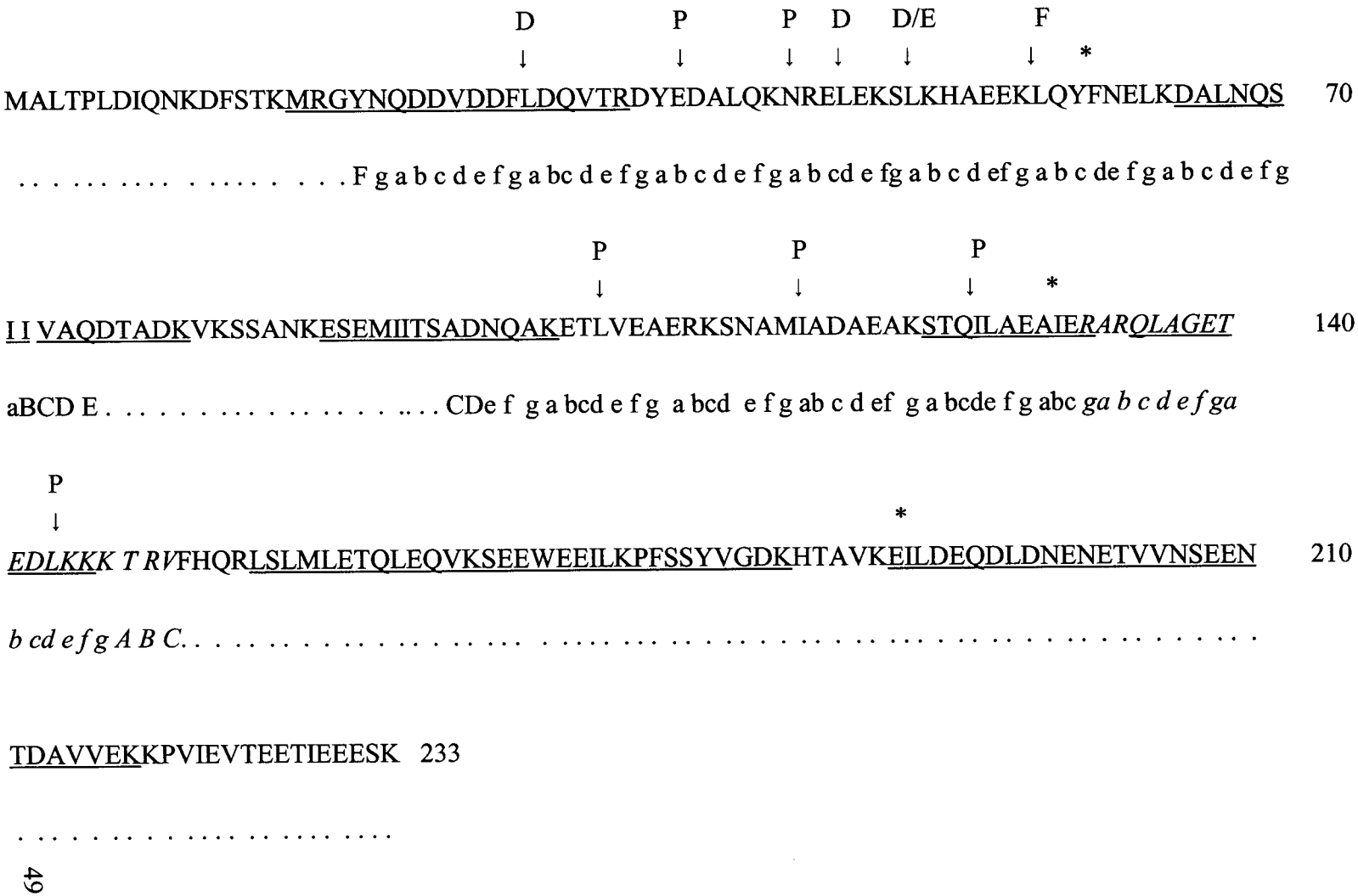
D P P D D/E F
↓ ↓ ↓ ↓ ↓ ↓ *
MALTPLDIQNKDFSTKMRGYNQDDVDDFLDQVTRDYEDALQKNRELEKSLKHAEEKLQYFNELKDALNQS 70
. . . . . F g a b c d e f g a bc d e f g a b c d e f g a b cd e fg a b c d ef g a b c de f g a b c d e f g
P P P
↓ ↓ ↓ *
I I VAQDTADKVKSSANKESEMIITSADNQAKETLVEAERKSNAMIADAEAKSTQILAEAIERARQLAGET 140
aBCD E . . . . . CDe f g a bcd e f g a bcd e f g ab c d ef g a bcde f g abc ga b c d e f ga
P *
↓
EDLKKK T RVFHQRLSLMLETQLEQVKSEEWEEILKPFSSYVGDKHTAVKEILDEQDLDNENETVVNSEEN 210
b cd e f g A B C. . . . . .
TDAVVEKKPVIEVTEETIEEESK 233
. . . . . .

Figure 9 - Discrepancies between the bioinformatically and experimentally determined molecular weight of $DivIVA_{Ef}$.

A) SDS-PAGE analysis indicates that $DivIVA_{Ef}$ has an apparent molecular weight of approximately 40 kDa while bioinformatics indicates the molecular weight should only be 27 kDa. Lanes 1-5 represents increasing loading volumes of purified $DivIVA_{Ef}$ from 5-25 uL in 5 uL increments. The arrow indicates a secondary band identified as $DivIVA_{Ef}$ by mass spectrometry analysis. B) Western blot analysis using α-$DivIVA_{Ef}$ antiserum of 1) *E. faecalis* cell lysate, 2) *E. faecalis* overexpressing $DivIVA_{Ef}$, 3) *E. faecalis* with *$divIVA_{Ef}$* knocked out and 4) Purified $DivIVA_{Ef}$-6xHis

Figure 9

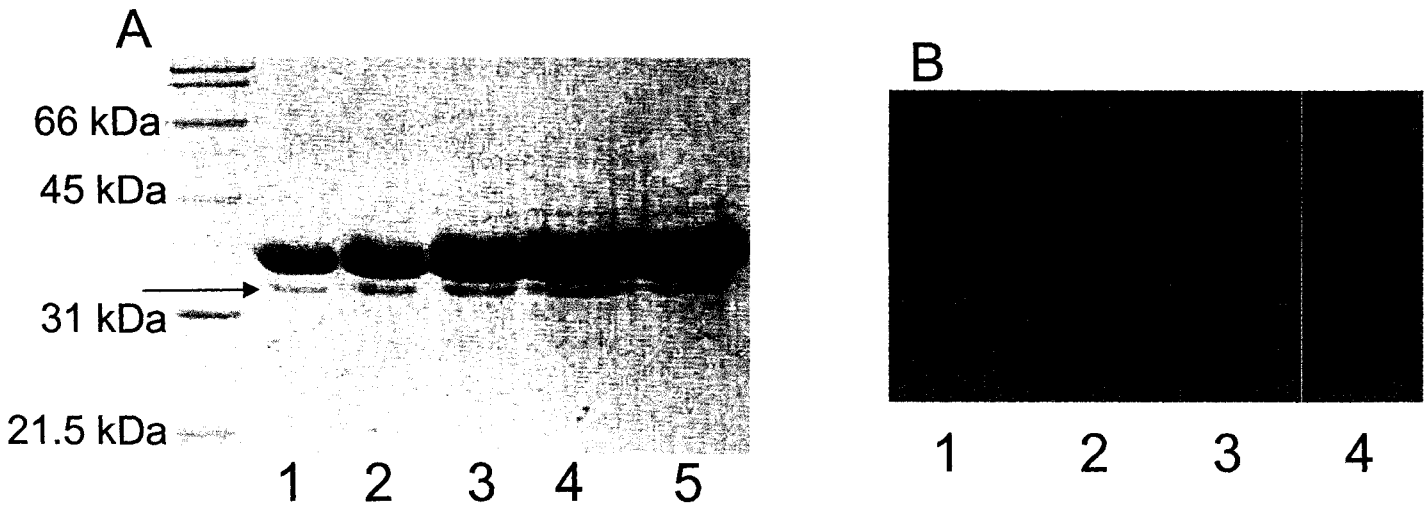

DivIVA$_{Ef}$, confirming that no other proteins were present in the sample. Specifically, peptides MRGYNQDDVDDFLDQVTR, GYNQDDVDDFLDQVTR, DALNQSIIVAQDTADK, ESEMIITSADNQAK, STQILAEAIER, QLAGETEDLKK, LSLMLETQLEQVK, SEEWEEILKPFSSYVGDK, and EILDEQDLDNENETVVNSEENTDAVVEK were identified from each sample. These sequences represent approximately 55% of DivIVA$_{Ef}$ and are underlined in Figure 8. To verify that DivIVA$_{Ef}$ was not being altered during the overexpression and purification processes, Western blotting analysis using α-DivIVA$_{Ef}$ antiserum was performed. As indicated in Figure 9B, the purified DivIVA$_{Ef}$ (lane 4) migrated identically to DivIVA$_{Ef}$ present in *E. faecalis* cell lysates (lanes 1 and 2), suggesting that DivIVA$_{Ef}$ is not adversely affected by purification and that the 6xHis tag present in the purified samples is not affecting electrophoretic mobility. While this aberrant mobility is not seen for all DivIVA homologs, it has been observed for the DivIVA homolog of *Staphylococcus epidermitis* (S. Ramirez-Arcos, Personal communication).

In order to attempt to determine the cause of the mobility shift, the purified DivIVA$_{Ef}$ was subjected to Urea SDS-PAGE analysis and tested for post-translational glycosylation. No difference in migration was observed when 5M urea was added to the gel, running buffer, and sample buffer as indicated in Figure 10A. Also, DivIVA$_{Ef}$ does not appear to undergo post-translational glycosylation as indicated in Figure 10B.

Aberrant electrophoretic mobility was also observed for DivIVA$_{Ef}$ that had been either truncated or deleted (MR6, MR7, and MR9, Data not shown). Using the IEP online software, the isoelectric point for DivIVA$_{Ef}$, MR6, MR7, and MR9 was calculated along with a predicted net charge of each protein at pH 8.5 (Table 4). Comparing the

Figure 10 - Attempts to resolve the discrepancy between the observed and predicted molecular weight of $DivIVA_{Ef}$

A) SDS-PAGE-Urea gel of purified $DivIVA_{Ef}$ stained with Sypro Ruby red, demonstrating that $DivIVA_{Ef}$ mobility is not affected by addition of urea. B) Glycosylation assay to determine if $DivIVA_{Ef}$ is being post-translationally glycosylated. Lane 1 contained a prestained protein marker with molecular weights indicated beside each band. Lane 2 (+) and Lane 3 (-) represent horseradish peroxidase (HRP) and soybean trypsin inhibitor (STI) control samples respectively. Lane 4 contained purified $DivIVA_{Ef}$ and lane 5 was left empty. Lanes 1-5 were stained using the Pierce GelCode kit, lanes 6-7 were stained with Coomassie blue to ensure proper sample application with a standard molecular weight ladder in lane 6 (molecular weights indicated outside lane 7) and $DivIVA_{Ef}$ in lane 7.

Figure 10

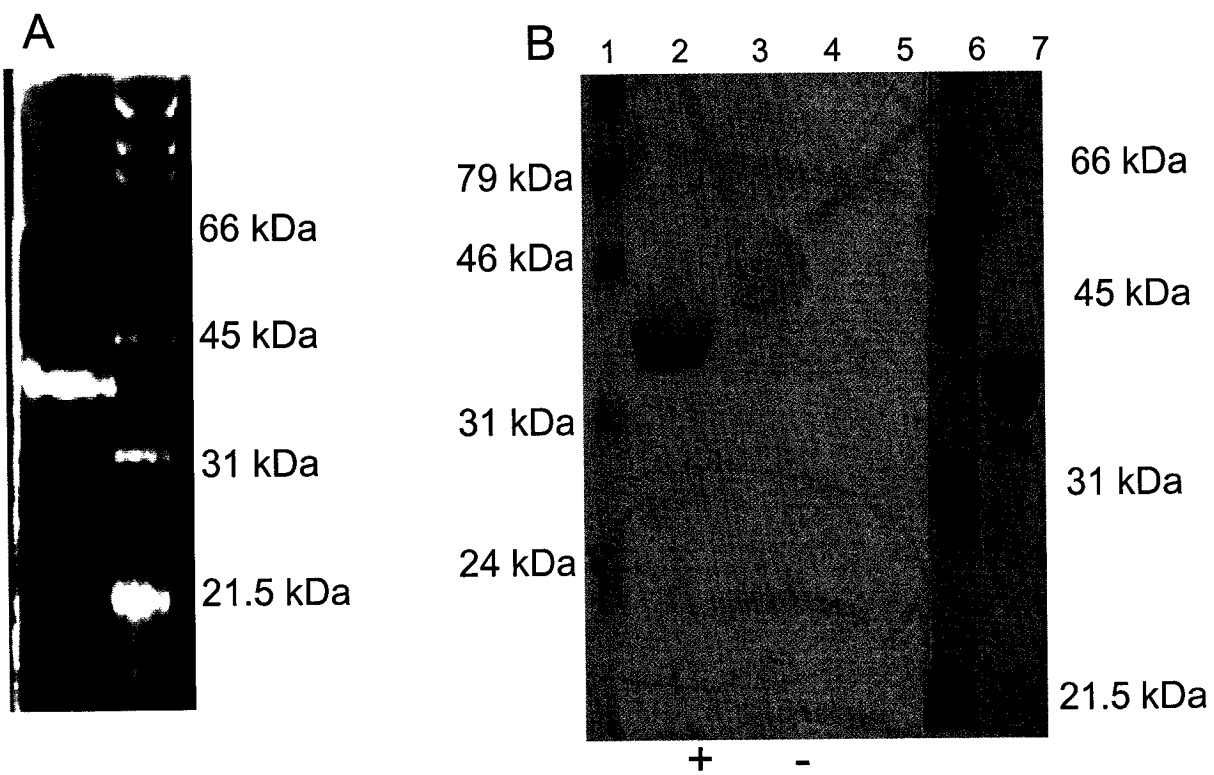
A
66 kDa
45 kDa
31 kDa
21.5 kDa
B
1 2 3 4 5 6 7
79 kDa
46 kDa
31 kDa
24 kDa
66 kDa
45 kDa
31 kDa
21.5 kDa
+
-

Table 4 – Comparison between aberrant electrophoretic mobility and predicted protein charge for wild type and deletion mutants of $DivIVA_{Ef}$

Protein	Predicted Molecular Weight (kDa)	Observed Molecular Weight (kDa)[1]	Percent Aberrant Migration[2]	Predicted charge at pH 8.5
Wild type $DivIVA_{Ef}$	26.64	39.46	48.12 %	-24.62
MR6 ($DivIVA_{Ef\ 1\text{-}190}$)	21.75	30.09	38.37 %	-11.61
MR7 ($DivIVA_{\ Ef\ \Delta\ 130\text{-}190}$)	19.68	33.54	70.43 %	-24.58
MR9 ($DivIVA_{\ Ef\ \Delta\ 60\text{-}130}$)	19.20	28.00	45.83 %	-19.59

[1] Mass calculated based on electrophoretic mobility of standards
[2] Percent aberrant migration = (Observed Molecular weight - Predicted Molecular weight) / Predicted Molecular weight

amount of aberrant mobility to the charge of the protein revealed that as the charge decreased, the amount of aberrant mobility decreased (Table 4).

3.3 Gel Filtration Standard Curve

The total column volume (V_t) used for these experiments was 100 mL. To determine the void volume (V_o), Blue Dextran 2000 was used and the volume measured to be 30 mL post-injection. These values were consistent between both the Superdex-200 and the Superose-6 columns. The elution profiles for the individual standards (Figure 11A) were combined into a single data series (Figure 11B) to facilitate visual comparison between the standards and purified protein samples. The standard curve used to calculate the molecular mass of the DivIVA protein complexes based on their partition coefficient is shown in Figure 11C. Only the standard curve for the Superose-6 column is shown since most samples were run using this resin.

3.4 Analysis of N-terminal DivIVA$_{Ef}$ point mutations

The predicted disruptions of the N-terminal coiled-coil domain as determined by Coils analysis are shown in Figure 12. Specifically, the L29D mutation (Figure 12A, MR1) pushes the start of the coiled-coil domain back from the wild type position (Figure 6A), the E37P mutation (Figure 12B, MR2) causes a disruption at the beginning of the coiled-coil domain, the combination of E37P, N43P, and L46D (Figure 12C, MR3) disrupts the first half of the domain and finally the combination of E37P, N43P, L46D, L50(D/E) and L57F (Figure 12D, MR4/MR5) disrupts the entire N-terminal coiled-coil domain. Following purification and concentration of wild type DivIVA$_{Ef}$ and the N-terminal DivIVA$_{Ef}$ mutants MR1 through MR5, the proteins were analysed by size exclusion chromatography (both Superdex-200 and Superose-6 resin) and native gel

Figure 11 - Generation of a standard curve to calculate the molecular weight of a protein complex based on its elution volume by size exclusion chromatography

A) Standard curve generated using Superose-6 resin. Although recommended by the kit, Ferritin, Albumin, and Aldolase could not be resolved from each other when run together due to the detection method. B) Combined standard curve extrapolated from A indicating each protein sample and corresponding mass. This curve was used to compare sample elution profiles to the standards. C) Extrapolation of the line of best fit and equation used to calculate the molecular weight of DivIVA$_{Ef}$ and the various mutant proteins based on the elution volume.

Figure 11

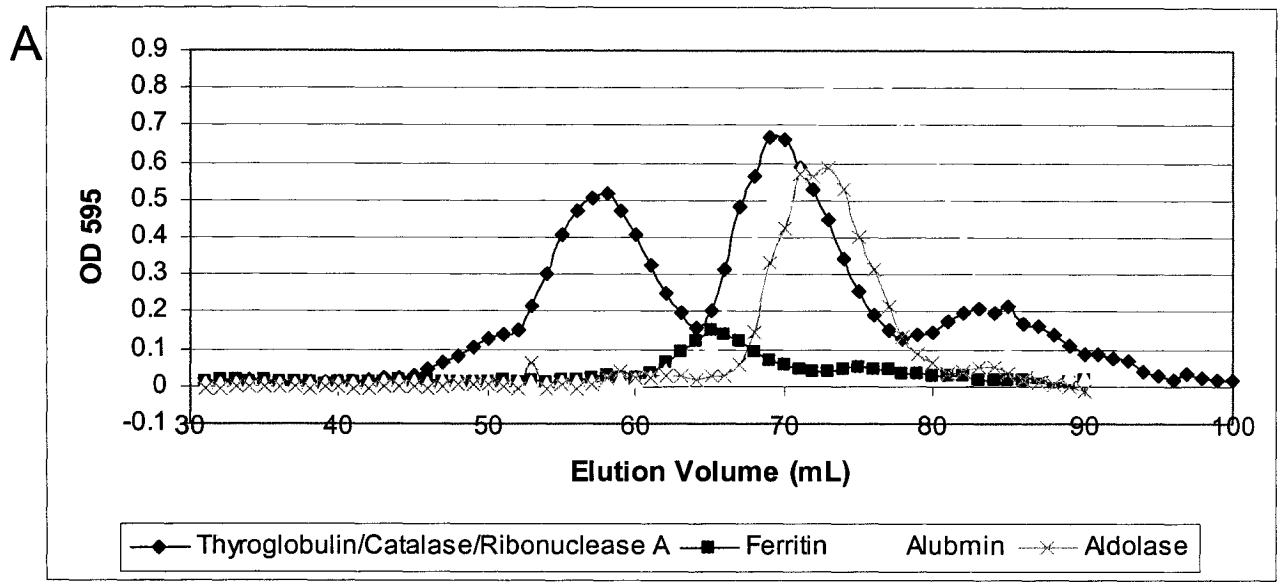
A
OD 595
0.9
0.8
0.7
0.6
0.5
0.4
0.3
0.2
0.1
0
-0.1
30
40
50
60
70
80
90
100
Elution Volume (mL)
Thyroglobulin/Catalase/Ribonuclease A
Ferritin
Alubmin
Aldolase

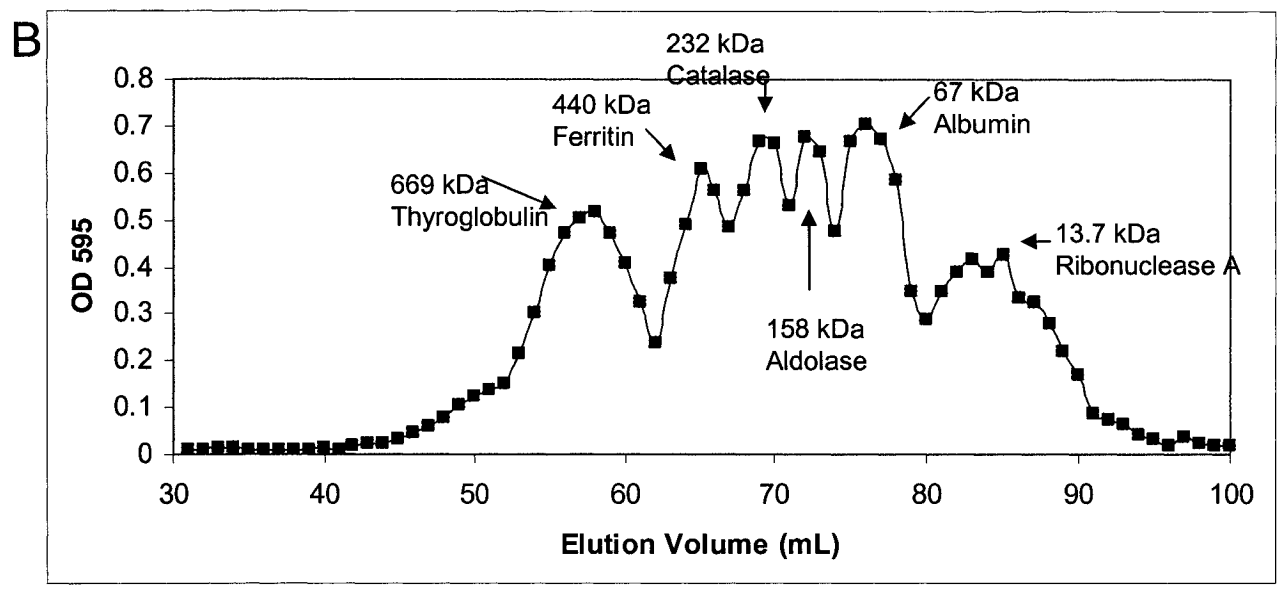
B
OD 595
232 kDa
Catalase
440 kDa
Ferritin
67 kDa
Albumin
669 kDa
Thyroglobulin
13.7 kDa
Ribonuclease A
158 kDa
Aldolase
0.8
0.7
0.6
0.5
0.4
0.3
0.2
0.1
0
30
40
50
60
70
80
90
100
Elution Volume (mL)

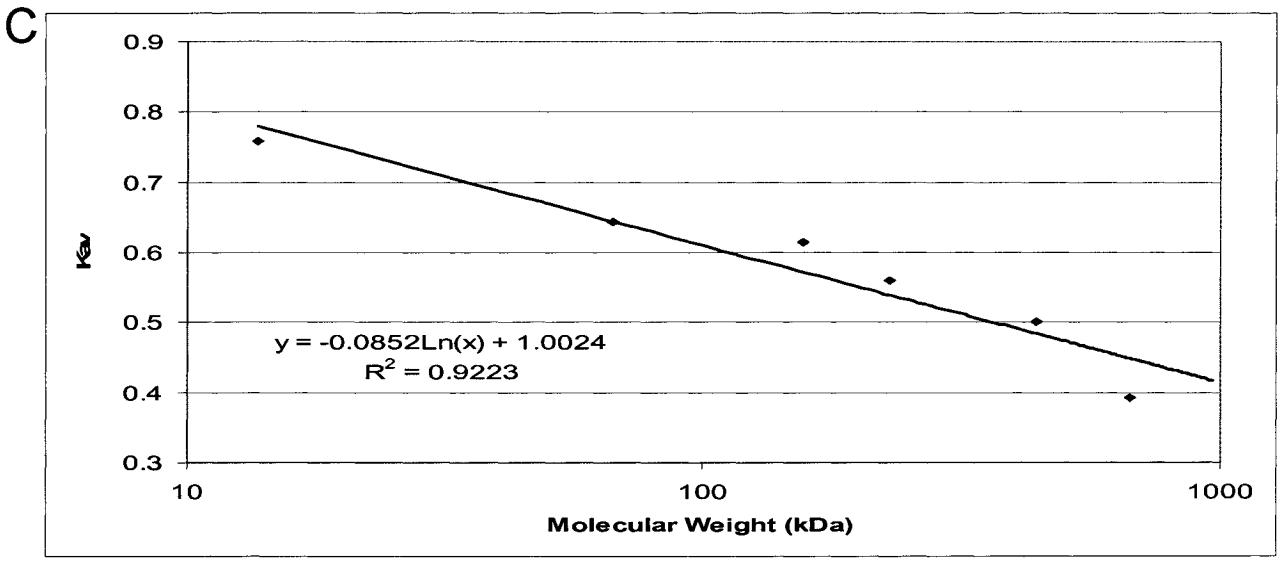
C
Kav
0.9
0.8
0.7
0.6
0.5
0.4
0.3
y = -0.0852Ln(x) + 1.0024
R2 = 0.9223
10
100
1000
Molecular Weight (kDa)

Figure 12 - Effect of introducing mutations to the N-terminal coiled-coil domain prediction

Coiled-coil domain predictions generated using the Coils program for $DivIVA_{Ef}$ to select mutations to the N-terminal domain, specifically $DivIVA_{Ef\ L29D}$ (MR1, A), $DivIVA_{Ef\ E37P}$ (MR2, B), $DivIVA_{Ef\ E37P,\ N3P,\ L46D}$ (MR3, C), and $DivIVA_{Ef\ E37P,\ N3P,\ L46D,\ L50D(E),\ L57F}$ (MR4(5), D) indicating that the specific mutation should disrupt the predicted coiled-coil domains.

Figure 12

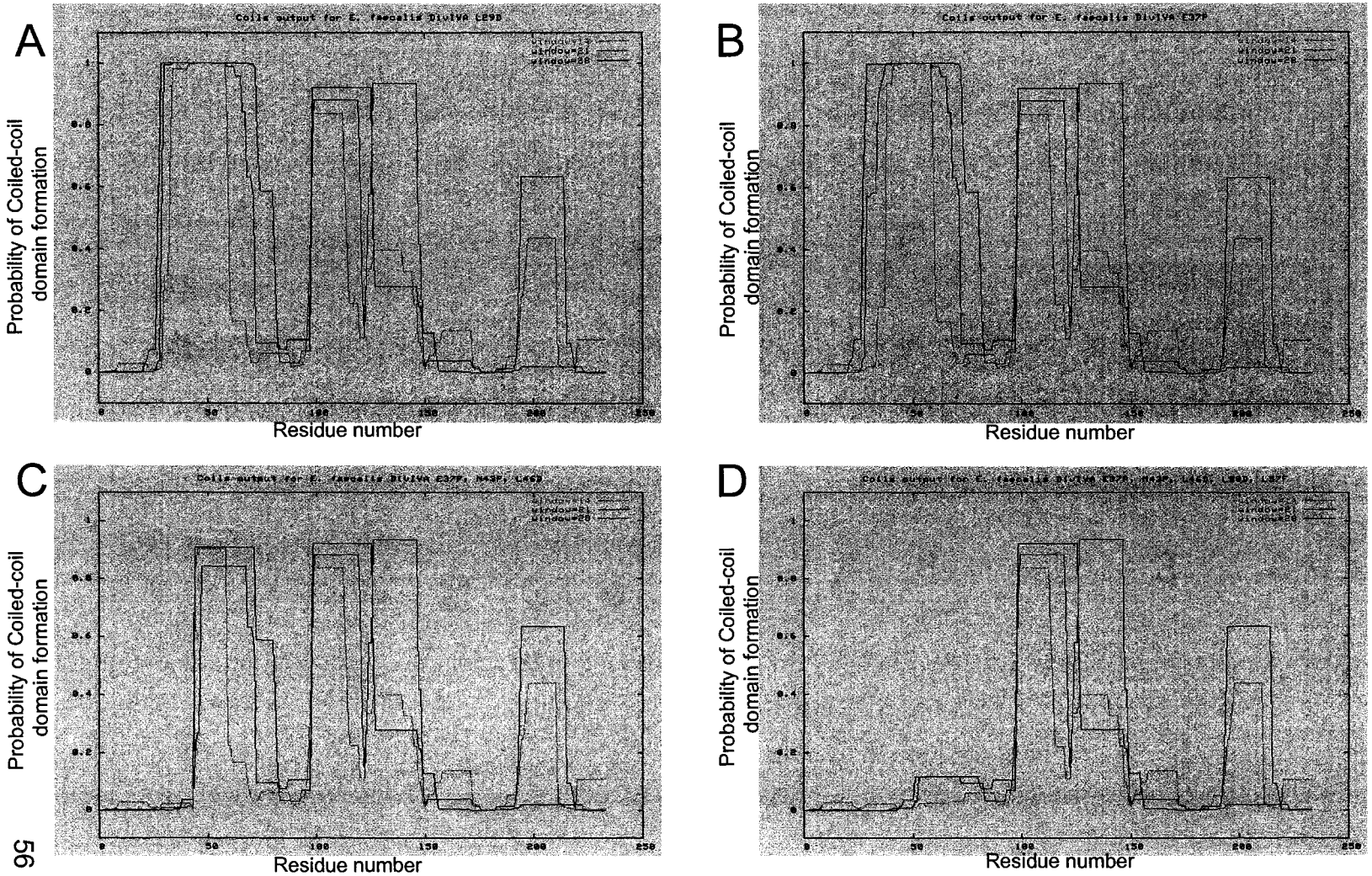
A
B
C
D
Probability of Coiled-coil domain formation
Residue number

electrophoresis. In all cases, both the wild type protein and those containing N-terminal mutations showed similar complex formation as determined by the calculated number of monomers making up the complex (Table 5). While the calculated number of DivIVA monomers associated within the complex was different for the two types of resin and the native gel calculations, the results were consistent within the method. Although the calculated complex size of the wild type $DivIVA_{Ef}$ and MR1 through MR5 samples (~1000 kDa) as measured using Superose-6 resin appears to be well above the highest calibration standard (Thyroglobulin, 669 kDa, Figure 11B) the elution profile for the $DivIVA_{Ef}$ and the N-terminal mutants eluted within the standards as shown in Figure 13. Native gel electrophoresis results for $DivIVA_{Ef}$ and the N-terminal mutants showed normal variation in terms of monomer count (between 10 and 12 monomers) according to literature (Muchova *et al.*, 2002a) and are presented in Figure 14. Circular dichroism analysis of $DivIVA_{Ef}$ and proteins carrying N-terminal mutations showed very similar spectra indicative of a primarily α-helical structure characterized by minima at approximately 208 and 220 nm (Figure 15).

In contrast to the gel filtration and native gel electrophoresis results, yeast two hybrid analysis of the N-terminal mutations revealed a statistically significant decrease in the interaction strength of the mutations as compared to the wild type (Table 5, Figure 16). With the exception of MR2 which had an approximately 50% decrease in interaction ($P>0.001$ by Student's T-test), all the N-terminal mutations showed at least a 66% decrease in interaction ($P=0.001$ by Student's T-test).

Table 5 – Mutations to N-terminal coiled-coil domain and deletion of the C-terminal coiled-coil domain do no affect $DivIVA_{Ef}$ oligomerization

Protein	Mutation(s)/Trunation	Gel Filtration		Yeast Two Hybrid		Native Gel Electrophoresis
		Superdex-200 (Complex Mass [kDa] /Number of monomers[1])	Superose-6 (Complex Mass [kDa] /Number of monomers)	Colony Lift	Liquid Assay (Miller Units)	(Complex Mass [kDa] /Number of monomers)
Wild Type	None	550 / 20	1011.83 / 37.47	Positive Interaction[2]	29.25 ± 6.70	288 / 10
MR1	L29D	532 / 20	1028.94 / 38.10	Positive Interaction	2.64 ± 1.16[3]	299 / 11
MR2	E37P	550 / 20	1046.33 / 38.75	Positive Interaction	17.53 ± 0.52[4]	332 / 12
MR3	E37P, N43P, L46D	470 / 18	962.19 / 35.63	Positive Interaction	7.36 ± 0.72[3]	344 / 12
MR4	E37P, N43P, L46D, L50D, L57F	526 / 20	1011.83 / 37.47	Positive Interaction	7.83 ± 1.50[3]	332 / 12
MR5	E37P, N43P, L46D, L50E, L57F	526 / 20	1003.38 / 37.16	Positive Interaction	8.69 ± 1.20[3]	332 / 12
MR6	Truncation after E190	550 / 25	834.4 / 38.40	Positive Interaction	23.65 ± 1.54	182 / 8

[1] Number of monomers based on molecular mass predicted by bioinformatics analysis
[2] Positive interaction indicates that only the combination of the DNA binding domain (BD) and transcriptional activation domain (AD) partners activated the reporter gene.
[3] Significant reduction (P = 0.001) by Student's T-test
[4] Significant reduction (P > 0.001) by Student's T-test

Figure 13 - Size exclusion chromatography indicates no difference in complex formation between wild type DivIVA$_{Ef}$ and proteins containing N-terminal mutants

Elution profile for DivIVA$_{Ef}$ and N-terminal mutations MR1 through MR5 using Superose-6 resin. All samples had an elution profile similar to that of thyroglobulin (669 kDa). Due to the low concentration of purified protein, the profile for MR3 was doubled to facilitate comparison on this scale.

Figure 13

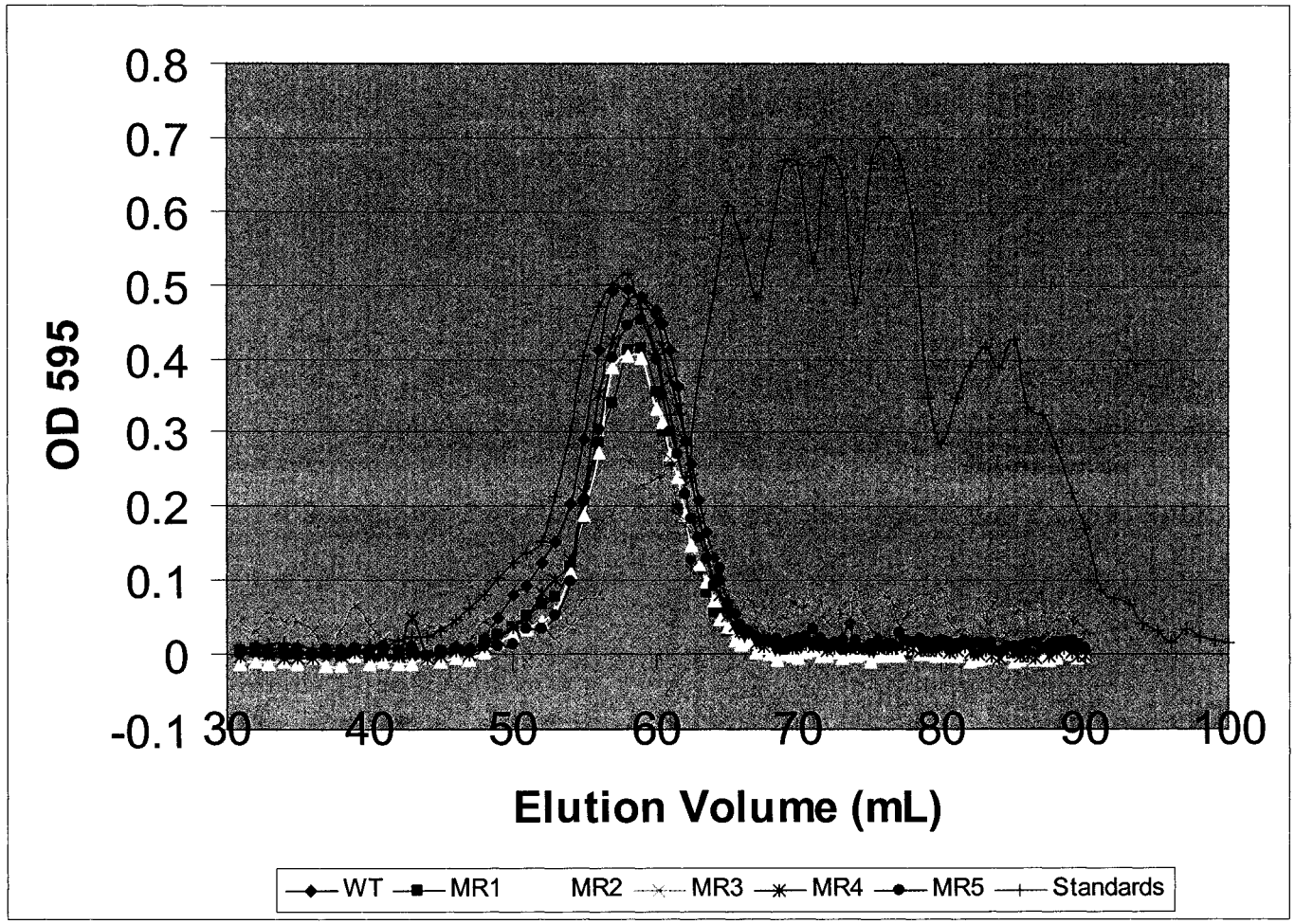
0.8
0.7
0.6
0.5
0.4
0.3
0.2
0.1
0
-0.1
OD 595
30
40
50
60
70
80
90
100
Elution Volume (mL)
WT
MR1
MR2
MR3
MR4
MR5
Standards

Figure 14 - Native gel electrophoresis reveals subtle differences in complex formation between wild type DivIVA$_{Ef}$ and proteins containing N-terminal mutants

Native gel electrophoresis of DivIVA$_{Ef}$ and N-terminal mutations. Samples were run on a 4-15% gradient Tris-HCl gel. 5 uL of each sample was loaded on the gel and the protein stained with Coomassie blue after elecrophoresis. Samples were loaded as follows: DivIVA$_{Ef}$ (Lane 1), MR1 (Lane 2), MR2 (Lane 3), MR3 (Lane 4), MR4 (Lane 5), MR5 (Lane 6).

Figure 14

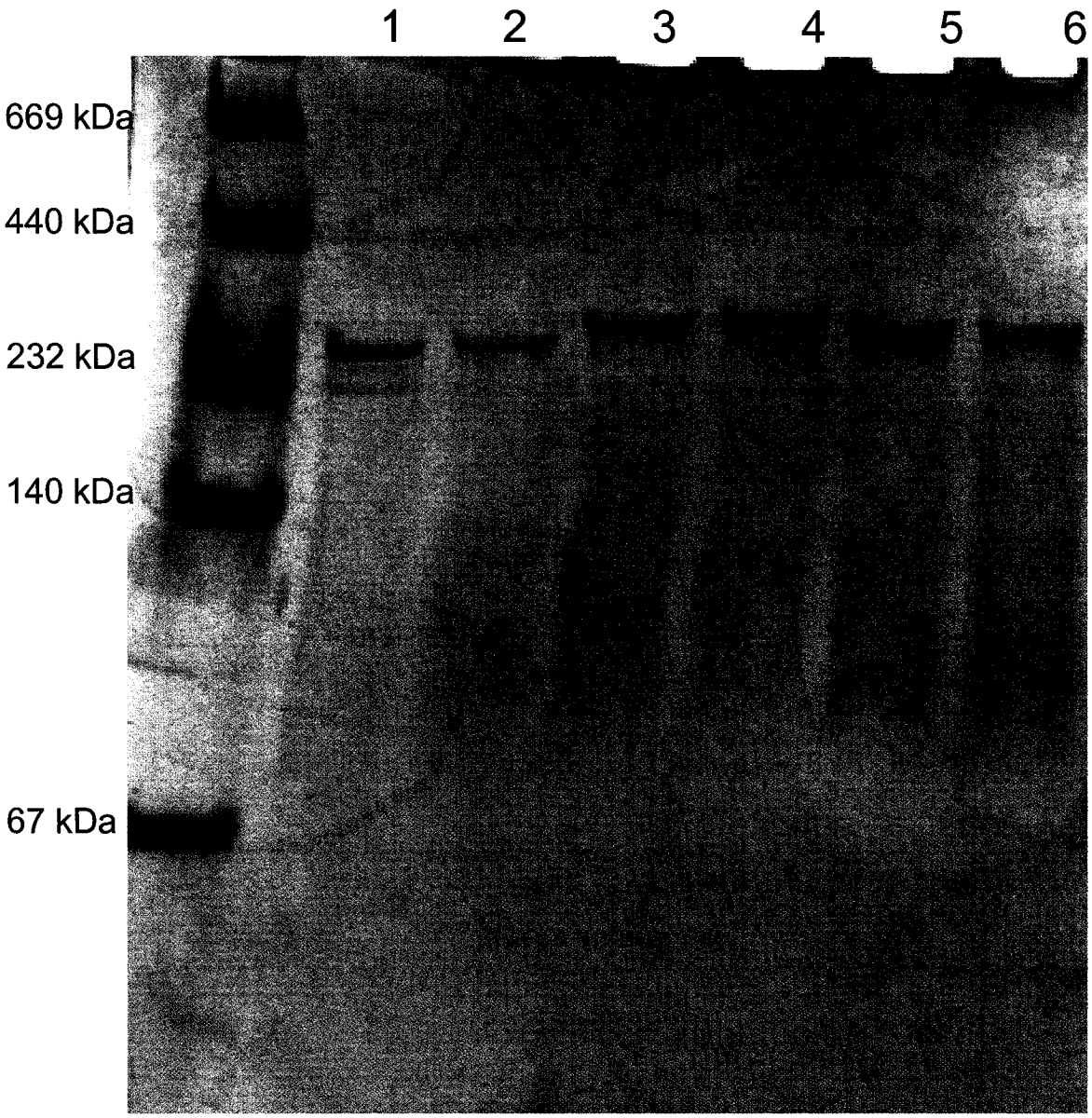

Figure 15 - Circular Dichroism analysis of DivIVA$_{Ef}$ and four of the N-terminal mutants.

While the overall secondary structures of the mutant proteins do not show significant variations from DivIVA$_{Ef}$, there is a slight increase in molar ellipticity at 208 nm for the mutations. Data points below 195 nm are not reliable since the signal strength exceeded 400V. No data was obtained for MR3 due to insufficient protein concentration.

Figure 15

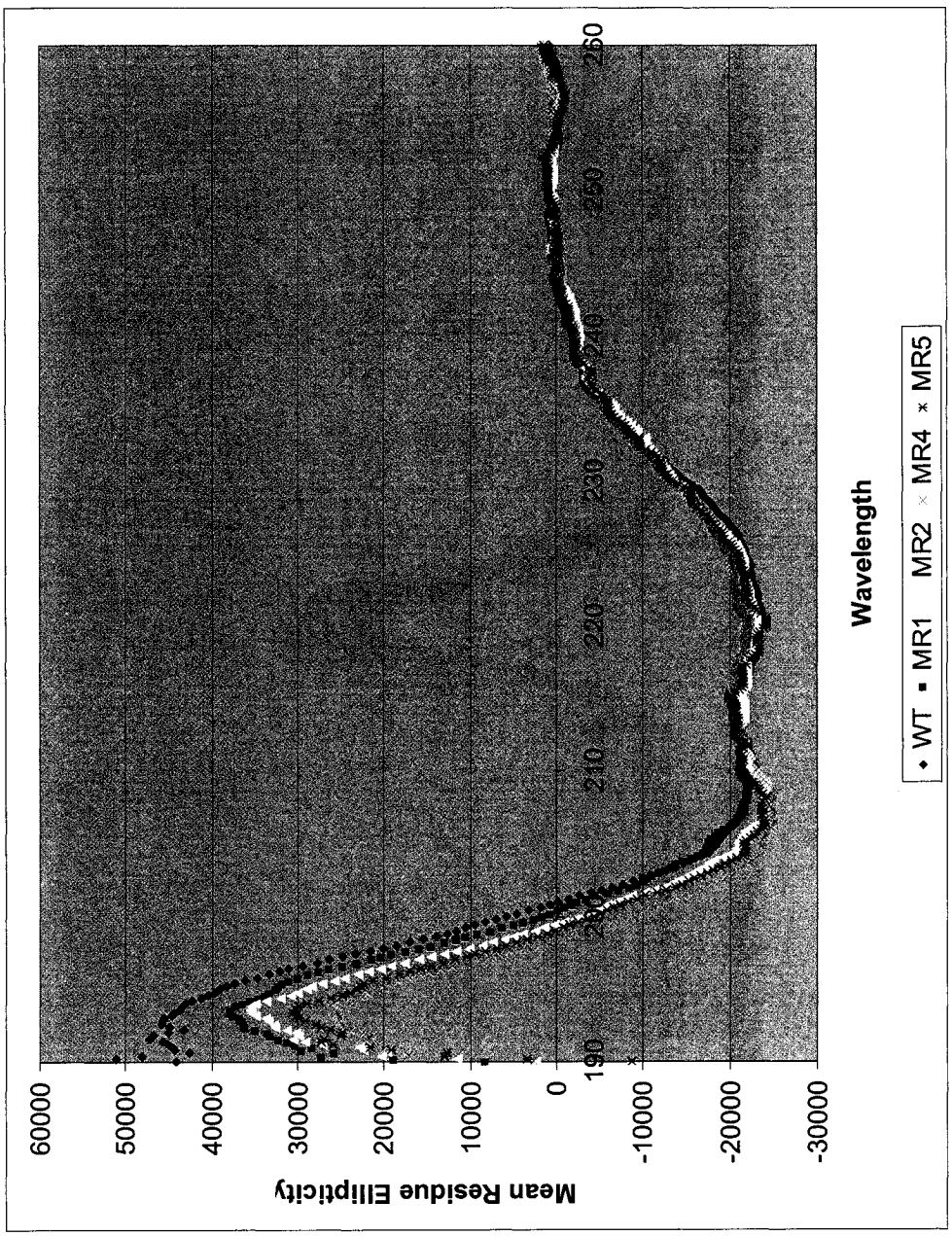
Mean Residue Ellipticity
60000
50000
40000
30000
20000
10000
0
-10000
-20000
-30000
190
210
220
230
260
Wavelength
WT
MR1
MR2
MR4
MR5

Figure 16 - Yeast two hybrid analysis of N-terminal mutants indicates significant decrease in interaction strength compared to wild type DivIVA$_{Ef}$

Quantification of interaction strength between DivIVA$_{Ef}$ and the N-terminal mutants. Samples were tested in combination with the corresponding mutations (e.g. pMR1-AD + pMR1-BD). * indicates P>0.001 and ** indicates P=0.001 using the Student's T-test with n=6.

Figure 16

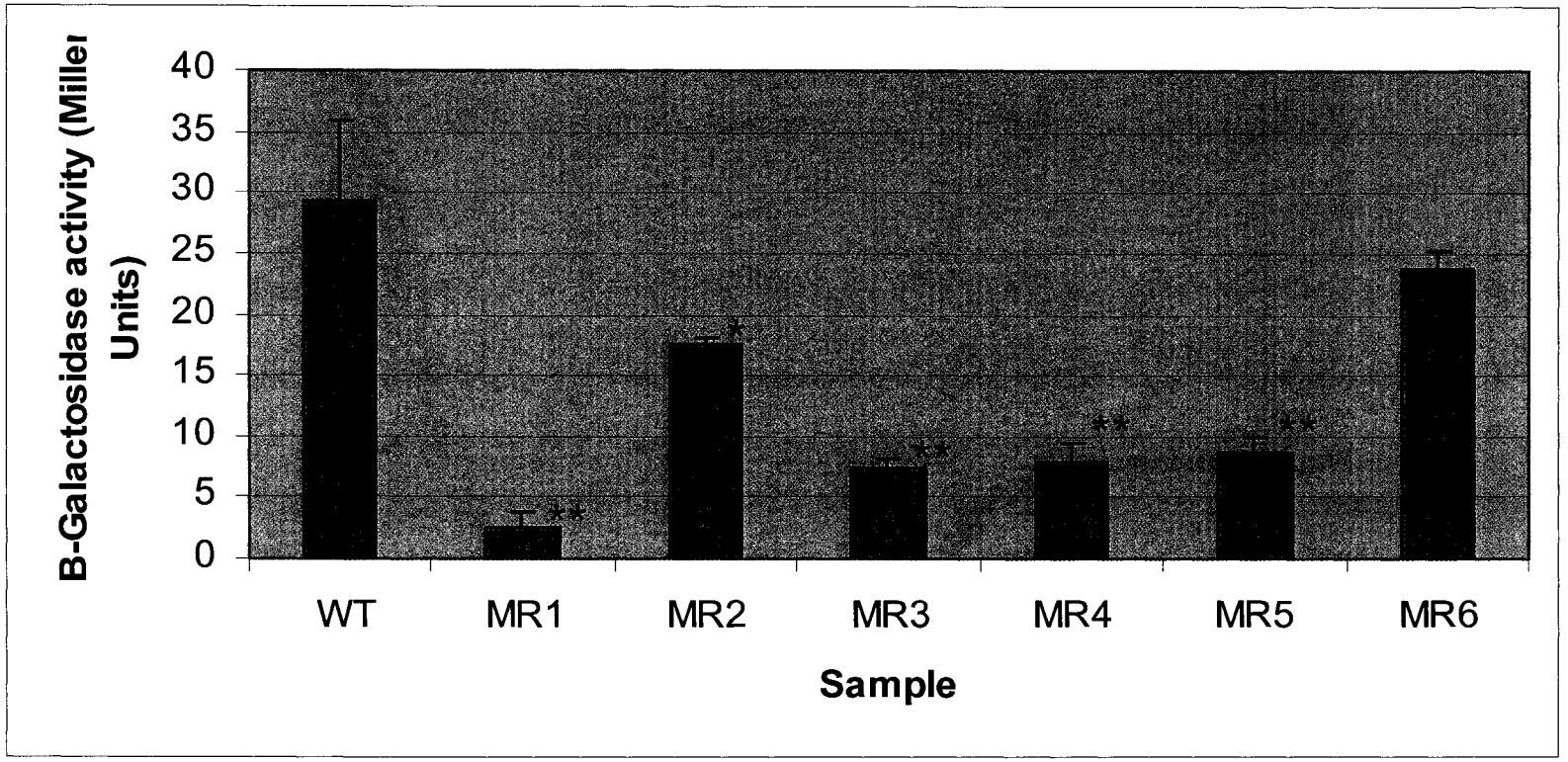

* P>0.001 by Student's T-test

** P=0.001 by Student's T-test

3.5 Analysis of C-terminal DivIVA$_{Ef}$ truncation

Deletion of the 43 C-terminal residues of DivIVA$_{Ef}$ (MR6) had no effect on DivIVA$_{Ef}$ oligomerization. Size exclusion chromatography of MR6 using either Superdex-200 or Superose-6 demonstrated that the number of monomers in the complex was similar to that of wild type DivIVA$_{Ef}$ despite the change in the size exclusion chromatography profile between the two proteins (Table 5, Figure 17). Similarly, although native gel electrophoresis of MR6 demonstrated a large decrease in overall complex size as compared to DivIVA$_{Ef}$ (182 kDa and 288 kDa respectively), the calculated number of monomers present in the complex was quite similar with 10 monomers for DivIVA$_{Ef}$ and 8 monomers for MR6 (Table 5, Figure 18).

Yeast two hybrid analysis of the C-terminal DivIVA$_{Ef}$ truncation demonstrated similar interaction strength to the wild type DivIVA$_{Ef}$, as shown in Figure 16.

3.6 Analysis of deletions and point mutations of the central coiled-coil domains

Deletion of either of the central coiled-coil domains of DivIVA$_{Ef}$ (MR7 and MR9) showed a decreased protein complex size as measured by native gel electrophoresis (Table 6). As shown in Figure 18, the MR7 (lane 3) and MR9 (lane 4) proteins show a significant decrease as compared to either DivIVA$_{Ef}$ or the C-terminal truncation with the corresponding calculated number of monomers being decreased by 50% from the wild type (Table 6). Gel filtration also revealed a similar decrease in both overall protein complex size and calculated number of monomers as compared to wild type for the MR7 protein (Table 6, Figure 19). Gel filtration data was only obtained for MR7 since protein with a high enough concentration could not be obtained for MR9 and no protein could be expressed or purified from the deletion of both central coiled-coil domains (MR8). Yeast

Figure 17 – Size exclusion chromatography indicates no difference in complex formation between wild type DivIVA$_{Ef}$ and a C-terminal 43 amino acid truncation

Size exclusion chromatography elution profile for DivIVA$_{Ef\ 1\text{-}190}$ (MR6) compared to DivIVA$_{Ef}$ using Superose-6 resin. Both proteins demonstrated full complex formation with MR6 having a slight shift due to the missing 43 amino acids per monomer.

Figure 17

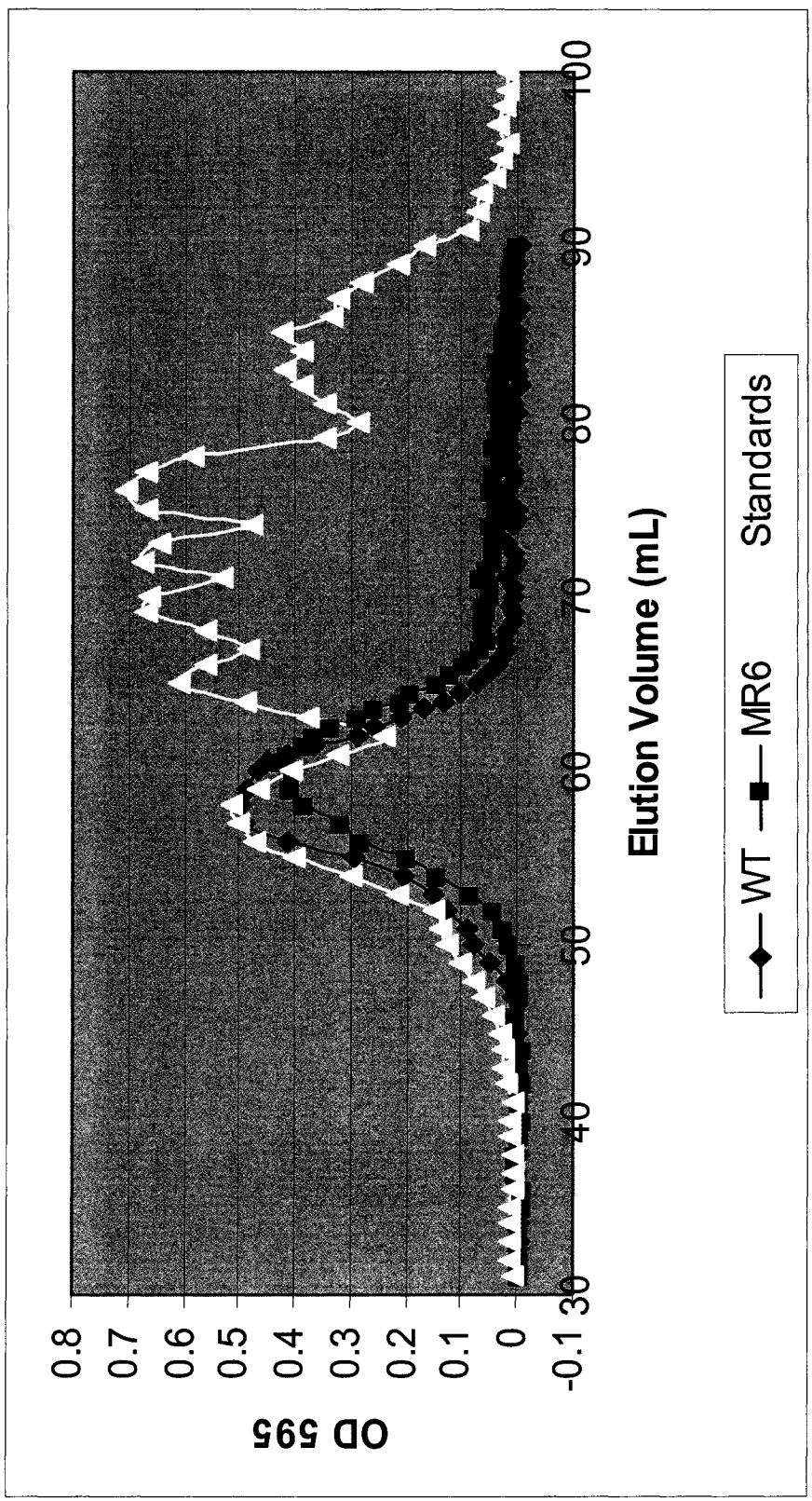
OD 595
0.8
0.7
0.6
0.5
0.4
0.3
0.2
0.1
0
-0.1
30
40
50
60
70
80
90
100
Elution Volume (mL)
WT
MR6
Standards

Figure 18 – Native gel electrophoresis of DivIVA$_{Ef}$ and the truncations/deletions constructed in this study

Native Gel electrophoresis of DivIVA$_{Ef}$ (Lane 1), MR6 (Lane 2), MR7 (Lane 3) and MR9 (Lane 4). Samples were run on a 4-15% gradient Tris-HCl gel and stained with Coomassie blue. Both MR7 and MR9 show approximately 50% decreased complex formation as compared to either DivIVA$_{Ef}$ or MR6.

Figure 18

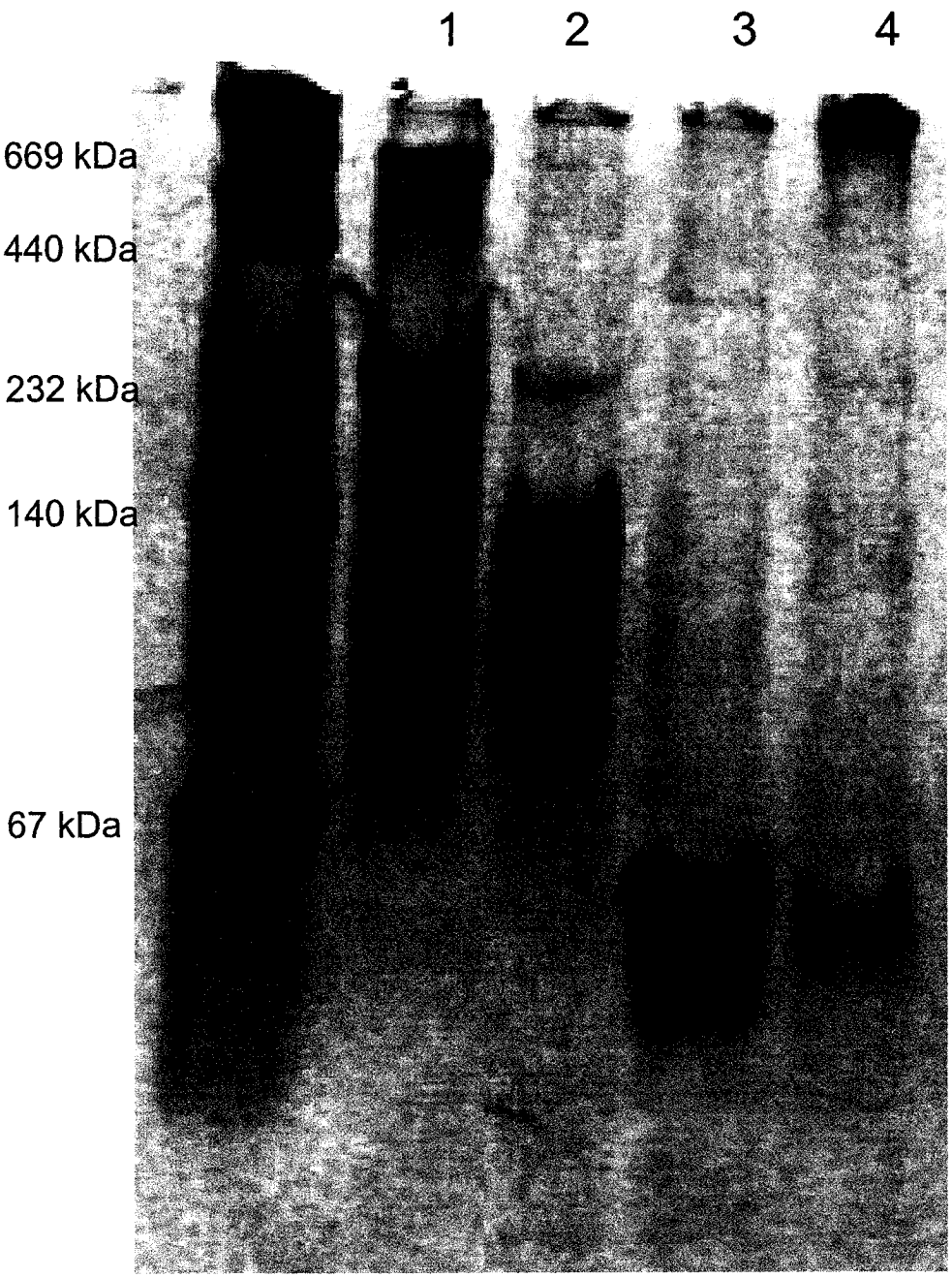

Table 6 – Mutations or deletions to the central coiled-coil domains of $DivIVA_{Ef}$ results in decreased $DivIVA_{Ef}$ oligomerization

Protein	Mutation/Deletion	Gel Filtration		Yeast Two Hybrid		Native Gel Electrophoresis
		Superdex-200 (Complex Mass [kDa] / Number of monomers[1])	Superose-6 (Complex Mass [kDa] / Number of monomers)	Interaction with Self	Interaction with Wild Type	Complex Mass [kDa] / Number of monomers
MR7	Deletion from I130-E190	170 / 9	260 / 13	NA[2]	Yes	52 / 3
MR9	Deletion from F60-I130	ND[3]	ND	NA	Yes	59 / 3
MR10	L143P	ND	ND	Not Detected	Yes	91 / 4
MR11	L104P	ND	841.1 / 31	ND	ND	125/4.6 and 78/2.8
MR12	L104P, L143P	ND	66.9 / 2.4	Not Deteted	Yes	64.2 / 2.4
MR13	L104P, I125P	ND	29.9 / 1.1	ND	ND	64.2 / 2.4
MR14	L104P, I125P, L143P	ND	100/3.7 and 28.9/1	ND	ND	69.8 / 2.6
MR15	L104P, I115P, I125P	ND	27 / 1.0	Not Detected	Yes	61.6 / 2.3
MR16	L104P, I115P, I125P, L143P	ND	40.4 / 1.5	Not Detected	Not Detected	66.9 / 2.5

[1] Number of monomers based on molecular mass predicted by bioinformatics analysis
[2] The DNA Binding Domain (BD) partner was able to activate the reporter gene independently of the transcriptional activation domain (AD) partner)
[3] ND = Experiment not preformed

Figure 19 – Size exclusion chromatography demonstrates a significantly decreased complex formation for protein lacking the third coiled-coil domain

Gel filtration profile for MR7 compared to DivIVA$_{Ef}$ and the standards. The increased elution volume for MR7 indicates disrupted complex formation.

Figure 19

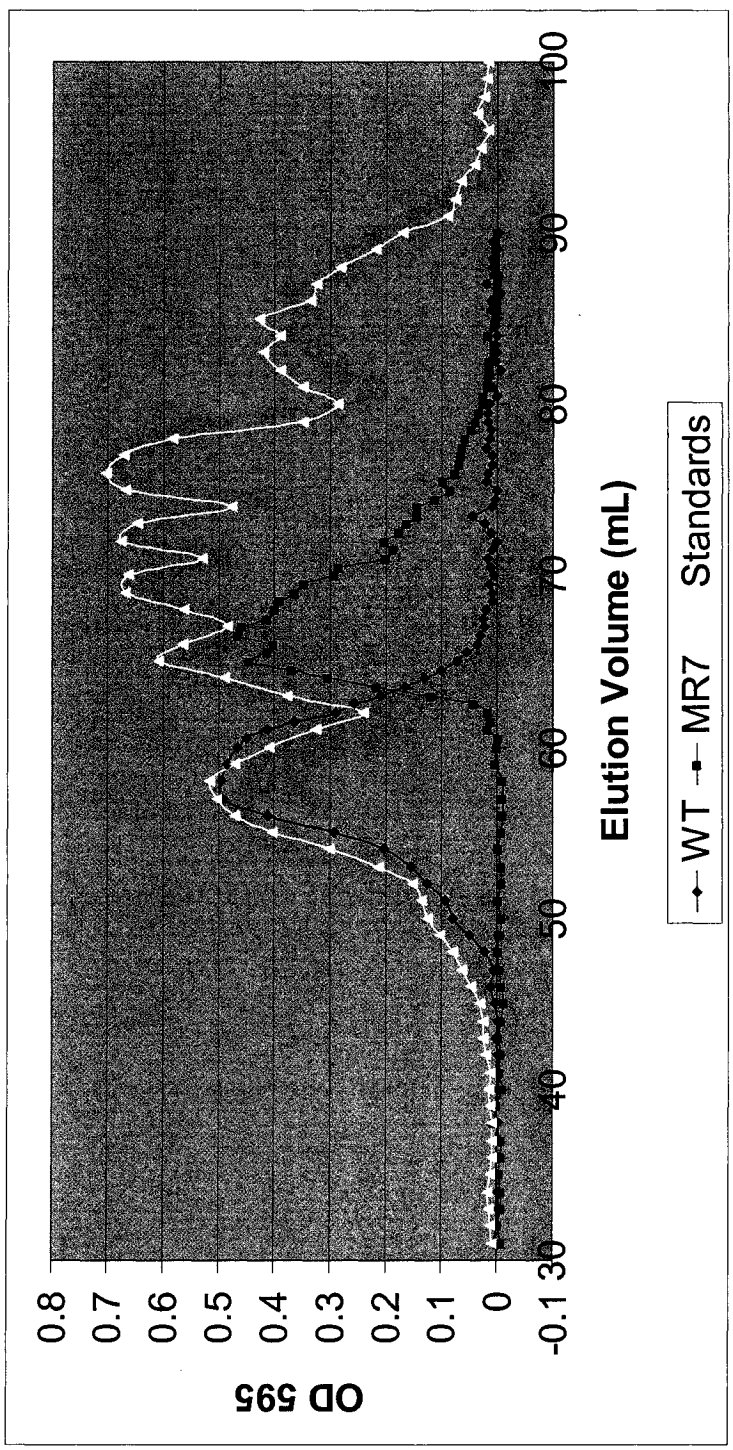
OD 595
0.8
0.7
0.6
0.5
0.4
0.3
0.2
0.1
0
-0.1
30
40
50
60
70
80
90
100
Elution Volume (mL)
WT
MR7
Standards

two hybrid data could not be obtained for these constructs since the DNA binding domain partner was able to activate the β-galactosidase reporter gene in the absence of the transcriptional activation domain partner.

Once the deletions identified the regions surrounding the central coiled-coil domains as the likely site of oligomerization, point mutations were designed to further characterize the domains. Predictions of the coiled-coil domain disruptions for MR10 through MR16 are shown in Figure 20 and 21. Figure 20 shows the effects of the L143P mutation (A, MR10), which abrogates the second central coiled-coil domain, the L104P mutation (B, MR11), which abrogates the first of the central coiled-coil domains, and a combination of both L104P and L143P (C, MR12) which abrogates both the first and second coiled-coil domain. Although the predicted disruptions for MR13 (L104P, I125P, Figure 21A) and MR15 (L104P, I115P, L143P, Figure 21C) are essentially identical to the MR11 prediction (Figure 20B), the addition of the I115P and I125P mutations helps ensure complete abrogation by disrupting the internal region of the first central coiled-coil domain and not just the end of the domain, as shown by the location of the mutations in Figure 8. Similarly, the predictions for MR14 (L104P, I125P, L143P, Figure 21B) and MR16 (L104P, I115P, I125P, L143P, Figure 21D) are nearly identical to MR12 (Figure 20C) and serve to ensure complete abrogation of both central coiled-coil domains. Size exclusion chromatography of proteins with mutational disruption of the central coiled-coil domains demonstrated decreased and abrogated complex formation. As shown in Figure 22, the elution profiles for MR12, MR13, MR14, MR15, and MR16 are largely decreased and exhibit a predominantly monomeric peak based on the standards. In contrast, MR11 has a wild type profile, suggesting that the L104P mutation has no effect

Figure 20 - Effect of introducing leucine to proline mutations at residues 104 and 143 of DivIVA$_{Ef}$ to the central coiled-coil domain predictions

Coiled-coil domain predictions for DivIVA$_{Ef}$ containing mutations to the central coiled-coil domains. A) DivIVA$_{Ef\ L143P}$ (MR10) B) DivIVA$_{Ef\ L104P}$ (MR11) and C) DivIVA$_{Ef\ L104P,\ L143P}$ (MR12)

Figure 20

A

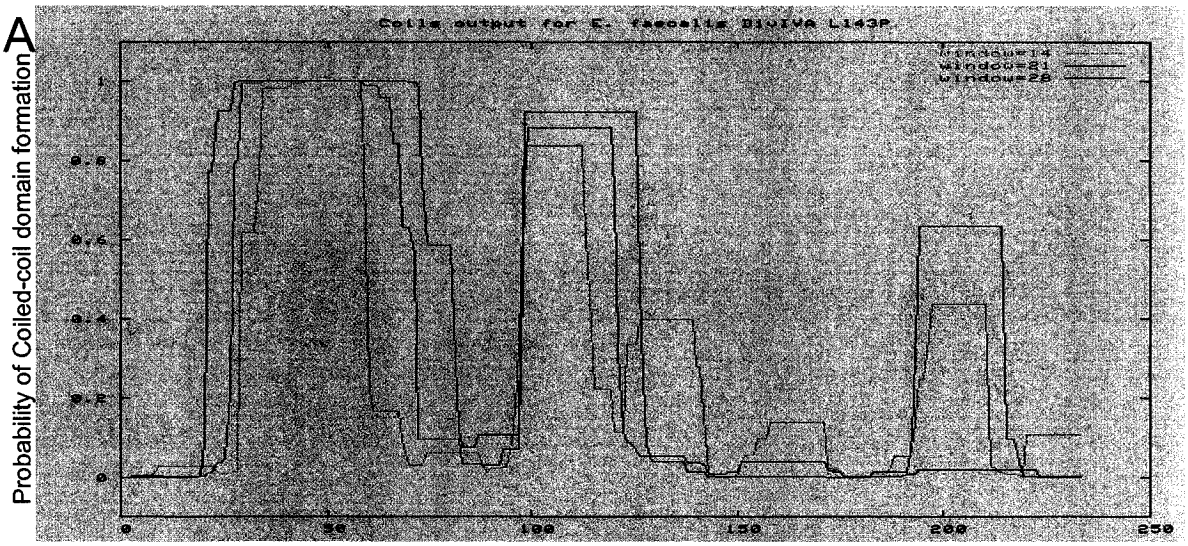

Probability of Coiled-coil domain formation

Residue number

B

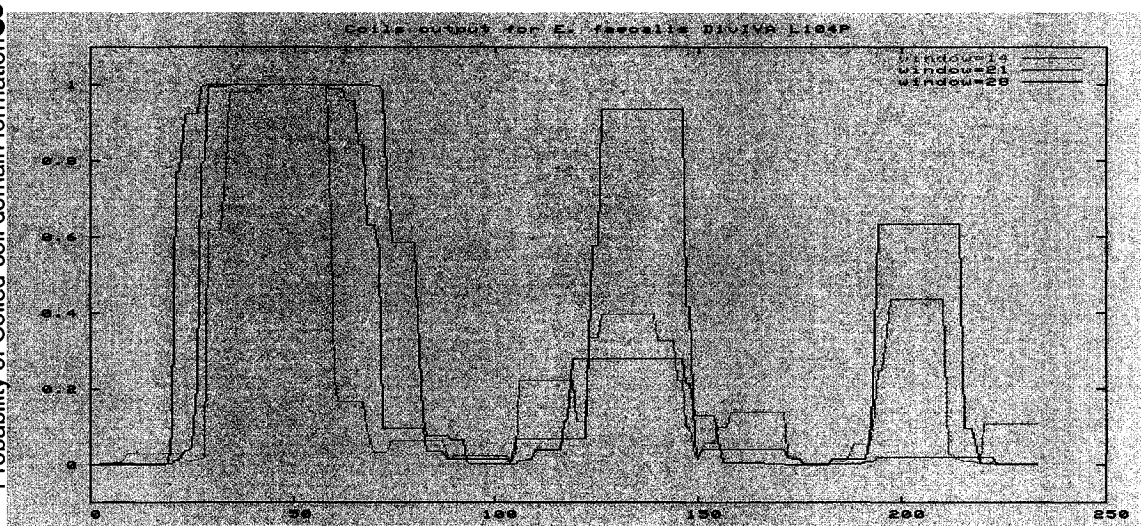

Probability of Coiled-coil domain formation

Residue number

C

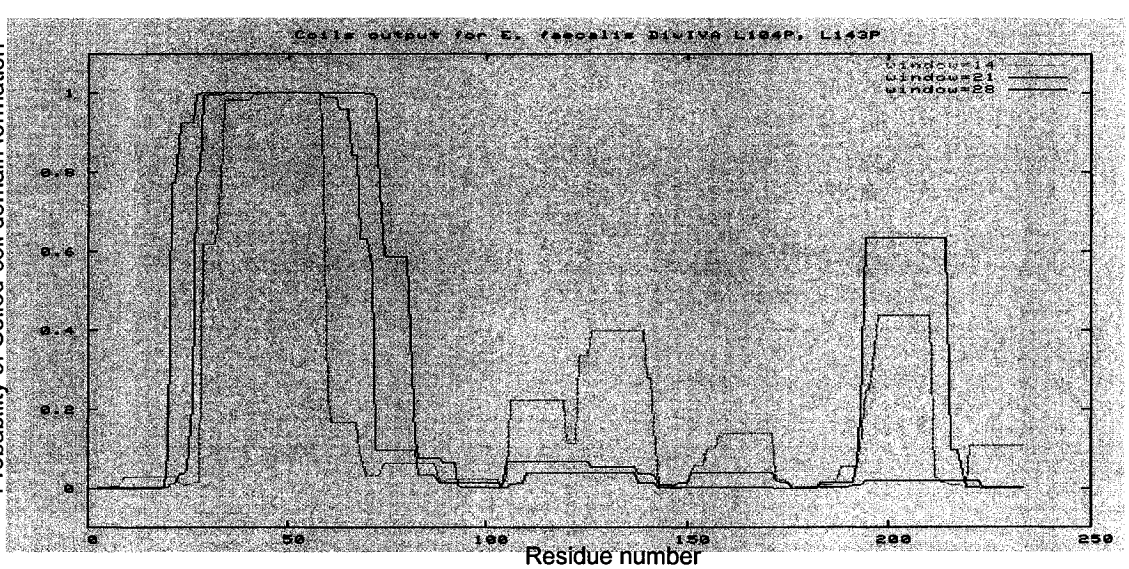

Probability of Coiled-coil domain formation

Residue number

Figure 21 - Effect of introducing additional isoleucine to proline mutations at residues 115 and 125 of DivIVA$_{Ef}$ to the central coiled-coil domain predictions.

Coiled-coil domain predictions for DivIVA$_{Ef}$ containing mutations to the central coiled-coil domains. A) DivIVA$_{Ef\ L104P,\ I125P}$ (MR13), B) DivIVAEf$_{L104P,\ I125P,\ L143P}$ (MR14), C) DivIVA$_{Ef\ L104P,\ I115P,\ I125P}$ (MR15) and D) DivIVA$_{Ef\ L104P,\ I115P,\ I125P,\ L143P}$ (MR16)

Figure 21

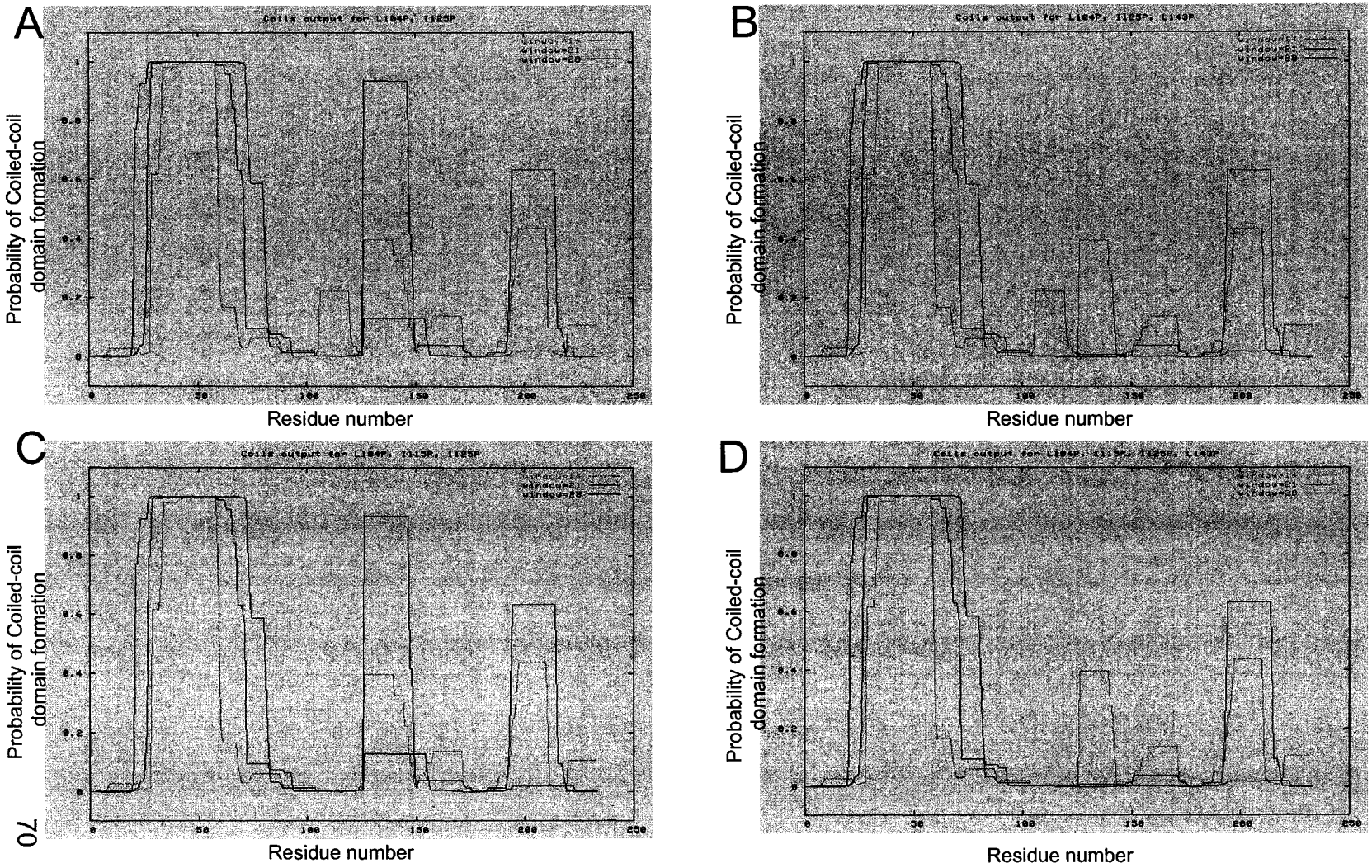
A
B
C
D
Probability of Coiled-coil domain formation
Residue number

Figure 22 – Size exclusion chromatography of proteins carrying mutations to the central coiled-coil domains

Gel filtration profiles for $DivIVA_{Ef}$ containing central coiled-coil domain mutations. Profiles are shown for MR11, MR12, MR13, MR14, MR15 and MR16. While MR11 seems to have full complex size, the remaining samples show a large shift down to a monomeric range. The two peaks for MR14 correspond to a 50% decrease and a monomeric peak. The standards were divided by 4 and MR11 by 2 in order to provide sufficient resolution for the other peaks.

Figure 22

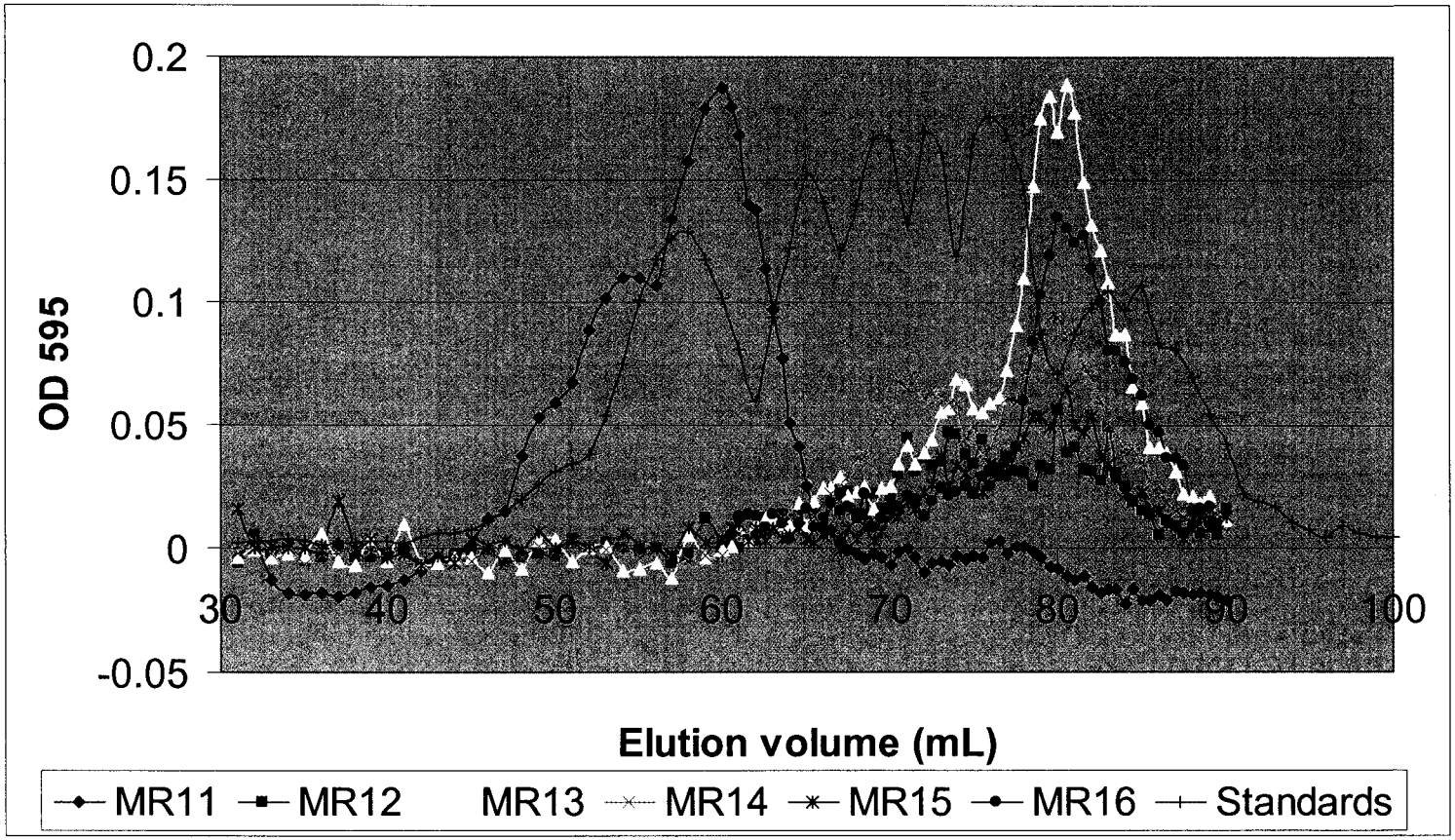
0.2
0.15
0.1
0.05
0
-0.05
OD 595
30
40
50
60
70
80
90
100
Elution volume (mL)
MR11
MR12
MR13
MR14
MR15
MR16
Standards

on complex formation. No data is presented for MR10 since protein of sufficient concentration for size exclusion chromatography could not be produced. In contrast, native gel electrophoresis data for MR10, MR12, MR13, MR14, MR15, and MR16 indicates only a 50% decrease in the number of monomers present in the complex as compared to the wild type (Table 6, data not shown). Again, MR11 is the exception showing a mixture of wild type and 50% decreased calculated monomer count by native gel electrophoresis (Table 6, data not shown).

When mutations of the central coiled-coil domain were tested in the yeast two hybrid system, no self interaction was detected when the mutations containing central coiled-coil domain disruptions were tested against themselves (e.g. MR12-AD + MR12-BD). However, interaction with the wild type protein was detected for MR10, MR12 and MR15, but no interaction between MR16 and wild type DivIVA$_{Ef}$ was detected (Table 6).

3.7 Preliminary mapping of MLJD1/DivIVA$_{Ef}$ interaction

Yeast two hybrid colony lift assays revealed that DivIVA$_{Ef}$ and MLJD1 were capable of interaction as determined by colony lift assay when DivIVA$_{Ef}$ either carried mutations to the N-terminal coiled-coil domain (Figure 23A), had residues between I130 and E190 deleted (Figure 23C), or lacked its C-terminal 43 amino acids (Figure 23D). However, no interaction was detected when DivIVA$_{Ef}$ lacking residues between F60 and I130 was tested with MLJD1 (Figure 23B). This indicates that the region of interaction between DivIVA$_{Ef}$ and MLJD1 is located somewhere between residues 60 and 130 of DivIVA$_{Ef}$.

Figure 23 – Yeast two hybrid analysis of $DivIVA_{Ef}$/MLJD1 interaction indicates that residues 60-100 of $DivIVA_{Ef}$ are required for interaction with MLJD1

Yeast two hybrid colony lift results used to map the site of $DivIVA_{Ef}$/MLJD1 interaction. The presence of blue colonies in A (MLJD1 + MR5), C (MR7 + MLJD1) and D (MR6 + MLJD1) and lack of blue colonies in B (MR9 + MLJD1) indicates that residues between amino acids 60 and 130 are required for $DivIVA_{Ef}$/MLJD1 interaction.

Figure 23

A

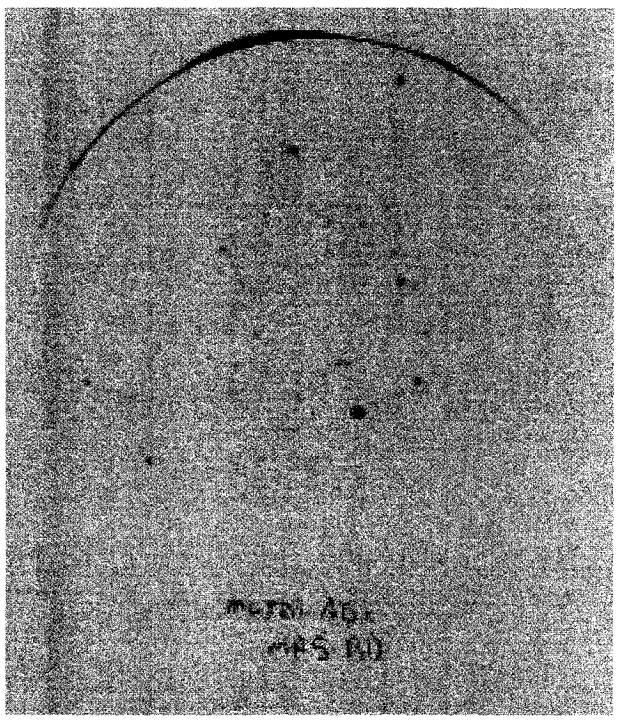

B

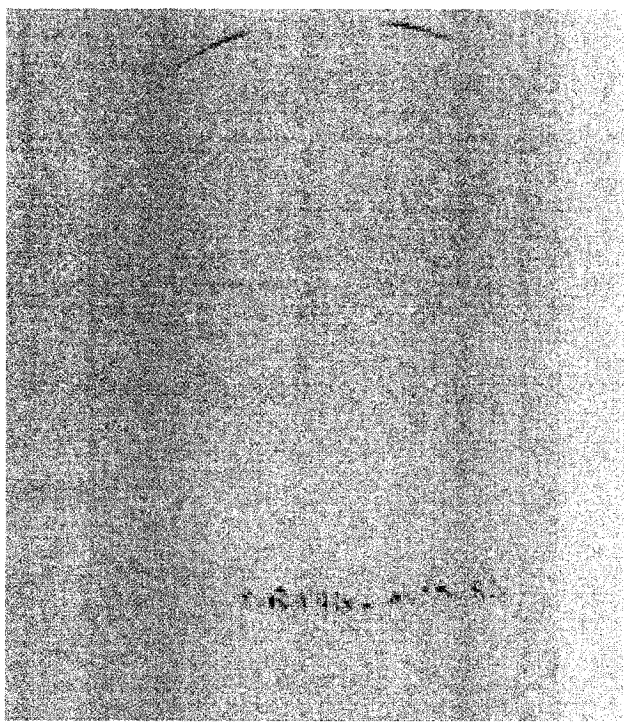

C

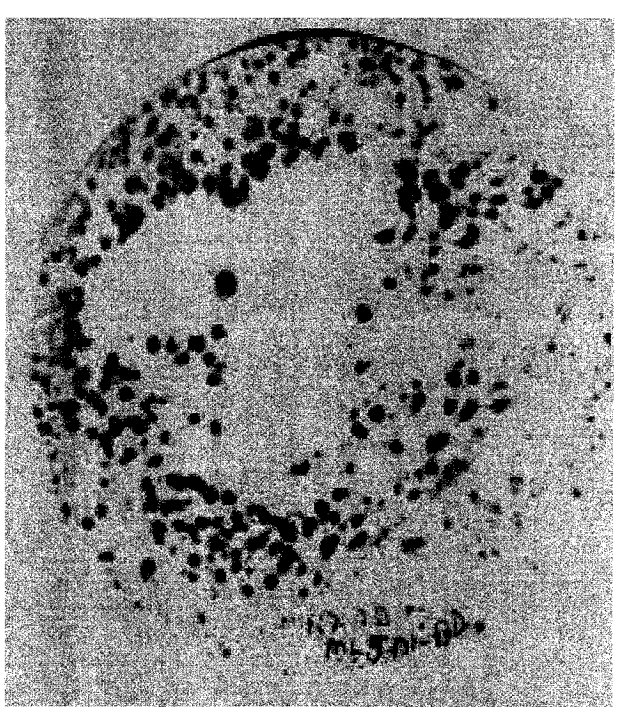

D

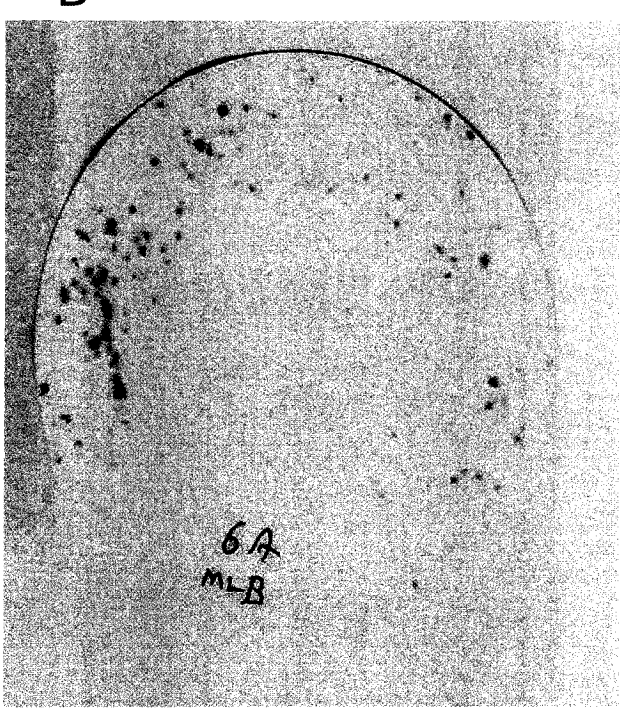

3.8 Preliminary DivIVA Localization studies

3.8.1 Localization in heterologous backgrounds

Localization of both GFP-DivIVA$_{Ef}$ and DivIVA$_{Ef}$-GFP in *E. coli* produced inconclusive results. When *E. coli* PB103 cells expressing the N-terminal GFP fusion to DivIVA$_{Ef}$ were examined microscopically, GFP appeared to localize at or near the cell poles in 80-90% of the cell population (Figure 24A`). However, bright field examination of the same cells showed inclusion bodies (indicated by arrows) in the same area, indicating that the observed GFP-DivIVA$_{Ef}$ fluorescence was not indicative of proper protein localization (Figure 24A). Unlike the N-terminal GFP fusion, PB103 expressing DivIVA$_{Ef}$ with a C-terminal GFP fusion showed very little fluorescence (data not shown). However, in cells where fluorescence was present it co-localized with inclusion bodies similar to the N-terminal fusion (data not shown).

Preliminary experiments expressing DivIVA$_{Ef}$-GFP in a *B. subtilis* background also produced inconclusive results. Although fluorescence was observed when *B. subtilis* cells were induced with 0.5% xylose to express the DivIVA$_{Ef}$-GFP fusion but not DivIVA$_{Bs}$ (Figure 24B`), a large number of inclusion bodies were seen distributed over the length of the cells (Figure 24B). It was later found that the plasmid used to transform *B. subtilis* carried an aspartic acid to methionine mutation at position 24 (D24M). Although several attempts were made to reconstruct the plasmid, random mutations were found in all subsequent plasmids. Attempts to work with a neutral arginine to lysine mutation at residue 188 (R188K) did not produce any fluorescence when incubated at either 30°C or 37°C. Despite confirming that the *amyE* gene was disrupted using starch-iodine testing, the *divIVA$_{Ef}$-gfp* fusion could not be amplified by PCR, suggesting that

Figure 24 – Attempts to localize DivIVA$_{Ef}$ heterologously in *E. coli* and *B. subtilis* by GFP fluorescence

A) Bright field (A) and fluorescence (A`) images for EGFP-DivIVA$_{Ef}$ localization in *E. coli* PB103. Samples were induced with 10 mM IPTG for two hours prior to mounting and imaging. Bright field (B) and fluorescence (B`) images for DivIVA$_{Ef}$-EGFP localization in *B. subtilis* 1756. Samples were induced with 0.5% xylose for two hours prior to mounting and imaging. Examples of inclusion bodies are indicated by arrows.

Figure 24

A

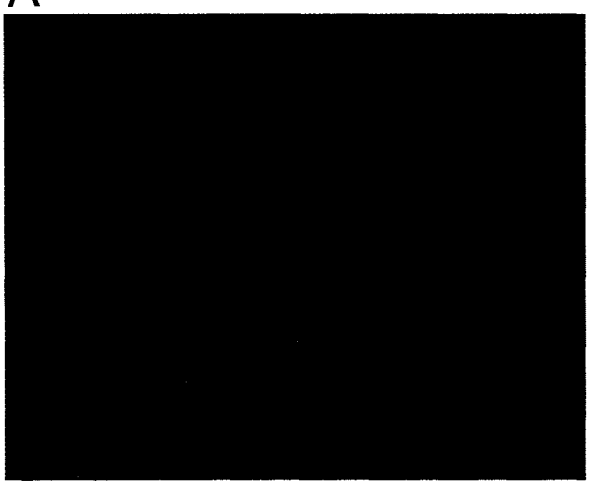

A`

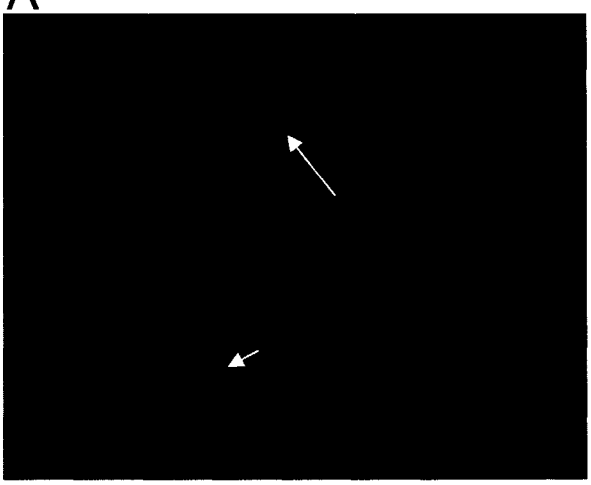

B

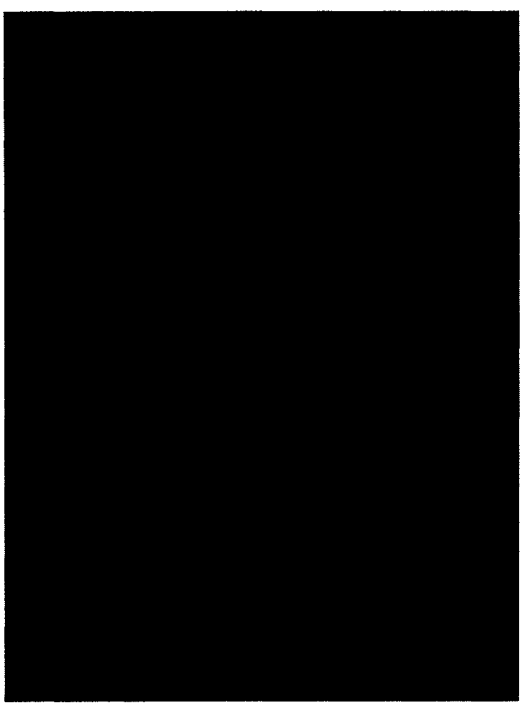

B`

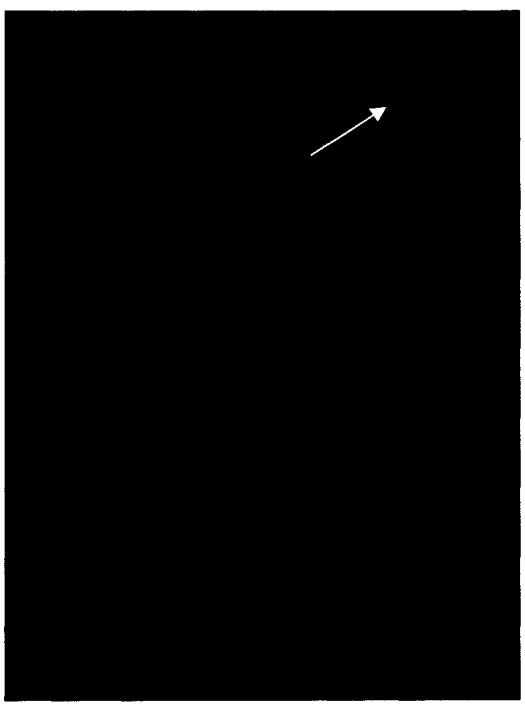

proper recombination between the plasmid and chromosome did not occur (data not shown).

3.8.2 Immunogold localization

Immunogold localization of $DivIVA_{Ef}$ in its native *E. faecalis* background revealed that the protein is associated primarily with the division septum and also localizes to cell poles. Of 19 cells observed that showed distinct localization, 8 showed localization primarily at the division septum (Figure 25A), 8 showed localization at the cell pole (Figure 25B), and 3 showed a band approximately halfway between the division septum and the cell pole (not shown).

Figure 25 – Immunogold localization of DivIVA in *Enterococcus faecalis* by electron microscopy

Immunogold localization of $DivIVA_{Ef}$ in *Enterococcus faecalis* demonstrating septal localization (A) and polar localization (B). α-$DivIVA_{Ef}$ was used at a final dilution of 1:250.

Figure 25

A

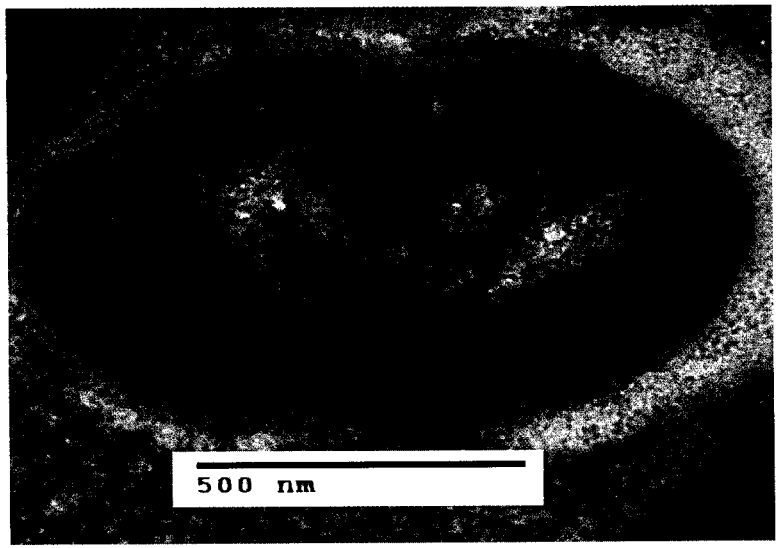

B

Discussion

4.1 Significance of this study

To date, most research involving DivIVA homologs has focused on division site localization and the effect of disrupting *divIVA* on cell division. Recently, Muchova *et al.* (2002a, b) and Stahlberg *et al.* (2004) began investigating the structure of DivIVA from *B. subtilis*. However, there has not been a detailed study of the biochemistry of DivIVA to determine what domains are responsible for the various properties of the protein, which include division site localization, oligomer formation and interaction with other proteins. This study has established that the central coiled-coil domain(s) of DivIVA are responsible for oligomerization and provides data that identifies the domain of DivIVA that interacts with the cell division protein MLJD1. This is also the first study to examine the biochemical properties of DivIVA from coccal bacteria.

4.2 Aberrant SDS-PAGE migration of $DivIVA_{Ef}$ is caused by excessive negative charge

As shown in Figure 9A, $DivIVA_{Ef}$ has a lower than expected mobility in SDS-PAGE, resulting in an observed molecular weight higher than expected by bioinformatic analysis. This aberrant SDS-PAGE mobility has been reported for a variety of proteins including the DNA repair protein XPA (Iakoucheva *et al.*, 2001), human papillomavirus E7 protein (Armstrong and Roman, 1993), *Cucumovirus* coat proteins (Hu and Ghabrial 1995), and the 70K U1 snRNP protein (Query *et al.*, 1989). It has been reported that several factors, including post-translational modifications such as phosphorylation or glycosylation, incomplete disulfide bond reduction, excessive positive or negative charge, or association of globular domains through flexible linkers containing unusual amino acid compositions (Iakoucheva *et al.*, 2001) can contribute to aberrant SDS-PAGE mobility.

Since Western blotting of purified DivIVA$_{Ef}$ and DivIVA in *E. faecalis* cell lysates show identical mobility (Figure 9B), the decreased mobility is not caused by sample preparation. While post-translational modifications are generally thought not to occur in prokaryotes, proteins in pathogenic bacteria including *E. coli and N. gonorrhoeae* and even some archaeal organisms have been shown to by glycosylated (Benz and Schmidt, 2002; Schmidt *et al.*, 2003). However, post-translational glycosylation was not demonstrated for DivIVA$_{Ef}$ (Figure 10B).

As mentioned previously, overall charge of a protein has been demonstrated to affect electrophoretic mobility in SDS-PAGE. Analysis of the predicted protein charge of DivIVA$_{Ef}$ and the deletion constructs MR6, MR7, and MR9 has demonstrated that as the charge on the protein decreases, the electrophoretic mobility becomes less aberrant, suggesting that charge is playing a role in DivIVA$_{Ef}$ migration. A charge of -22 has been shown to be sufficient to induce aberrant mobility of proteins in SDS-PAGE while protein samples show normal migration at a charge of -18 (Armstrong and Roman, 1993). While the overall charge of the protein does not account for the discrepancy between the observed and predicted molecular weight of DivIVA$_{Ef}$, it does appear to be a major contributor. Due to the net negative charge of the protein, SDS molecules are repelled from the protein and cannot coat the protein in a uniform fashion, as is assumed when calculating molecular mass based on electrophoretic mobility (Hu and Ghabrail, 1995).

This also explains why the addition of urea did not affect the electrophoretic mobility of DivIVA$_{Ef}$ (Figure 10A). Urea acts to cause protein denaturation by binding to the protein, similar to SDS (Monera *et al.*, 1994). Unlike SDS, urea is a neutrally charged molecule and thus cannot compensate for any charge imbalance on the protein

sample (Monera *et al.*, 1994). It is possible that using guanidine hydrochloride, a salt that acts as a protein denaturant at high concentration, would counteract the net charge of $DivIVA_{Ef}$ and allow proper electrophoretic mobility to occur (Monera *et al.*, 1994).

4.3 Native gel electrophoresis provides a more accurate estimate of the monomer content of the full sized DivIVA complex than size exclusion chromatography

As noted in Tables 5 and 6, there is a large discrepancy between the calculated monomer content obtained by size exclusion chromatography and native gel electrophoresis. The cause of this discrepancy is caused by the shape of the $DivIVA_{Ef}$ particle. Size exclusion chromatography assumes that the sample being analyzed occupies a spherical volume (Amersham Biosciences Gel Filtration Handbook, Edition A1). However, as demonstrated by Stahlberg *et al.* (2004), DivIVA forms an elongated particle which they described as a "doggy bone". In this elongated conformation, DivIVA is mostly excluded from the pores present in the gel matrix, allowing the sample to elute at a volume corresponding to a molecular weight much higher than the actual size of the particle. In contrast, the "doggy bone" structure of DivIVA is ideally suited to native gel electrophoresis experiments. In its elongated conformation, DivIVA will migrate through the gel more efficiently than a spherical protein of the same molecular weight and arrive at its "buoyancy point" sooner. As such, native gel electrophoresis provides a more accurate estimation of the actual number of monomers present in the "doggy bone" complex. Since experiments on DivIVA from both *B. subtilis* and *E. faecalis* estimate the number of monomers in the complex at between 10 and 12 (Muchova *et al.*, 2002a), it is probable that DivIVA homologs from other organisms will have a similar complex size.

4.4 Decreased interaction strength of N-terminal mutants MR1 through MR5 as measured by yeast two hybrid assays

The decreased strength of interaction of the N-terminal mutants MR1 through MR5 as compared to the wild type DivIVA$_{Ef}$ is intriguing since the oligomer size of the mutant proteins is unaltered. While Circular Dichroism (CD) analysis has demonstrated that the secondary structures of DivIVA$_{Ef}$ and N-terminal mutants are very similar, the minimum at 208 nm becoming slightly more pronounced for the MR4 and MR5 proteins may indicate a slight shift in helix type (Figure 15). It has been reported that the CD spectrum of proteins containing coiled-coil domains have a molar ellipticity ratio for the minima at 208 and 220 nm of approximately 1 while the spectrum of a normal α-helix shows a more pronounced minimum at 208 nm (Monera *et al.*, 1994). This suggests that the mutations are relaxing the supercoiled α–helix of the N-terminal coiled-coil domain, which contains 3.5 residues per turn, into normal α-helices, which contain 3.6 residues per turn (Lupas, 1996, Voet *et al.*, 1999). However, additional experiments using different concentrations of the various proteins would be required to confirm this hypothesis. It is possible that the disruption of the supercoiled α-helices of the N-terminal coiled-coil domain by the mutations creates a slight steric hindrance between DivIVA$_{Ef}$ monomers, thus slowing the interaction rate. The N-terminal coiled-coil domain ends at approximately residue 75 and the central coiled-coil domains begin at approximately residue 95 (Figure 8). As such, there appears to be enough of a gap to allow proper interaction. However, without an appropriate model of the three dimensional structure of monomeric DivIVA$_{Ef}$, the proximity of these residues upon folding cannot be determined. This interaction between monomers containing N-terminal

mutations despite potential conformational changes suggests that once the coiled-coil association is made between the $DivIVA_{Ef}$ monomers that the interaction is quite stable.

4.5 Oligomerization of $DivIVA_{Ef}$ is mediated by coiled-coil interactions of the central domains

In support of my hypothesis that coiled-coil interactions mediate $DivIVA_{Ef}$ oligomerization, my data indicates that the two central coiled-coil domains of $DivIVA_{Ef}$ are responsible for oligomer formation. While the central location of these domains is constant between various DivIVA homologs (Figure 6), the amino acid sequence of this region is poorly conserved between species (Figure 5). In turn, this observation coupled with the results of this study suggests that the coiled-coil structure itself and not the individual amino acids that make up the domains are responsible for $DivIVA_{Ef}$ oligomer formation.

4.6 Proposed model for $DivIVA_{Ef}$ oligomerization

A model for $DivIVA_{Bs}$ oligomerization was proposed by Stahlberg *et al* (2004); however the results of my experiments suggest a different model of oligomer formation. Although the tertiary structure for $DivIVA_{Ef}$ has not been examined, it is likely that its tertiary structure is very similar to $DivIVA_{Bs}$. Despite the differences in length between DivIVA from *B. subtilis* (190 amino acids) and *E. faecalis* (233 amino acids), there is approximately 36% identity between the two proteins. According to homology modelling, by using *B. subtilis* DivIVA as a template for *E. faecalis* DivIVA, the resulting model should result in greater than 85% of the α-carbon atoms being within 3.5 angstroms of their correct position due to the identity between the two proteins (Burley and Bonanno, 2002).

The model proposed by Stahlberg *et al.* (2004) suggests that the individual $DivIVA_{Bs}$ monomers that form the "doggy bone" oligomer particle are composed of DivIVA dimers that are arranged in a stacked formation with the N and C termini both providing the site of monomer interaction in the middle of the structure and representing the top and bottom of the particle, similar to an α-keratin dimer (Figure 26). As shown in Figure 26C, DivIVA is proposed to first associates as linear dimers, represented by the red, blue, and black lines, and subsequently these dimers arrange themselves to form the final "doggy bone" structure. Following the Stalhberg *et al.* (2004) model, the DivIVA protein complex should be observable only as dimers or a full sized complex and a species corresponding to 50% of the full complex should not be observed. However, my results indicate disruption of the central coiled-coil domains results in a 50% decrease and then abrogated self interaction. It has also been demonstrated that $DivIVA_{Bs}$ forms a species half the size of the wild type complex when the L120P mutation is present (Muchova *et al.*, 2002a). Based on the Stahlberg model, the central coiled-coil domains can be though of as clover leafs extending above and below the plane of each monomer (Figure 27A). To apply the results of this study to the Stahlberg model in terms of orienting the DivIVA monomers, one of the coiled-coil domains is used for dimerization and the second to interact with other DivIVA dimers to form the "doggy bone" complex (Figure 27B). Subsequently, disruption or deletion of one of the coiled-coil domains would result in a population of DivIVA dimers instead of the 50% decrease observed in this study (Figure 27C). Also, a clover leaf-type model does not provide a mechanism to explain why the DivIVA complex is limited to 6-10 monomers instead of polymerizing into a complex containing an unlimited number of monomers.

Figure 26 - Comparison of transmission electron microscopy (TEM) model of DivIVA from *B. subtilis* to the coiled-coil protein α-keratin.

A) α-keratin dimer demonstrating polar arrangement of the N-termini and C-termini. Adapted from Voet *et al.*, 1999. B) TEM image of $DivIVA_{Bs}$ "doggy bone" particle, adapted from Stahlberg *et al.*, 2004. C) Model for DivIVA organization in the "doggy bone" particles proposed by Stahlberg *et al* (2004). Each coloured strand represents a $DivIVA_{Bs}$ dimer.

Figure 26

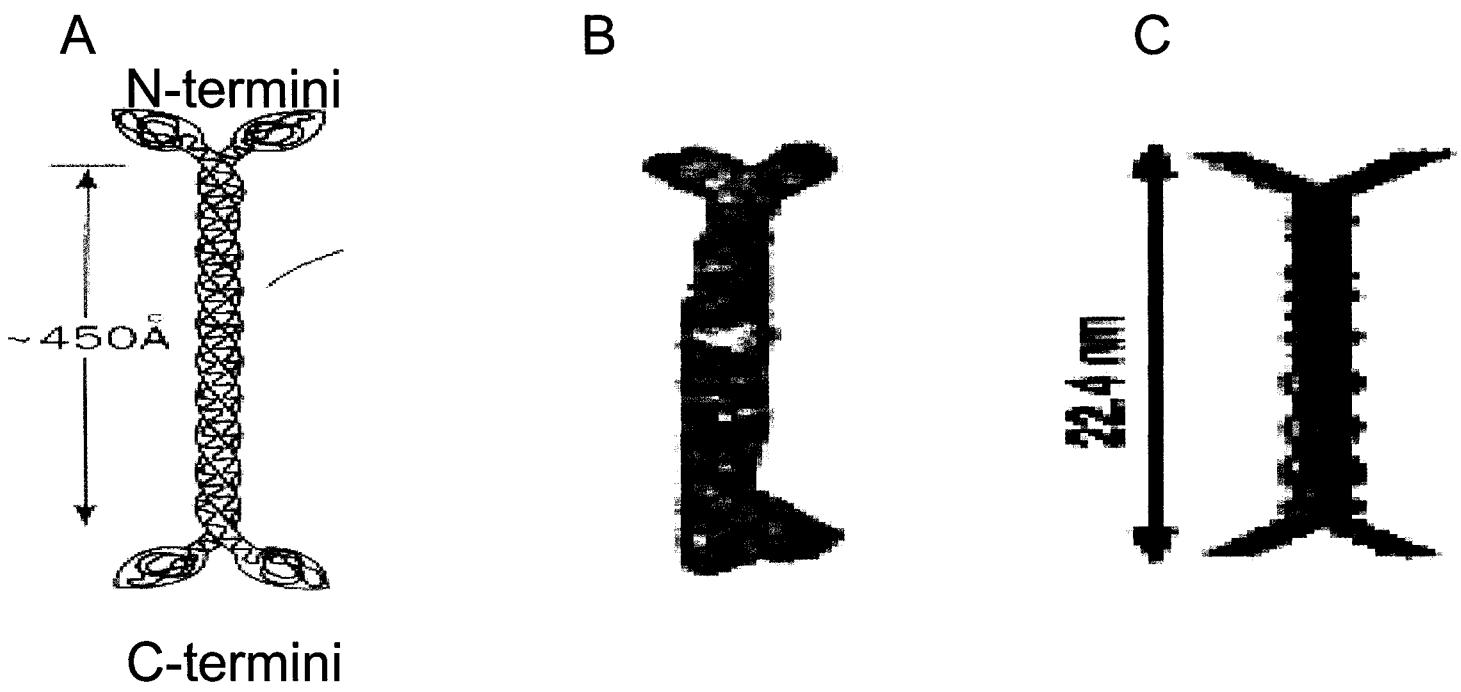

Figure 27 – Cloverleaf model for DivIVA oligomerization

Applying the results of this study to the model proposed by Stahlberg *et al.* A) A DivIVA monomer with the coiled-coil domains represented in gold, the N-terminal in blue and the C-terminal in red. B) Interaction between two DivIVA dimers following the cloverleaf model. In this situation, one coiled-coil domain from each monomer is used for dimerization and the second coiled-coil domain is responsible for inter-dimer interactions. C) Model of cloverleaf association with one of the central coiled-coil domains disrupted. Under these conditions, only DivIVA dimers can form.

Figure 27

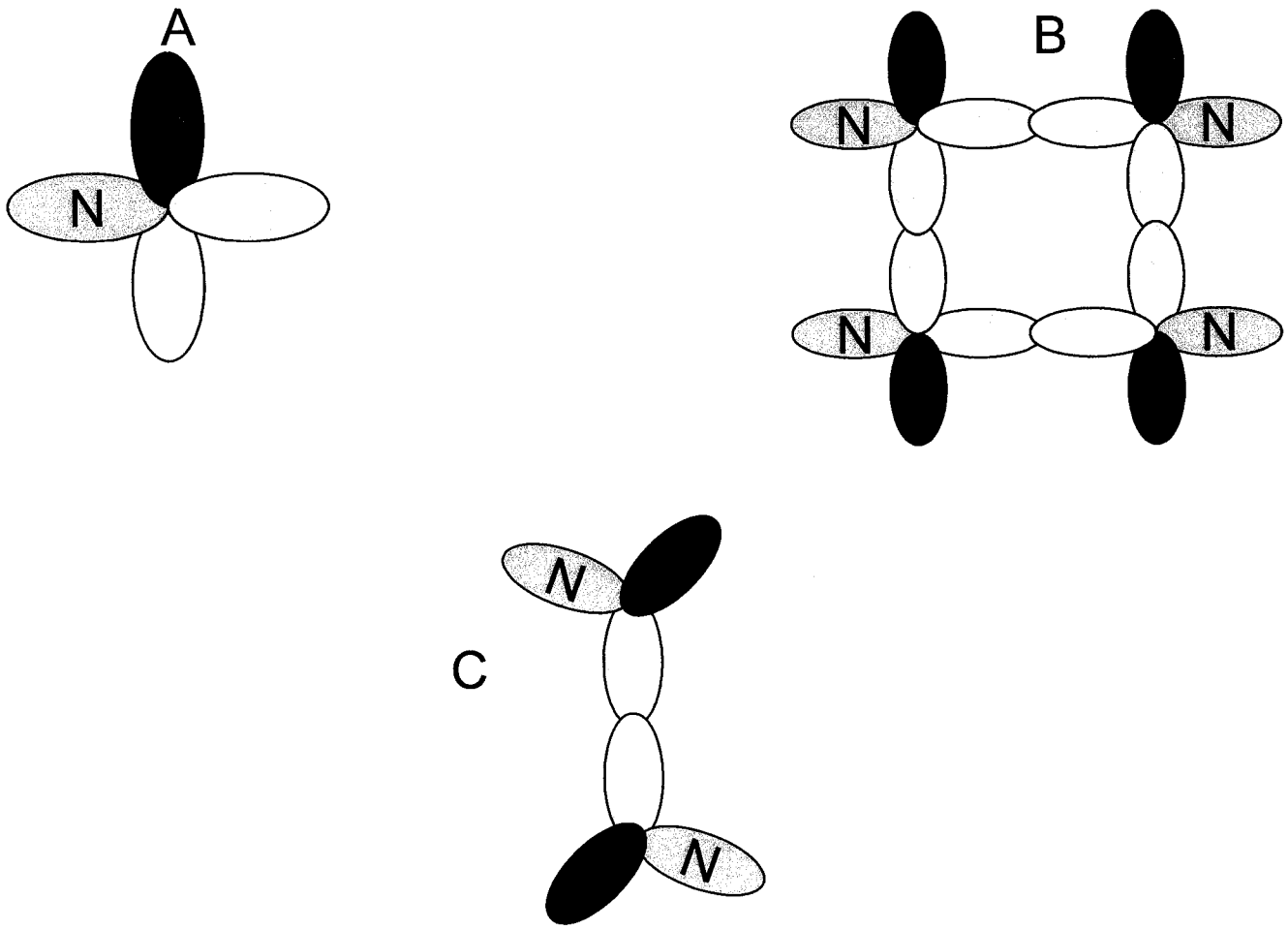

As such, I am proposing a zipper model for DivIVA oligomerization. My yeast two hybrid data indicates that the two central coiled-coil domains do not interact with their corresponding domain on another monomer but rather with the opposite domain. Specifically, domain 2 only interacts with domain 3 since no interaction is seen when mutations are tested against themselves, however interaction with the wild type protein is maintained (Table 6, Figure 28B). This suggests that monomers come together in either a staggered (Figure 28) or step (Figure 29) formation. Since the central coiled-coil domains of DivIVA are predicted to have a three stranded structure, it is possible for the domains to extend both above and below the plane of the monomer, allowing binding on the top and bottom faces to create a stacked array (Figure 28C, 29A). This array would be capped at 3-4 monomers either by electrostatic repulsion of the C-termini, which carries a net charge of -13 from the end of the central coiled-coil domains to the end of the C-terminus in the case of *E. faecalis*, or more probably by steric hindrance from the approximately 100 amino acids that make up the N-terminus, or an as yet unidentified method. As demonstrated in figure 28D and 29B, this stacked array allows for incorporation of a second array beside the first one, generating the 6-8 monomer DivIVA "doggy bone" particle. It is presently not possible to determine whether the step or staggered arrangement of the arrays is the correct one since both will result in a "doggy bone" structure similar to that observed by Stahlberg *et al.* However, the step conformation would facilitate interaction between the monomers in each "doggy bone" particles. Both the step and staggered conformation allow formation of the higher order structures described below. Also, the free N-terminal and C-terminal at the "top" and

Figure 28 - Staggered zipper model of DivIVA oligomerization.

A) DivIVA monomer showing the N-terminal (Blue), C-terminal (Red) and central coiled-coil domains (numbered 2 and 3). B) Dimerization occurs by interaction between domain 2 of one monomer and domain 3 of another monomer. C) Stacked array representing one side of the DivIVA staggered zipper oligomer. D) Complete DivIVA oligomer consisting of 8 staggered zipper monomers.

Figure 28

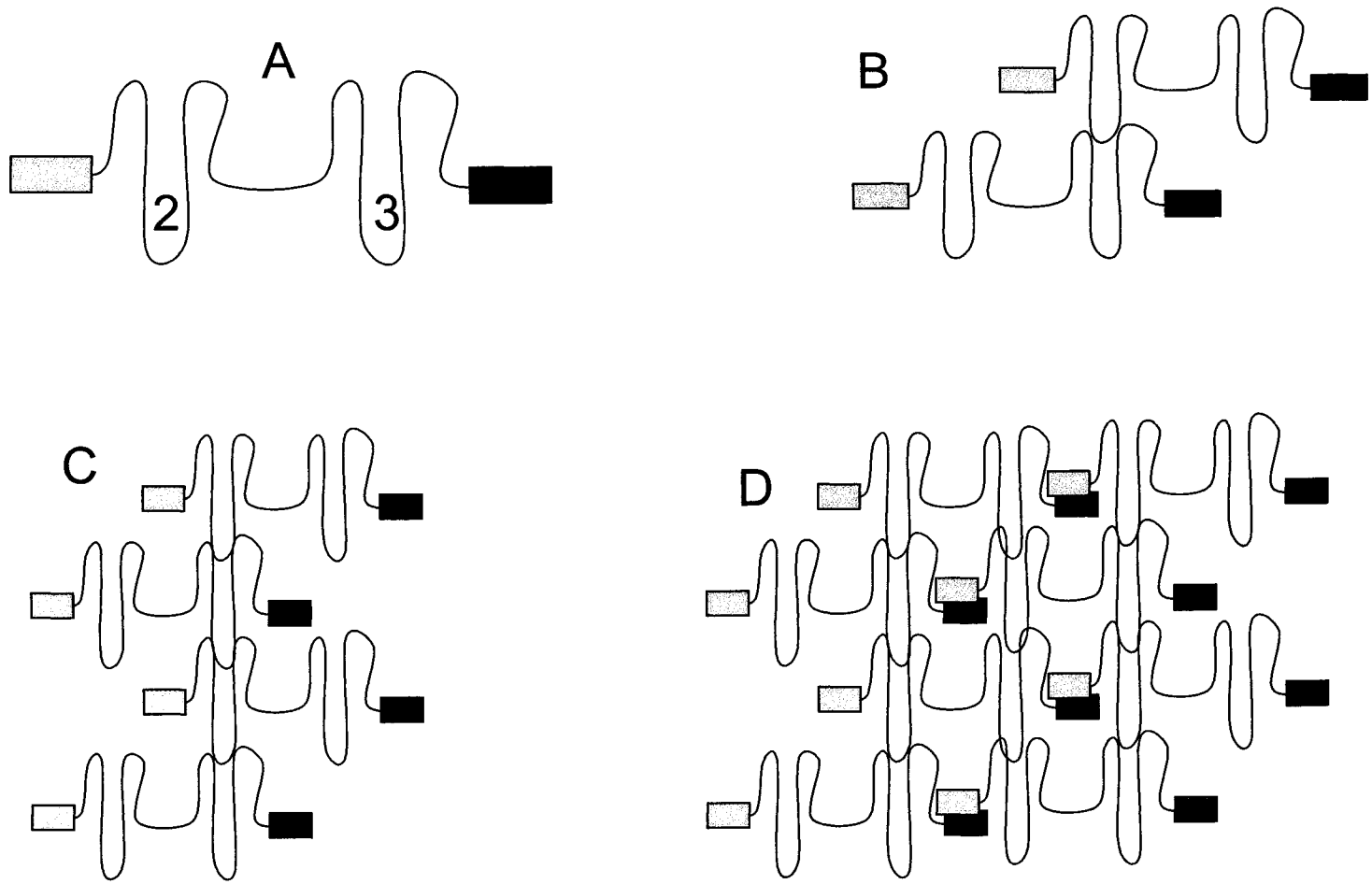

Figure 29 - Step model of DivIVA oligomerization.

A) Stacked array representing one side of the array. B) Full DivIVA step zipper complex comprising 8 monomers. N-termini and C-termini are shown in Blue and Red respectively

Figure 29

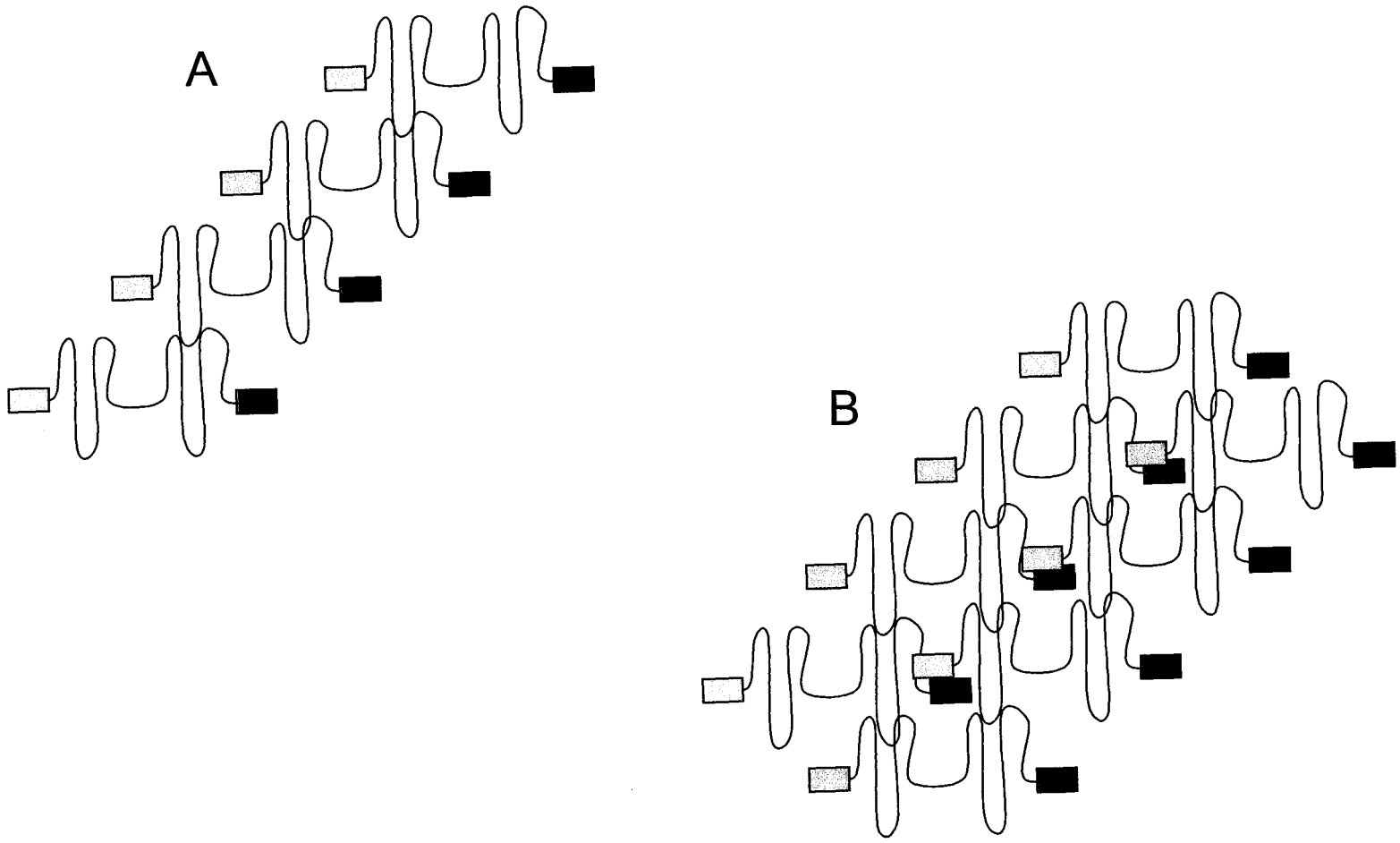

bottom" of the step arrangements could form the tips of the "doggy bone" structure with greater ease due to lack of steric interference as demonstrated in Figure 30.

This zipper model also allows for co-ordination of the highly conserved N-termini of each monomer in the "doggy bone", which would facilitate the proposed division site localization role of the N-terminus. This co-ordination of the N-termini would naturally lead to co-ordination of each monomer's C-terminus, allowing for the electrostatic repulsion to produce the capping as described above. While co-ordination is also possible for the Stahlberg model, it is more likely that the N-terminus and C-terminus are arranged opposite each other in at the top and bottom of the "doggy bone" particle similar to α-keratin. However, if each "tip" represents 4 N-termini or C-termini then the electrostatic or stearic effects discussed above would be even more prominent and the complex potentially very difficult to assemble.

Stahlberg *et al.* (2004) were able to image not only the "doggy bone" particle but also several higher order DivIVA complexes. While no model for assembly of the "doggy bone" particles is presented by Stahlberg *et al.* (2004), the formation of the higher order complexes can be explained using the zipper model since the various higher order complexes can be assembled using the open faces of the "doggy bone" zipper particle shown in figures 28D and 29B. It is likely that the individual particles assemble so that the N-terminal and C-terminal domains are on the same side of the "doggy bone" as the adjoining particle however would not be directly aligned in order to overcome the capping effects of the individual particles.

Although the zipper model suggests that DivIVA complex formation should be completely abolished when either of the central coiled-coil domains is disrupted, my

Figure 30 - Three dimensional schematic of DivIVA monomer locations inside the "doggy bone" complex based on the zipper model

Front (A), Side (B) and Top (C) views. As with the other models, the N-termini of various monomers are shown in blue, C-termini in red, and coiled-coil domains (in B and C) in gold.

Figure 30

A – Front view

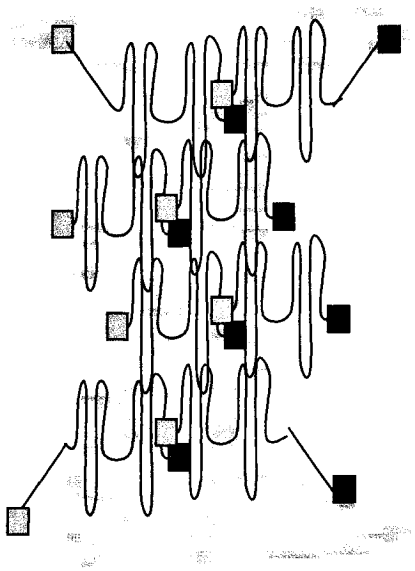

B – Side view

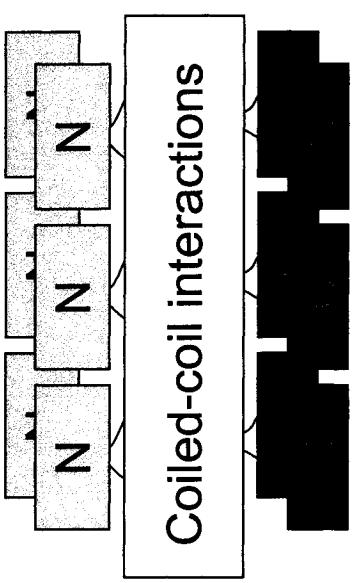

C – Top view

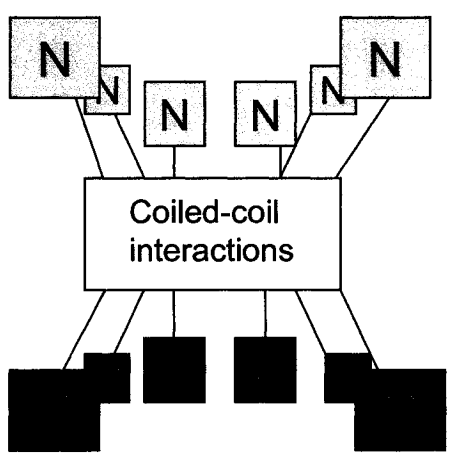

results indicate that only a 50% decrease occurs when disrupting or deleting only one of the two domains (Table 6). This suggests that the central coiled-coil domains can still interact with their corresponding domains to a certain degree. This is contrary to my yeast two hybrid data that indicates that the central coiled-coil domains only interact in a staggered fashion. One possible explanation is that the coiled-coil domains are not completely disrupted as predicted by bioinformatics. This is apparent when looking at the size exclusion chromatography data for MR11. According to the coiled-coil domain prediction software (Fig 20B), the first of the two central coiled-coil domains is abrogated by the L104P mutation, which should correspond to a 50% decrease in $DivIVA_{Ef}$ oligomerization. However, as shown in Table 6, the complex size for MR11 remains identical to the wild type protein by gel filtration analysis and shows a mixture of full complex size and a 50% decreased complex as measured by native gel electrophoresis. This suggests that there are still enough residues present after the mutation to form a partial coiled-coil domain that could maintain interaction with the other $DivIVA_{Ef}$ monomers.

While the possibility of improper coiled-coil domain predictions can explain the discrepancy observed for MR11, it cannot explain the oligomerization of the deletion mutants MR7 and MR9. In these cases, the residues that make up either of the two central coiled-coil domains are removed entirely, leaving no possibility of forming a coiled-coil structure to help maintain oligomerization. This further suggests that domains 2 and 3 are capable of interaction with their corresponding domains on another monomer. However, this arrangement would only allow one side of the "zipper" to form since there would be no other coiled-coil domain for the second half of the zipper to interact with,

resulting in the 50% decrease in complex size indicated by both size exclusion chromatography and native gel electrophoresis. This could also explain why higher order aggregates of DivIVA were not seen with the DivIVA2 mutation, which also shows decreased self interaction (Muchova *et al.,* 2002a, Stahlberg *et al.,* 2004).

Taken together, this information suggests that the interaction between the two central coiled-coil domains is a preferential arrangement that allows for the largest complex to form. In turn, the potential preferential arrangement implies that complex formation is extremely important for proper DivIVA function. In fact, it has been shown that disruption of the DivIVA oligomer (e.g. DivIVA2) can result in severe defects in cell division of *B. subtilis* (Muchova *et al.,* 2002a)

In order to answer some of the questions surrounding the model, transmission electron microscopy of my C-terminal $DivIVA_{Ef}$ deletion (MR6) could serve to indicate how the N-termini and C-termini are arranged in the "doggy bone" particle. Since I have demonstrated that this deletion has no effect on oligomer formation, I believe the differences between the wild type and truncated images would reveal a significant amount of information which could be used to refine the zipper model.

4.7 Role of the remaining domains of $DivIVA_{Ef}$

While the role of the remaining domains of $DivIVA_{Ef}$ cannot be determined in this study, hypothetical roles of these domains based on data collected in this study and available literature on DivIVA can be proposed. First, due to the high sequence conservation the N-terminal domain is likely involved in division site localization. Previous results demonstrating that $DivIVA_{Bs}$ can localize to sites of nascent and used cell division in both prokaryotes and the eukaryote *Schizosaccharomyces pombe*

(Edwards *et al.,* 2000) suggest that DivIVA recognizes a highly conserved component of the cell division apparatus. This hypothesis can be tested once proper GFP localization experiments can be conducted on both $DivIVA_{Ef}$ and mutations that affect the highly conserved residues of $DivIVA_{Ef}$ such as the L29D and E37P mutations. With regards to the C-terminus of DivIVA, the variability in protein length of the various DivIVA homologs, as well as the inconsistent predictions of a coiled-coil domain, suggest that this region of $DivIVA_{Ef}$ is involved in species-specific interactions, possibly involving hitherto unidentified DivIVA binding proteins.

4.8 $DivIVA_{Ef}$/MLJD1 interaction occurs between amino acids 60 and 100 of $DivIVA_{Ef}$

Yeast two hybrid studies demonstrated that $DivIVA_{Ef}$ and MLJD1 interact between residues 60 and 130 of $DivIVA_{Ef}$. Since the central coiled-coil domains occur approximately between residues 100 and 150 of $DivIVA_{Ef}$, the region between residues 100 and 130 is unavailable for interaction with MLJD1. As such, this leaves the region between residues 60 and 100 available for interaction. Further interaction studies should be able to narrow this region even further and subsequently specify the residues of MLJD1 that are required for interaction with $DivIVA_{Ef}$.

4.9 Future refinements for GFP localization Experiments

Localization of DivIVA in various organisms has predominantly been done using a C-terminal GFP fusion (Edwards and Errington, 1997, Edwards *et al.,* 2000, Ding *et al.,* 2002). Also, publications dealing with purified DivIVA always use a C-terminal 6xHis tag (Muchova *et al.,* 2002a, b, Stahlberg *et al.,* 2004). This implies that the N-terminal must remain unaltered for proper DivIVA function. In this study, I attempted both N-terminal and C-terminal GFP fusions to $DivIVA_{Ef}$, both of which resulted in the

formation of inclusion bodies. For the N-terminal fusion, I believe the formation of inclusion bodies and subsequent lack of localization was caused either by improper folding of DivIVA$_{Ef}$ caused by the fusion or blockage of localization caused by the placement of GFP. Blockage of localization is the more probable explanation if my earlier hypothesis that the N-terminus of DivIVA$_{Ef}$ is responsible for localization is correct. In this scenario, the large number of GFP molecules brought together by DivIVA$_{Ef}$ oligomerization would prevent proper localization. The resulting non-functional protein complex would then become an inclusion body as seen in Figure 24.

For the C-terminal GFP fusion, inclusion body formation was most likely caused by a frameshift between *divIVA$_{Ef}$* and the upstream *lacZ*. Although *divIVA$_{Ef}$* and *gfp* are properly aligned as confirmed by DNA sequencing, the restriction sites selected for cloning (*Bam*HI and *Nco*I) also allow GFP expression starting from the *lacZ* start codon. Briefly, inserting *divIVA$_{Ef}$* at the *Bam*HI site results in a +2 frameshift from *lacZ*. To ensure proper fusion to *gfp*, a single nucleotide must be added at the end of *divIVA$_{Ef}$* to compensate for the *gfp* start codon being in the middle of the *Nco*I site, yielding a +3, or in frame, product with *lacZ*. As such, there is no way to determine whether expressed GFP was generated from the DivIVA$_{Ef}$ start codon or the LacZ start codon. This problem can be resolved by adding a nucleotide between *Bam*HI and *divIVA$_{Ef}$* to ensure that GFP can only be expressed in one reading frame.

With regards to *B. subtilis* localization, while the mutations present in DivIVA$_{Ef}$ undoubtedly affected the experiments, the major problem being faced is the native DivIVA$_{Bs}$. Experiments performed in Dr. Dillon's lab have shown that *divIVA$_{Ef}$* does not complement a *divIVA$_{Bs}$* knockout, although the two DivIVA proteins do interact

(Ramirez-Arcos *et al.*, unpublished data; Liao *et al.*, unpublished data). As such, $DivIVA_{Bs}$ expression must be significantly decreased in order to observe $DivIVA_{Ef}$ localization, which is possible using *B. subtilis* 1756 since $divIVA_{Bs}$ is under the control of the IPTG inducible P_{spac} promoter (Edwards and Errington, 1997). However, when the amount of $DivIVA_{Bs}$ is decreased, *B. subtilis* can no longer divide properly and forms long rods similar to those shown in Figure 24B (Cha and Stewart, 1997, Edwards and Errington, 1997). Thus, any DivIVA localization that occurs happens in a cell that is not behaving normally. It may be preferable to attempt the localization experiments in a *B. subtilis* strain lacking both *divIVA* and *minD* since the double mutation has been shown to divide almost normally (Edwards and Errington, 1997).

4.10 Applicability of this study to other DivIVA homologs

Despite the variation in primary sequence and length of the various known DivIVA homologs, the results of this study can be broadly applied. As mentioned previously, coiled-coil predictions of various DivIVA homologs show similar trends across species (Figure 6). While there is variability in the size of the individual domains, their relative positions and sizes are similar. Previous work done by Muchova *et al.* (2002a) has demonstrated that a mutation of $DivIVA_{Bs}$ at position 120 (L120P) results in decreased self interaction. I have demonstrated that the corresponding mutation of $DivIVA_{Ef}$ (L143P, MR10) also shows decreased self interaction, indicating that mutations corresponding to those I created in *E. faecalis* should produce similar results in other DivIVA homologs. The biological significance of DivIVA oligomerization requires further analysis; however this work is an important step in understanding the properties of DivIVA not only in *E. faecalis* but also in other bacteria having DivIVA homologs.

Subsequent work on DivIVA should help illuminate its role in cell division and chromosome segregation and produce a model from Gram positive cell division that may be used to create future antibiotics.

References

1. **Aarestrup, F. M., P. Butaye, and W. Witte.** 2002. Nonhuman Reservoirs of Enterococci, p. 55-99. *In* The Enterococci: Pathogenesis, Molecular Biology and Antibiotic Resistance. M. S. Gilmore (ed.), ASM Press, Washington, D.C.

2. **Amersham Biosciences.** 2002. Gel Filtration: Principles and Methods. Amersham Biosciences.

3. **Armstrong, D. J. and A. Roman.** 1993. The anomalous electrophoretic behavior of the human papillomavirus type 16 E7 protein is due to the high content of acidic amino acid residues. Biochem.Biophys.Res.Commun. **192**:1380-1387.

4. **Bateman, A.** 1997. The structure of a domain common to archaebacteria and the homocystinuria disease protein. Trends Biochem.Sci. **22**:12-13.

5. **Begg, K. J. and W. D. Donachie.** 1985. Cell shape and division in *Escherichia coli*: experiments with shape and division mutants. J.Bacteriol. **163**:615-622.

6. **Benz, I. and M. A. Schmidt.** 2002. Never say never again: protein glycosylation in pathogenic bacteria. Mol.Microbiol. **45**:267-276.

7. **Bi, E. F. and J. Lutkenhaus.** 1991. FtsZ ring structure associated with division in *Escherichia coli.* Nature **354**:161-164.

8. **Bramhill, D. and C. M. Thompson** . 1994. GTP-dependent polymerization of *Escherichia coli* FtsZ protein to form tubules. Proc.Natl.Acad.Sci.U.S.A **91**:5813-5817.

9. **Burley, S. K. and J. B. Bonanno** . 2002. Structuring the universe of proteins. Annu.Rev.Genomics Hum.Genet. **3**:243-262.

10. **Cha, J. H. and G. C. Stewart.** 1997. The *divIVA* minicell locus of Bacillus subtilis. J.Bacteriol. **179**:1671-1683.

11. **Chien, C. T., P. L. Bartel, R. Sternglanz, and S. Fields.** 1991. The two-hybrid system: a method to identify and clone genes for proteins that interact with a protein of interest. Proc.Natl.Acad.Sci.U.S.A **88**:9578-9582.

12. **de Boer, P. A., R. E. Crossley, and L. I. Rothfield.** 1989. A division inhibitor and a topological specificity factor coded for by the minicell locus determine proper placement of the division septum in E. coli. Cell **56**:641-649.

13. **Dewar, S. J. and R. Dorazi.** 2000. Control of division gene expression in *Escherichia coli.* FEMS Microbiol.Lett. **187**:1-7.

14. **Ding, Z., Z. Zhao, S. J. Jakubowski, A. Krishnamohan, W. Margolin, and P. J. Christie.** 2002. A novel cytology-based, two-hybrid screen for bacteria applied to protein-protein interaction studies of a type IV secretion system. J.Bacteriol. **184**:5572-5582.

15. **Edwards, D. H. and J. Errington.** 1997. The *Bacillus subtilis* DivIVA protein targets to the division septum and controls the site specificity of cell division. Mol.Microbiol. **24**:905-915.

16. **Edwards, D. H., H. B. Thomaides, and J. Errington.** 2000. Promiscuous targeting of *Bacillus subtilis* cell division protein DivIVA to division sites in *Escherichia coli* and fission yeast. EMBO J. **19**:2719-2727.

17. **Errington, J.** 2001. Septation and chromosome segregation during sporulation in *Bacillus subtilis*. Curr.Opin.Microbiol. **4**:660-666.

18. **Fadda, D., C. Pischedda, F. Caldara, M. B. Whalen, D. Anderluzzi, E. Domenici, and O. Massidda.** 2003. Characterization of *divIVA* and other genes located in the chromosomal region downstream of the *dcw* cluster in *Streptococcus pneumoniae*. J.Bacteriol. **185**:6209-6214.

19. **Flardh, K.** 2003a. Essential role of DivIVA in polar growth and morphogenesis in *Streptomyces coelicolor* A3(2). Mol.Microbiol. **49**:1523-1536.

20. **Flardh, K.** 2003b. Growth polarity and cell division in Streptomyces. Curr.Opin.Microbiol. **6**:564-571.

21. **Francis, F., S. Ramirez-Arcos, H. Salimnia, C. Victor, and J. R. Dillon.** 2000. Organization and transcription of the division cell wall (*dcw*) cluster in *Neisseria gonorrhoeae*. Gene **251**:141-151.

22. **Fu, X., Y. L. Shih, Y. Zhang, and L. I. Rothfield.** 2001. The MinE ring required for proper placement of the division site is a mobile structure that changes its cellular location during the *Escherichia coli* division cycle. Proc.Natl.Acad.Sci.U.S.A **98**:980-985.

23. **Gilmore, M. S., P. S. Coburn, S. R. Nallapareddy, and B. E. Murray.** 2002. Enterococcal Virulence, p. 301-354. *In* The Enterococci: Pathogenesis, Molecular Biology and Antibiotic Resistance. M. S. Gilmore (ed.), ASM Press, Washington, D.C.

24. **Gilmour, M. W., J. E. Gunton, T. D. Lawley, and D. E. Taylor.** 2003. Interaction between the IncHI1 plasmid R27 coupling protein and type IV secretion system: TraG associates with the coiled-coil mating pair formation protein TrhB. Mol.Microbiol. **49**:105-116.

25. **Gugolya, Z., A. Muskotal, A. Sebestyen, Z. Dioszeghy, and F. Vonderviszt.** 2003. Interaction of the disordered terminal regions of flagellin upon flagellar filament formation. FEBS Lett. **535**:66-70.

26. **Hamoen, L. W. and J. Errington** . 2003. Polar targeting of DivIVA in *Bacillus subtilis* is not directly dependent on FtsZ or PBP 2B. J.Bacteriol. **185**:693-697.

27. **Harborth, J., J. Wang, C. Gueth-Hallonet, K. Weber, and M. Osborn.** 1999. Self assembly of NuMA: multiarm oligomers as structural units of a nuclear lattice. EMBO J. **18**:1689-1700.

28. **Harry, E. J.** 2001. Bacterial cell division: regulating Z-ring formation. Mol.Microbiol. **40**:795-803.

29. **Harry, E. J. and P. J. Lewis.** 2003. Early targeting of Min proteins to the cell poles in germinated spores of *Bacillus subtilis*: evidence for division apparatus-independent recruitment of Min proteins to the division site. Mol.Microbiol. **47**:37-48.

30. **Hebrard, E., M. Drucker, D. Leclerc, T. Hohn, M. Uzest, R. Froissart, J. M. Strub, S. Sanglier, A. van Dorsselaer, A. Padilla, G. Labesse, and S. Blanc.** 2001. Biochemical characterization of the helper component of Cauliflower mosaic virus. J.Virol. **75**:8538-8546.

31. **Hu, C. C. and S. A. Ghabrial.** 1995. The conserved, hydrophilic and arginine-rich N-terminal domain of cucumovirus coat proteins contributes to their anomalous electrophoretic mobilities in sodium dodecylsulfate-polyacrylamide gels. J.Virol.Methods **55**:367-379.

32. **Hu, Z., A. Mukherjee, S. Pichoff, and J. Lutkenhaus.** 1999. The MinC component of the division site selection system in *Escherichia coli* interacts with FtsZ to prevent polymerization. Proc.Natl.Acad.Sci.U.S.A **96**:14819-14824.

33. **Iakoucheva, L. M., A. L. Kimzey, C. D. Masselon, R. D. Smith, A. K. Dunker, and E. J. Ackerman**. 2001. Aberrant mobility phenomena of the DNA repair protein XPA. Protein Sci. **10**:1353-1362.

34. **Jones, L. J., R. Carballido-Lopez, and J. Errington**. 2001. Control of cell shape in bacteria: helical, actin-like filaments in *Bacillus subtilis*. Cell **104**:913-922.

35. **Kak, V. and J. W. Chow.** 2002. Acquired Antiobiotic Resistances in Enterococci, p. 355-384. *In* The Enterococci: Pathogenesis, Molecular Biology and Antibiotic Resistance. M. S. Gilmore (ed.), ASM Press, Washington, D.C.

36. **Liao, M., D. Sikora, M. Rigden, S. Marthaler, S. Ramirez-Arcos, and J.R. Dillon**. 2004. A novel DivIVA binding protein is involved in bacterial cell division in *Enterococcus faecalis*. Manuscript in Preparation

37. **Lupas, A., M. Van Dyke, and J. Stock**. 1991. Predicting coiled coils from protein sequences. Science **252**:1162-1164.

38. **Lupas, A.** 1996. Prediction and analysis of coiled-coil structures. Methods Enzymol. **266**:513-525.

39. **Margolin, W.** 2001. Spatial regulation of cytokinesis in bacteria. Curr.Opin.Microbiol. **4**:647-652.

40. **Margolin, W.** 2003. Bacterial division: the fellowship of the ring. Curr.Biol. **13**:R16-R18.

41. **Marston, A. L., H. B. Thomaides, D. H. Edwards, M. E. Sharpe, and J. Errington**. 1998. Polar localization of the MinD protein of *Bacillus subtilis* and its role in selection of the mid-cell division site. Genes Dev. **12**:3419-3430.

42. **Marston, A. L. and J. Errington**. 1999. Selection of the midcell division site in *Bacillus subtilis* through MinD-dependent polar localization and activation of MinC. Mol.Microbiol. **33**:84-96.

43. **Massidda, O., D. Anderluzzi, L. Friedli, and G. Feger**. 1998. Unconventional organization of the division and cell wall gene cluster of *Streptococcus pneumoniae*. Microbiology **144 (Pt 11)**:3069-3078.

44. **Miroux, B. and J. E. Walker**. 1996. Over-production of proteins in *Escherichia coli*: mutant hosts that allow synthesis of some membrane proteins and globular proteins at high levels. J.Mol.Biol. **260**:289-298.

45. **Monera, O. D., C. M. Kay, and R. S. Hodges**. 1994. Protein denaturation with guanidine hydrochloride or urea provides a different estimate of stability depending on the contributions of electrostatic interactions. Protein Sci. **3**:1984-1991.

46. **Muchova, K., E. Kutejova, D. J. Scott, J. A. Brannigan, R. J. Lewis, A. J. Wilkinson, and I. A. Barak**. 2002a. Oligomerization of the *Bacillus subtilis* division protein DivIVA. Microbiology **148**:807-813.

47. **Muchova, K., E. Kutejova, L. Pribisova, A. J. Wilkinson, and I. Barak**. 2002b. *Bacillus subtilis* division protein DivIVA - sceen for stable oligomer state conditions. Acta Crystallogr.D.Biol.Crystallogr. **58**:1542-1543.

48. **Nath, N., R. R. McCartney, and M. C. Schmidt**. 2002. Purification and characterization of Snf1 kinase complexes containing a defined Beta subunit composition. J.Biol.Chem. **277**:50403-50408.

49. **Park, Y. C., V. Burkitt, A. R. Villa, L. Tong, and H. Wu**. 1999. Structural basis for self-association and receptor recognition of human TRAF2. Nature **398**:533-538.

50. **Paulsen, I. T., L. Banerjei, G. S. Myers, K. E. Nelson, R. Seshadri, T. D. Read, D. E. Fouts, J. A. Eisen, S. R. Gill, J. F. Heidelberg, H. Tettelin, R. J. Dodson, L. Umayam, L. Brinkac, M. Beanan, S. Daugherty, R. T. DeBoy, S. Durkin, J. Kolonay, R. Madupu, W. Nelson, J. Vamathevan, B. Tran, J. Upton, T. Hansen, J. Shetty, H. Khouri, T. Utterback, D. Radune, K. A. Ketchum, B. A. Dougherty, and C. M. Fraser**. 2003. Role of mobile DNA in the evolution of vancomycin-resistant *Enterococcus faecalis*. Science **299**:2071-2074.

51. **Pichoff, S. and J. Lutkenhaus**. 2001. *Escherichia coli* division inhibitor MinCD blocks septation by preventing Z-ring formation. J.Bacteriol. **183**:6630-6635.

52. **Query, C. C., R. C. Bentley, and J. D. Keene**. 1989. A common RNA recognition motif identified within a defined U1 RNA binding domain of the 70K U1 snRNP protein. Cell **57**:89-101.

53. **Ramirez-Arcos, S., H. Salimnia, I. Bergevin, M. Paradis, and J. A. Dillon**. 2001a. Expression of *Neisseria gonorrhoeae* cell division genes *ftsZ, ftsE* and *minD* is influenced by environmental conditions. Res.Microbiol. **152**:781-791.

54. **Ramirez-Arcos, S., J. Szeto, T. Beveridge, C. Victor, F. Francis, and J. Dillon**. 2001b. Deletion of the cell-division inhibitor MinC results in lysis of *Neisseria gonorrhoeae*. Microbiology **147**:225-237.

55. **Ramirez-Arcos, S., J. Szeto, J. A. Dillon, and W. Margolin**. 2002. Conservation of dynamic localization among MinD and MinE orthologues: oscillation of *Neisseria gonorrhoeae* proteins in *Escherichia coli*. Mol.Microbiol. **46**:493-504.

56. **Ramirez-Arcos, S., V. Greco, H. Douglas, D. Tessier, D. Fan, J. Szeto, J. Wang, and J. R. Dillon**. 2004a. Conserved glycines in the C terminus of MinC proteins are implicated in their functionality as cell division inhibitors. J.Bacteriol. **186**:2841-2855.

57. **Ramirez-Arcos, S., Liao, M., Marthaler, S., Rigden, M., and Dillon, J. R**. 2004b. *Enterococcus faecalis divIVA*: An Essential Gene Involved in Cell Division, Cell Growth, and Chromosome Segregation. Submitted to Microbiology, Manuscript 27718.

58. **Ramos, A., M. P. Honrubia, N. Valbuena, J. Vaquera, L. M. Mateos, and J. A. Gil**. 2003. Involvement of DivIVA in the morphology of the rod-shaped actinomycete *Brevibacterium lactofermentum*. Microbiology **149**:3531-3542.

59. **Raskin, D. M. and P. A. de Boer**. 1999. MinDE-dependent pole-to-pole oscillation of division inhibitor MinC in *Escherichia coli*. J.Bacteriol. **181**:6419-6424.

60. **Reeve, J. N., N. H. Mendelson, S. I. Coyne, L. L. Hallock, and R. M. Cole**. 1973. Minicells of *Bacillus subtilis*. J.Bacteriol. **114**:860-873.

61. **Rothfield, L. I. and S. S. Justice**. 1997. Bacterial cell division: the cycle of the ring. Cell **88**:581-584.

62. **Rothfield, L. I., Y. L. Shih, and G. King**. 2001. Polar explorers: membrane proteins that determine division site placement. Cell **106**:13-16.

63. **Roy, S., A. Sahu, and S. Adhya** . 2002. Evolution of DNA binding motifs and operators. Gene **285**:169-173.

64. **Sambrook, J., E. F. Fritschand and T. Maniatis.** 1980. Molecular Cloning: A Laboratory Manual. Cold Spring Harbor Press, New York.

65. **Schmidt, M. A., L. W. Riley, and I. Benz**. 2003. Sweet new world: glycoproteins in bacterial pathogens. Trends Microbiol. 11:554-561.

66. **Scott, J. W., S. A. Hawley, K. A. Green, M. Anis, G. Stewart, G. A. Scullion, D. G. Norman, and D. G. Hardie**. 2004. CBS domains form energy-sensing modules whose binding of adenosine ligands is disrupted by disease mutations. J.Clin.Invest **113**:274-284.

67. **Shih, Y. L., T. Le, and L. Rothfield**. 2003. Division site selection in *Escherichia coli* involves dynamic redistribution of Min proteins within coiled structures that extend between the two cell poles. Proc.Natl.Acad.Sci.U.S.A **100**:7865-7870.

68. **Stahlberg, H., E. Kutejova, K. Muchova, M. Gregorini, A. Lustig, S. A. Muller, V. Olivieri, A. Engel, A. J. Wilkinson, and I. Barak**. 2004. Oligomeric structure of the *Bacillus subtilis* cell division protein DivIVA determined by transmission electron microscopy. Mol.Microbiol. **52**:1281-1290.

69. **Sun, Q. and W. Margolin**. 2004. Effects of perturbing nucleoid structure on nucleoid occlusion-mediated toporegulation of FtsZ ring assembly. J.Bacteriol. **186**:3951-3959.

70. **Szeto, J., S. Ramirez-Arcos, C. Raymond, L. D. Hicks, C. M. Kay, and J. A. Dillon**. 2001. Gonococcal MinD affects cell division in *Neisseria gonorrhoeae* and *Escherichia coli* and exhibits a novel self-interaction. J.Bacteriol. **183**:6253-6264.

71. **Szeto, J., S. Acharya, N. F. Eng, and J. A. Dillon**. 2004. The N Terminus of MinD Contains Determinants Which Affect Its Dynamic Localization and Enzymatic Activity. J.Bacteriol. **186**:7175-7185.

72. **Tannock, G. W. and G. Cook.** 2002. Enterococci as Members of the Intestinal Microflora of Humans, p. 101-132. *In* The Enterococci: Pathogenesis, Molecular Biology and Antibiotic Resistance. M. S. Gilmore (ed.), ASM Press, Washington, D.C.

73. **Thomaides, H. B., M. Freeman, M. El Karoui, and J. Errington**. 2001. Division site selection protein DivIVA of *Bacillus subtilis* has a second distinct function in chromosome segregation during sporulation. Genes Dev. **15**:1662-1673.

74. **Voet, D., J. G. Voet and C. W. Pratt.** 1999. Fundamentals of Biochemistry. John Wiley & Sons, Inc, New York.

75. **Weiss, D. S., J. C. Chen, J. M. Ghigo, D. Boyd, and J. Beckwith**. 1999. Localization of FtsI (PBP3) to the septal ring requires its membrane anchor, the Z ring, FtsA, FtsQ, and FtsL. J.Bacteriol. **181**:508-520.

76. **Wiegert, T. and W. Schumann**. 2003. Analysis of a DNA-binding motif of the *Bacillus subtilis* HrcA repressor protein. FEMS Microbiol.Lett. **223**:101-106.

77. **Wu, L. J. and J. Errington**. 2003. RacA and the Soj-Spo0J system combine to effect polar chromosome segregation in sporulating *Bacillus subtilis*. Mol.Microbiol. **49**:1463-1475.

RESEARCH ASSISTANT — MAY 1 -AUGUST 31, 2000 (CO-OP)
APRIL 17 - AUGUST 31, 2001 (CO-OP)
Health Canada — *Ottawa, Ontario*

- Developed and implemented protocols for lipid oxidation analysis.
- Developed and implemented Hepatocyte harvesting and testing techniques.
- Participated in all aspects of toxicological testing.
- Preformed endpoint analysis of biological samples.

LABORATORY ASSISTANT — FEBRUARY 4 - JUNE 9, 1997 (CO-OP)
Health Canada — *Ottawa, Ontario*

- Cleaned and analyzed biological samples
- Operated clinical chemistry analyzer
- Assisted in development of new experimental protocols.

INTERESTS AND ACTIVITIES

- Member of RA badminton club since 1990.
- Volunteer at various badminton tournaments at the RA badminton club.
- Former Patroller and Dispatcher for Carleton University Foot Patrol (1998-2001).
- Former Member of Carleton Chemistry and Biochemistry Society (1998-2001)
- Active member of Ottawa-Carleton Ultimate Association (2000-Present)

AWARDS

- Graduated Ontario scholar with Certificat d'études en Français (1997).
- Recipient of entrance scholarship to Carleton University (1997).
- Recipient of NSERC USRA in industry (2001)

EMPLOYMENT ELIGIBILITY

I am a Canadian Citizen.

REFERENCES

Available upon request.